

# **Wif1 Inhibits the Growth of Basal Cell Carcinoma**

Dissertation  
for the award of the degree  
“Doctor rerum naturalium”  
of the Georg-August-Universität Göttingen

within the doctoral program Molecular Biology of Cells  
of the Georg-August University School of Science (GAUSS)

submitted by

Marco Becker  
from Gelsenkirchen

Göttingen 2015

## **Thesis Committee**

**Prof. Dr. Heidi Hahn**

Dept. of Human Genetics; University Medical Center Göttingen

**Prof. Dr. Matthias Dobbelstein**

Dept. of Molecular Oncology; Georg-August-University Göttingen

**Prof. Dr. Tobias Pukrop**

Dept. of Hematology and Oncology; University Medical Center Regensburg

## **Members of the Examination Board**

Referee: **Prof. Dr. Heidi Hahn**

Dept. of Human Genetics; University Medical Center Göttingen

Co- referee: **Prof. Dr. Matthias Dobbelstein**

Dept. of Molecular Oncology; Georg-August-University Göttingen

## **Further members of the Examination Board**

**Prof. Dr. Holger Bastians**

Dept. of Molecular Oncology; Georg-August-University Göttingen

**Prof. Dr. Steven Johnsen**

Clinic for General, Visceral and Pediatric surgery; University Medical Center Göttingen

**Prof. Dr. Gregor Bucher**

Dept. of Developmental Biology; Georg-August-University Göttingen

**Prof. Dr. Sigrid Hoyer-Fender**

Dept. of Developmental Biology; Georg-August-University Göttingen

Date of oral examination: 1<sup>st</sup> of September, 2015

## Affidavit

I, Marco Becker, hereby declare that the PhD thesis entitled "Wif1 Inhibits the Growth of Basal Cell Carcinoma" has been written independently and with no other sources and aids than quoted.

---

Marco Becker

July, 2015

Göttingen

“We have done it that way ever since.”

-absolutely everybody

# Content

Affidavit.....	III
Content.....	V
List of Figures .....	VIII
List of Tables .....	XI
I Summary .....	1
II Introduction.....	2
II.1 Basal cell carcinoma (BCC) .....	2
II.2 Signaling pathways in BCC.....	4
II.3 Hh signaling.....	7
II.4 Wnt signaling.....	9
II.5 Wnt signaling in BCC.....	13
II.6 Wif1 .....	15
II.7 Objectives.....	17
III Material and methods .....	18
III.1 Software .....	18
III.2 Databases and web pages .....	18
III.3 Equipment .....	19
III.4 Consumables.....	21
III.5 Chemicals and reagents .....	22
III.6 Ready-to-use reaction systems.....	23
III.7 Buffers and solutions .....	24
III.8 Media.....	27
III.8.1 Media for bacteria culture .....	27
III.8.2 Agar plates .....	28
III.8.3 Media and reagents for cultivation of eukaryotic cell lines.....	28
III.9 Biological material.....	29
III.9.1 Bacterial strain.....	29
III.9.2 Eukaryotic cell lines .....	29
III.9.3 Mouse lines .....	30
III.10 Plasmids.....	30
III.11 Synthetic oligonucleotides .....	31
III.11.1 Synthetic DNA-oligonucleotides for qRT-PCR .....	31
III.11.2 Synthetic DNA-oligonucleotides for cloning .....	33
III.11.3 Synthetic DNA-oligonucleotides for sequencing.....	33
III.11.4 Synthetic DNA-oligonucleotides for genotyping .....	33
III.12 Enzymes.....	34
III.13 Antibodies.....	35

## Content

III.13.1	Primary antibodies.....	35
III.13.2	Secondary antibodies .....	36
III.14	Molecular biological methods.....	37
III.14.1	Isolation of nucleic acids.....	37
III.14.2	Polymerase chain reaction .....	40
III.14.3	Cloning techniques.....	43
III.14.4	Cell biological techniques .....	47
III.14.4.1	Transformation of bacteria .....	47
III.14.4.2	Culture of eukaryotic cells .....	48
III.14.4.3	Isolation and cultivation of BMDMs .....	48
III.14.4.4	Conditioned media (CM) .....	48
III.14.4.4.1	Generation and use of Wnt3a and Wnt5a CM .....	48
III.14.4.4.2	Generation and use of L929 CM.....	49
III.14.4.5	Concentration of Wif1-containing media.....	49
III.14.4.6	Transfection of eukaryotic cells .....	49
III.14.4.7	Nucleofection of eukaryotic cells .....	50
III.14.4.8	Retroviral transduction of eukaryotic cells .....	50
III.14.4.9	<i>TOP/FOP</i> reporter assay .....	51
III.14.4.10	Proliferation assay.....	52
III.14.4.10.1	5-Bromo-2'-deoxyuridine assay.....	52
III.14.4.10.2	Coculture proliferation assay .....	52
III.14.4.11	Cell cycle analysis.....	52
III.14.4.12	Cell viability assay.....	53
III.14.4.13	Annexin V assay .....	53
III.14.4.14	Transwell migration assay.....	53
III.14.4.15	Ca <sup>2+</sup> -flux assay.....	54
III.14.5	Western blot (WB) .....	54
III.14.5.1	Isolation of proteins from cell culture .....	54
III.14.5.2	Isolation of proteins from tissue samples.....	55
III.14.5.3	Western blot.....	55
III.14.6	Animal experiments .....	56
III.14.6.1	Mouse keeping.....	56
III.14.6.2	Genotyping PCR.....	56
III.14.6.3	Intramuscular tamoxifen injection .....	56
III.14.6.4	BCC mouse model and <i>Wif1</i> knockout.....	57
III.14.6.5	Allograft.....	57
III.14.7	Histological stainings .....	58

## Content

III.14.7.1	Hematoxylin and eosin (H&E) staining .....	58
III.14.7.2	Immunohistochemistry (IHC) .....	59
III.14.7.3	TdT-mediated dUTP-biotin nick end labeling (TUNEL) .....	59
III.14.7.4	Ladewig staining .....	60
IV	Results .....	61
IV.1	WIF1 expression in human BCC .....	61
IV.2	Generation of a Wif1 expression vector .....	64
IV.2.1	Cloning strategy .....	64
IV.2.2	Selection of stably transfected cells and verification of Wif1 expression .....	65
IV.3	Functional analysis of Wif1 <i>in vitro</i> .....	67
IV.3.1	TOP/FOP reporter assay for assessment of Wif1 activity .....	67
IV.3.2	Analysis of Hh and Wnt pathway activity and Ca <sup>2+</sup> measurement .....	70
IV.4	Effect of Wif1 overexpression on various cellular processes of ASZ001 <i>in vitro</i> .....	72
IV.4.1	Effect of Wif1 on cell viability <i>in vitro</i> .....	73
IV.4.2	Effect of Wif1 on apoptosis <i>in vitro</i> .....	73
IV.4.3	Effect of Wif1 on cell cycle regulation and proliferation <i>in vitro</i> .....	74
IV.4.4	Effect of Wif1 on migration <i>in vitro</i> .....	78
IV.4.5	Effect of Wif1 on differentiation <i>in vitro</i> .....	78
IV.5	Effect of Wif1 <i>in vivo</i> .....	79
IV.5.1	Effect of Wif1 on Hh, Wnt and Akt signaling pathways <i>in vivo</i> .....	83
IV.5.2	Cellular response on Wif1 <i>in vivo</i> .....	87
IV.5.3	Summary of the effects of Wif1 overexpression .....	98
IV.6	Targeted disruption of <i>Wif1</i> in murine BCC .....	99
V	Discussion .....	103
V.1	WIF1 in human tumors of the skin .....	103
V.2	Wif1 overexpression in the BCC cell line ASZ001 .....	105
V.2.1	Validation of Wif1 overexpression, secretion and functionality .....	105
V.2.2	Effects of Wif1 overexpression on the BCC cell line ASZ001 .....	106
V.2.2.1	Effect of Wif1 on Wnt, Hh and EGFR signaling pathways .....	106
V.3	Wif1 depletion in murine BCC .....	115
V.4	Outlook .....	116
VI	References .....	119
VII	Abbreviations .....	132
VIII	Acknowledgements .....	142
IX	Curriculum vitae .....	144

## List of Figures

Fig. 1: EGFR signaling pathway.....	7
Fig. 2: Pathologically activated Hh signaling pathway.....	9
Fig. 3: canonical Wnt signaling pathway .....	11
Fig. 4: Wnt/Ca <sup>2+</sup> signaling pathway .....	13
Fig. 5: Gel electrophoresis of amplified and purified <i>Wif1</i> insert .....	45
Fig. 6: Gel electrophoresis of hydrolyzed <i>Wif1</i> insert and <i>pMSCV</i> vector backbone .....	46
Fig. 7: Gel electrophoresis of restriction hydrolyzed <i>pMSCV-Wif1</i> .....	47
Fig. 8: Antibody staining of WIF1 in human BCC .....	61
Fig. 9: Evaluation of <i>WIF1</i> qRT-PCR of microdissected BCC subtypes, SCC and melanomas .....	63
Fig. 10: Functional structure <i>Wif1</i> .....	64
Fig. 11: Schematic of <i>pMSCV-Wif1</i> .....	65
Fig. 12: PCR detecting <i>Wif1</i> of <i>pMSCV</i> and <i>pMSCV-Wif1</i> transduced ASZ001 cells.....	66
Fig. 13: Western blot detecting <i>Wif1</i> of <i>pMSCV</i> and <i>pMSCV-Wif1</i> transduced ASZ001 cells.....	66
Fig. 14: Western blot detecting <i>Wif1</i> in supernatant and cellular extracts of ASZ- <i>pMSCV</i> and ASZ- <i>Wif1</i> .....	67
Fig. 15: <i>TOP/FOP</i> reporter assay of Wnt signaling in ASZ001 cells incubated with Wnt3a .....	68
Fig. 16: <i>TOP/FOP</i> reporter assay in HEK-293 cells incubated with Wnt3a and <i>Wif1</i> -concentrated supernatant.....	70
Fig. 17: qRT-PCR of <i>Axin2</i> and <i>Gli1</i> in ASZ- <i>pMSCV</i> and - <i>Wif1</i> .....	71
Fig. 18: Ca <sup>2+</sup> -influx assay of ASZ- <i>pMSCV</i> and - <i>Wif1</i> .....	72
Fig. 19: WST-1 assay of ASZ- <i>pMSCV</i> and - <i>Wif1</i> .....	73
Fig. 20: Annexin V assay of uninduced and staurosporine induced ASZ- <i>pMSCV</i> and - <i>Wif1</i> .....	74
Fig. 21: Distribution of ASZ- <i>pMSCV</i> and - <i>Wif1</i> in respective phases of cell cycle.....	75
Fig. 22: BrdU assay of ASZ- <i>pMSCV</i> and - <i>Wif1</i> .....	76

## List of Figures

Fig. 23: Cell proliferation assay of ASZ- <i>pMSCV</i> and ASZ- <i>Wif1</i> cocultured with B9, L cells, Wnt3A L cells, NIH/3T3, Wnt5a-NIH/3T3 or BMDMs .	77
Fig. 24: Transwell migration assay of ASZ- <i>pMSCV</i> and – <i>Wif1</i> .....	78
Fig. 25: qRT-PCR of <i>Krt10</i> in ASZ- <i>pMSCV</i> and - <i>Wif1</i> .....	79
Fig. 26: Growth curve of ASZ- <i>pMSCV</i> and ASZ- <i>Wif1</i> allografts in nude mice .....	80
Fig. 27: Tumor weight of ASZ- <i>pMSCV</i> and ASZ- <i>Wif1</i> allografts after dissection .....	81
Fig. 28: H&E stainings of ASZ- <i>pMSCV</i> and ASZ- <i>Wif1</i> allografts .....	82
Fig. 29: Total sections of ASZ- <i>pMSCV</i> and ASZ- <i>Wif1</i> allografts.....	82
Fig. 30: Vital tumor area of ASZ- <i>pMSCV</i> and ASZ- <i>Wif1</i> allografts.....	83
Fig. 31: qRT-PCR of <i>Gli1</i> , <i>Axin2</i> and <i>c-Myc</i> expression in ASZ- <i>pMSCV</i> and ASZ- <i>Wif1</i> allografts .....	84
Fig. 32: Antibody staining of $\beta$ -catenin in ASZ- <i>pMSCV</i> and ASZ- <i>Wif1</i> allografts .....	84
Fig. 33: Western blot of pJNK and pCaMKII in ASZ- <i>pMSCV</i> and ASZ- <i>Wif1</i> allografts .....	85
Fig. 34: Western blot of pAkt, Akt, pS6 and S6 in ASZ- <i>pMSCV</i> and ASZ- <i>Wif1</i> allografts .....	86
Fig. 35: Western blot of pPKC in ASZ- <i>pMSCV</i> and ASZ- <i>Wif1</i> .....	86
Fig. 36: Western blot of pErk1 and 2 and Erk1 and 2 in ASZ- <i>pMSCV</i> and ASZ- <i>Wif1</i> allografts .....	87
Fig. 37: qRT-PCRs of early and late keratinocyte differentiation markers in ASZ- <i>pMSCV</i> and ASZ- <i>Wif1</i> allografts.....	88
Fig. 38: Proportion of keratinous tissue in ASZ- <i>pMSCV</i> and ASZ- <i>Wif1</i> allografts .....	89
Fig. 39: qRT-PCRs of EMT markers in ASZ- <i>pMSCV</i> and ASZ- <i>Wif1</i> allografts .....	90
Fig. 40: Number of CD34 positive blood vessels in ASZ- <i>pMSCV</i> and ASZ- <i>Wif1</i> allografts .....	91
Fig. 41: Western blot of Caspase 3 in ASZ- <i>pMSCV</i> and ASZ- <i>Wif1</i> allografts .....	92
Fig. 42: Nuclear p53 staining of ASZ- <i>pMSCV</i> and ASZ- <i>Wif1</i> allografts. ....	92
Fig. 43: TUNEL staining of ASZ- <i>pMSCV</i> and ASZ- <i>Wif1</i> allografts.....	93
Fig. 44: Ladewig staining of ASZ- <i>pMSCV</i> and ASZ- <i>Wif1</i> allografts .....	94

## List of Figures

Fig. 45: Collagen proportion in ASZ- <i>pMSCV</i> and ASZ- <i>Wif1</i> allografts.....	95
Fig. 46: Western blot of Sdc-2 in ASZ- <i>pMSCV</i> and ASZ- <i>Wif1</i> allografts.....	95
Fig. 47: Evaluation of Ki67 staining of ASZ- <i>pMSCV</i> and ASZ- <i>Wif1</i> allografts .....	96
Fig. 48: Western blot of cyclin D1 in ASZ- <i>pMSCV</i> and ASZ- <i>Wif1</i> allografts.	97
Fig. 49: antibody staining of F4/80 in ASZ- <i>pMSCV</i> and ASZ- <i>Wif1</i> allografts	97
Fig. 50: Antibody staining of $\alpha$ Sma in ASZ- <i>pMSCV</i> and ASZ- <i>Wif1</i> allografts .....	98
Fig. 51: Antibody staining of Wif1 in murine BCC .....	99
Fig. 52: Western blot of Wif1 in murine BCC .....	100
Fig. 53: Planimetric measurement of tumor size in <i>Ptch</i> <sup>flox/flox</sup> <i>CreERT2</i> <sup>T/-</sup> and <i>Ptch</i> <sup>flox/flox</sup> <i>CreERT2</i> <sup>T/-</sup> <i>Wif1</i> <sup>-/-</sup> skin samples 45d after induction .....	101
Fig. 54: Planimetric measurement of tumor size in <i>Ptch</i> <sup>flox/flox</sup> <i>CreERT2</i> <sup>T/-</sup> and <i>Ptch</i> <sup>flox/flox</sup> <i>CreERT2</i> <sup>T/-</sup> <i>Wif1</i> <sup>-/-</sup> skin samples 90d after induction .....	101
Fig. 55: Evaluation of anti-Ki67 antibody staining in <i>Ptch</i> <sup>flox/flox</sup> <i>CreERT2</i> <sup>T/-</sup> and <i>Ptch</i> <sup>flox/flox</sup> <i>CreERT2</i> <sup>T/-</sup> <i>Wif1</i> <sup>-/-</sup> skin samples 45d and 90d after induction .....	102
Fig. 56: Putative autocrine and paracrine signaling mechanism in ASZ- <i>Wif1</i> allografts .....	117

## List of Tables

Table 1: Software.....	18
Table 2: Databases and web pages.....	18
Table 3: Equipment.....	19
Table 4: Consumables.....	21
Table 5: Chemicals and reagents.....	22
Table 6: Ready-to-use reaction systems.....	23
Table 7: Cell culture media and supplements for eukaryotic cell lines.....	28
Table 8: Eukaryotic cell lines.....	29
Table 9: Mouse lines.....	30
Table 10: Plasmids.....	31
Table 11: Oligonucleotides for qRT-PCR analyses.....	32
Table 12: Oligonucleotides for cloning.....	33
Table 13: Oligonucleotides for sequencing of <i>mWif1</i> .....	33
Table 14: Oligonucleotides for genotyping.....	33
Table 15: Enzymes.....	34
Table 16: Primary antibodies for immunohistochemistry.....	35
Table 17: Primary antibodies for Western blot.....	35
Table 18: Secondary antibodies.....	36
Table 19: Scheme of plasmid combinations for nucleofection.....	50

# I Summary

Basal cell carcinoma (BCC) belongs to the group of non-melanoma skin cancers and is the most commonly diagnosed cancer in fair-skinned individuals. In the majority of BCC the tumor suppressor gene *patched1* (*PTCH*) is mutated resulting in aberrant hedgehog (HH) signaling. Analysis of human and murine BCC shows that the putative tumor suppressor Wnt inhibitory factor 1 (Wif1) is highly expressed by this tumor entity. However, malignant forms of skin cancer, *i.e.* squamous cell carcinomas and melanomas, also express Wif1. Thus, the objective of this thesis was to analyze the role of Wif1 in BCC by Wif1 overexpression in the BCC cell line ASZ001 and by Wif1 depletion in the BCC mouse model *Ptch<sup>flox/flox</sup>CreERT2<sup>T/-</sup>*.

Indeed, tumor-intrinsic Wif1 overexpression in ASZ001 significantly inhibits tumor growth in nude mice. The Wif1-mediated tumor suppression was not due to diminished vascularization or alterations in canonical Wnt, Hh or PI3K/Akt signaling activity. It also was not due to induction of differentiation or apoptosis. However, we found that Wif1-expressing tumors were characterized by a decrease in Ki67 positive cells which was accompanied by phosphorylation of PKC and Erk1 along with moderately increased deposition of collagens. *Vice versa*, BCC growth is enhanced in *Ptch*-knockout mice on a Wif1-deficient background due to an increase in proliferation. Together, the data suggest that Wif1 is both necessary and sufficient to restrict BCC growth and may be one of the factors that are responsible for the very low metastatic potential of this tumor entity.

## **II Introduction**

### **II.1 Basal cell carcinoma (BCC)**

BCC belongs to the group of non-melanoma skin cancers and is the most commonly diagnosed cancer in fair-skinned individuals. As it is not reported to cancer registries, the precise incidence of BCC is unknown. However, it is estimated that BCC account for nearly half of all cancers in the United States of America (USA). In Europe, the incidence of BCC ranges from 44.6 to 128 per 100,000 inhabitants (Rubin *et al.* 2005; Trakatelli *et al.* 2007)(American Cancer Society 2015). The average lifetime risk for fair-skinned individuals to develop a BCC is approximately 30 % (Abdulla *et al.* 2005). Thus, BCC is the most common tumor in humans.

In contrast to other skin tumors such as squamous cell carcinoma (SCC) and melanoma, BCC are semi-malignant tumors. They have a good overall prognosis, with a high chance of cure when diagnosed early (Robinson and Dahiya 2003). This is due to the fact that BCC have a low metastatic potential as metastasis occurs in only 0.0028-0.55 % of all patients (Soleymani *et al.* 2008). In addition, approximately 20 % of BCC show signs of spontaneous regression (Curson and Weedon 1979). However, BCC can cause substantial morbidity due to its multiplicity, local recurrence and tissue invasion and destruction (Basset-Seguin *et al.* 2015).

The clinical presentation of BCC is diverse. Consequently, BCC can be classified histopathologically as indolent-growth or aggressive-growth subsets. The indolent-growth variants comprise superficial and nodular BCC subtypes with nodular BCC being the most common BCC subtype (Crowson 2006). Aggressive-growth tumors include infiltrative BCC, metatypical BCC and morpheaform or sclerosing BCC.

BCC can also be classified according to their differentiation status. This includes keratotic, infundibulocystic, follicular, pleomorphic BCC, BCC with eccrine differentiation, BCC with sebaceous differentiation, the fibroepithelioma of Pinkus and BCC with myoepithelial differentiation (Crowson 2006).

BCC most frequently occur at sun-exposed sites of the skin (Nakayama *et al.* 2011) and several epidemiologic studies indicate that exposure to sun light is the main risk factor for BCC formation. Other risk factors comprise fair skin, age, immune suppression and exposure to arsenic (Boonchai *et al.* 2000; Dessinioti *et al.* 2010).

Although the vast majority of BCC occur sporadically, a rare heritable disorder exists, that predisposes patients to the development of multiple BCC during their lifetime. This syndrome is known as basal-cell nevus syndrome (BCNS), or Gorlin-Goltz syndrome or nevoid basal-cell carcinoma syndrome. By genetic linkage analysis of relatives with BCNS, the mutation bearing locus was mapped to human chromosome 9q22 and then to the *patched 1* (*PTCH*) gene (Hahn *et al.* 1996; Johnson *et al.* 1996). Indeed, mutations of *PTCH* are responsible for BCC development in BCNS patients. Upon this discovery, *PTCH* was shown to be mutated in about 90 % of all spontaneous BCC. Other BCC associated mutations are activating mutations in *smoothened* (*SMO*) (Lam *et al.* 1999), mutations in *suppressor of fused homolog* (*SUFU*) and in *tumor protein p53* (*TP53*) (Reifenberger *et al.* 2005). BCC also develop in *Ptch* mutant mice comprising the *Ptch*<sup>neo67/+</sup> (Mancuso *et al.* 2004) and the *Ptch*<sup>flox/flox</sup> (Zibat *et al.* 2009; Nitzki *et al.* 2010) mouse models, in a mouse model expressing a constitutively active Smo mutant (SmoM2) (Xie *et al.* 1998) and in a mouse model overexpressing sonic hedgehog (Shh) (Oro *et al.* 1997). These mouse models are valuable tools to investigate the molecular mechanisms of BCC pathogenesis.

The cellular origin of BCC is still debated. However, analysis of *Ptch* knockout or transgenic *SmoM2* mouse models revealed that BCC can originate from progenitor cells of the interfollicular epidermis and the upper infundibulum of the hair shaft (Youssef *et al.* 2010) and from hair follicle stem cells (Nitzki *et al.* 2010; Peterson *et al.* 2015) caused by aberrantly activated Hedgehog (Hh) signaling.

BCC treatment comprises surgical or non-surgical techniques depending on several tumor- and patient-related factors. The best results are achieved upon surgery including Mohs micrographic surgery, La Galette technique,

conventional surgery with tumor-adapted margins of safety, curettage, electrodesiccation, and cryosurgery (Goppner and Leverkus 2011). Non-surgical treatment options comprise radiotherapy, photodynamic therapy, and topical application of imiquimod and 5-fluorouracil. For advanced or metastatic BCC the Food and Drug Administration (FDA) approved the Smo inhibitor vismodegib (trade name Erivedge®) that can be either applied systemically or topically (Basset-Seguin *et al.* 2015). In particular, patients with multiple comorbidities and inoperable tumors benefit from these non-surgical techniques. However, compared to surgery non-surgical treatments can result in increased recurrence rates.

Due to its high and rising incidence and its increasing occurrence in young people BCC are becoming more and more problematic for the health care system. Non-melanoma skin cancer (i.e. BCC and SCC) account for 9% of the total costs of all cancers in 2000-2001 in Australia (Staples *et al.* 2006). Better therapeutic approaches may help to reduce these costs. This, however, necessitates a better knowledge about molecular events in BCC growth, progression or regression. Particularly factors and mechanisms that keep BCC a slowly growing tumor entity could enable us to employ these findings as prospective treatment options.

## II.2 Signaling pathways in BCC

Multiple pathways are known to be misregulated in BCC. Among these are the Hh and Wnt signaling pathway (see below). Moreover, components of pathways regulating cell cycle progression and controlling apoptosis are frequently found to be mutated (TP53) or misregulated (platelet derived growth factor receptor- $\alpha$  (PDGFR $\alpha$ ) and B cell leukemia/lymphoma 2 (BCL2)) in BCC (Xie *et al.* 2001; Vidal *et al.* 2004; Reifenberger *et al.* 2005).

Furthermore, epidermal growth factor receptor (EGFR) signaling plays an important role in BCC. Receptors of this pathway, ErbB1, 2 and 3 were shown to be expressed in BCC (Krahn *et al.* 2001; Schnidar *et al.* 2009) and epidermal-specific deletion or irreversible inhibition of EGFR inhibits BCC

growth (Eberl *et al.* 2012). Downstream of activated EGFR several signaling cascades including mitogen-activated protein kinase (MAPK) and phosphatidylinositol-4,5-bisphosphate 3-kinase/v-akt murine thymoma viral oncogene homolog (PI3K/Akt) signaling have been reported to be involved in BCC growth (Schnidar *et al.* 2009; Hafner *et al.* 2010). In particular, the inhibition of the Mapk kinase 1/2 (Mek1/2) was shown to suppress the proliferation of the BCC cell line ASZ001 (Xie *et al.* 2001).

As EGFR signaling is also relevant in this thesis a more detailed summary of this pathway is given. EGFR signaling is involved in the regulation of a variety of cellular responses including proliferation, differentiation, migration and apoptosis (Yarden and Sliwkowski 2001; Chong and Janne 2013) and has a crucial role in the initiation and maintenance of several solid tumors (Arteaga and Engelman 2014). In the extracellular space ligands containing epidermal growth factor (EGF)-like domains can bind to the v-erb-b2 erythroblastic leukemia viral oncogene homolog (ErbB) receptors (Yarden and Sliwkowski 2001). ErbB family members are receptor tyrosine kinases (RYKs) and comprise the epidermal growth factor receptor ErbB1 (EGFR, also HER1), ErbB2 (also HER2 or Neu), ErbB3, and ErbB4 (Yarden and Sliwkowski 2001). Upon binding of EGF-like growth factors to the extracellular domain, the ErbB receptors form homo- and heterodimers resulting in auto- or transphosphorylation of the cytoplasmic domains. The phosphorylated domains serve as binding sites for various proteins involved in the regulation of multiple intracellular signaling cascades (Yarden and Pines 2012). Which signaling cascade is activated depends on the respective receptor dimers, as all ErbB family members have distinct biochemical properties and interaction partners (see Fig. 1) (Nyati *et al.* 2006; Yarden and Pines 2012).

First, EGFR phosphorylation can induce the activation of signal transducer and activator of transcription (STAT) by Janus kinase (JAK). Activated STAT in turn translocates into the nucleus and directly regulates gene expression crucial for cell survival, proliferation, transformation and oncogenesis (Bowman *et al.* 2000).

Second, EGFR activates PI3K that phosphorylates PIP<sub>2</sub> to form phosphatidylinositol-3,4,5-triphosphate (PIP<sub>3</sub>), which then activates Akt by phosphorylation. Phosphorylated Akt has several effects, both in the cytoplasm and in the nucleus, which include the inhibition of proapoptotic factors such as BAD (BCL2 antagonist of cell death), pro-caspase 9 and the Forkhead (FKHR) family of transcription factors (FOXO). Moreover, Akt-mediated activation of mammalian target of rapamycin (mTOR) is involved in the regulation of cell proliferation by controlling the activity of ribosomal protein S6 (S6) (Wendel *et al.* 2004; Ruvinsky and Meyuhas 2006; Hemmings and Restuccia 2015).

Third, activation of small GTPase rat sarcoma virus oncogene homolog (Ras) by phosphorylation is mediated by son of sevenless (SOS) triggering a MAPK signaling cascade. Activated Ras binds to Raf (MAP3K), which in turn triggers the phosphorylation of MEK1/2 and MAPK3/1 (also named extracellular signal-regulated kinases (ERK) 1/2 or p44/p42). Phosphorylated ERK1/2 translocates into the nucleus and activates various transcription factors such as ELK1 (McCubrey *et al.* 2012).

Fourth, PLC binds to phosphorylated EGFR inducing its activity. Subsequently, PLC hydrolyses phosphatidylinositol-4,5-bisphosphate (PIP<sub>2</sub>) to 1,2 diacylglycerol (DAG) and inositol 1,4,5-triphosphate (IP<sub>3</sub>). DAG mediates the activation of protein kinase C (PKC) regulating cell-cycle progression, transformation, differentiation and apoptosis (Oliva *et al.* 2005).

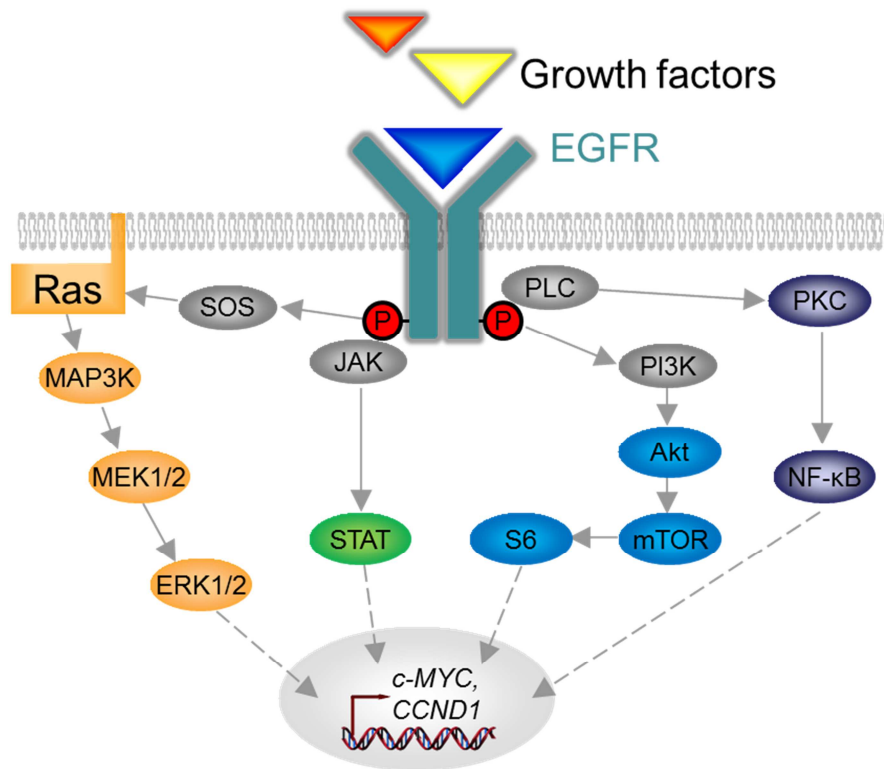


**Fig. 1: EGFR signaling pathway**

The shown signaling cascade does not include all the known components of a given pathway, and cross-talks are not shown for clarity. Activated EGFR signaling can result in the induction of different pathways leading to the activation of ERK, STAT, Akt, S6 and/or PKC. Modified from: (Nyati *et al.* 2006).

## II.3 Hh signaling

The Hh signaling pathway is highly conserved between the species and its signaling is required for tissue homeostasis and regeneration (Beachy *et al.* 2004). In brief, Hh is a morphogen and three mammalian homologues of the *Drosophila* segment polarity gene *hedgehog* exist. These are sonic (Shh), indian (Ihh) and desert (Dhh) hedgehog, all of which are all secreted proteins. Shh is the most broadly expressed Hh homologue. In vertebrate development Shh is mainly required for polarization and pattern formation of the limb bud and of the neural tube. Ihh regulates bone and cartilage development and Dhh is essential for germ cell development in the testis and peripheral nerve sheath formation (Petrova and Joyner 2014). Hh signaling requires the autoproteolytic cleavage of the Hh precursor into an N-terminal (Hh-N) and a C-terminal (Hh-C) moiety. After several post-translational modifications including an addition of a cholesterol moiety at the C-terminus

and palmitoylation at the N-terminus of Hh-N, it is secreted by means of the membrane transporter protein Dispatched (Disp) (Burke *et al.* 1999; Ma *et al.* 2002; Beachy *et al.* 2010).

In the extra cellular space the distribution of Hh is dependent on heparan sulfate proteoglycans (HSPGs) (Chang *et al.* 2011), where it can bind to the two extracellular loops of the 12-pass transmembrane receptor Ptch (Briscoe *et al.* 2001). The association of Hh to Ptch is increased by the transmembrane proteins cysteine dioxygenase 1, cytosolic (Cdo1) and biregional cell adhesion molecule-related/down-regulated by oncogenes (Cdon) binding protein (Boc) (Yao *et al.* 2006). Ptch is a negative regulator of the Hh signaling pathway (Epstein 2008); (Pasca di Magliano and Hebrok 2003). In the absence of Hh ligand, Ptch inhibits the activation of the G-protein coupled receptor Smo, in turn keeping glioma-associated oncogene family member (Gli) transcription factors inactive in the cytoplasm. When Hh is present, Ptch becomes internalized into the cell, resulting in suspension of Smo inhibition. Subsequently, Smo facilitates the translocation of the activator forms of Gli transcription factors into the nucleus where they induce the expression of Hh target genes (see Fig. 2) by binding to the conserved Gli binding site 5'-GACCACCCA-3' (Hallikas *et al.* 2006). The Gli protein family consists of 3 distinct proteins (Gli1, 2 and 3). Gli2 and Gli3 are bifunctional transcription factors facilitating either transcriptional repression or activation. When Hh signaling is inactive Gli2 and Gli3 are phosphorylated and subsequently proteolytically cleaved to generate the repressor forms (Gli2R and Gli3R, respectively). When Hh is present, the activation of Smo results in the transport of uncleaved, activated Gli2 and Gli3 proteins from the cilia to the nucleus. Gli1, which is a downstream target gene of active Hh signaling but not immediately involved in signal transduction, is a strong potentiator of the signaling cascade (Roberg-Larsen *et al.* 2014).

When Ptch is mutated, the resulting protein is incapable of inhibiting Smo. This results in pathological, constitutive active Hh signaling, ultimately leading to cancer formation such as BCC in both humans and mice (see Fig. 2) (Athar *et al.* 2006).

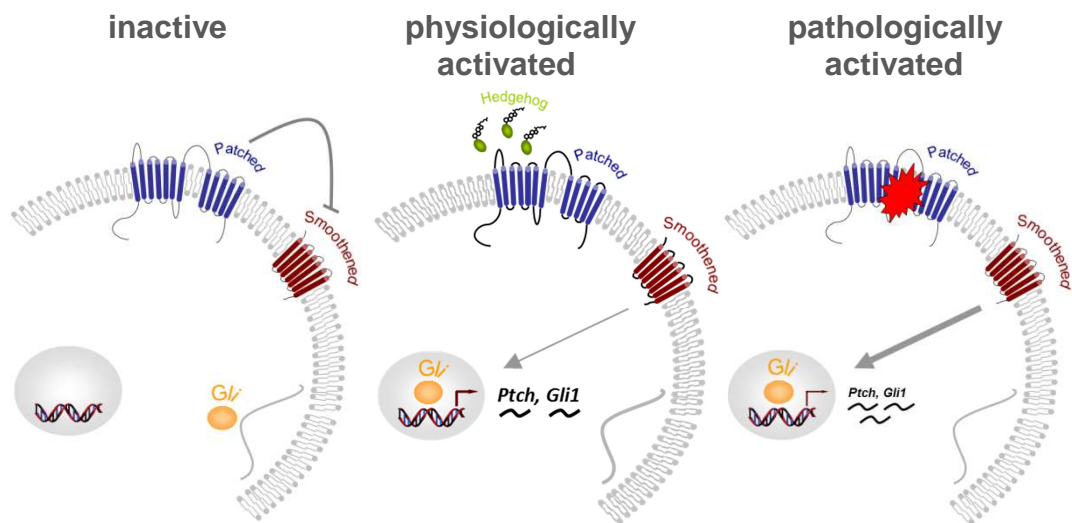


**Fig. 2: Pathologically activated Hh signaling pathway**

Left panel: inactive pathway, Ptc inhibits Smo and Gli transcription factors remain inactive in cytoplasm; middle panel: Hh binds to its receptor Ptc leading to a translocation of Gli transcription factors into the nucleus; right panel: mutated Ptc cannot inhibit Smo and Gli is constitutively triggering target gene expression. Modified from: (Nitzki 2008).

## II.4 Wnt signaling

The wingless-type MMTV integration site family member (Wnt) signaling is a central pathway in development, tissue regeneration and homeostasis. Wnts are secreted proteins that act as morphogens in the extracellular space. For secretion they require the activity of the palmitoyltransferase porcupine (Porcn) adding a palmitate modification to the premature Wnt proteins. This lipid modification leads to the binding of the 7-transmembrane protein wntless (Wls) conveying Wnt to the plasma membrane for secretion (Banziger *et al.* 2006). At the target cell Wnt ligands can induce the activity of  $\beta$ -catenin-dependent Wnt signaling (canonical) or  $\beta$ -catenin-independent (non-canonical) signaling. The non-canonical signaling comprises at least the Wnt/planar cell polarity (PCP) and Wnt/ $\text{Ca}^{2+}$  signaling.

In the extracellular space Wnt signaling can be blocked at the receptor level by dickkopf (Dkk) binding to the single-span transmembrane receptor LDL receptor-related protein 5/6 (Lrp5/6) or by direct binding and sequestration of Wnts either by the secreted frizzled-related protein (Sfrp) or by Wnt inhibitory factor 1 (Wif1) (Malinauskas and Jones 2014).

When canonical Wnt signaling is inactive,  $\beta$ -catenin is continuously phosphorylated by the serine/threonine kinases glycogen synthase kinase 3 (Gsk3) and casein kinase 1 (Ck1) as part of the destruction complex (composed of Gsk3, Ck1, dishevelled (Dvl), Axin1, adenomatosis polyposis coli (Apc) and beta-transducin repeat containing protein ( $\beta$ -TrCP)) (see Fig. 3). Phosphorylated  $\beta$ -catenin is subsequently ubiquitinated by  $\beta$ -TrCP, a component of the E3 ubiquitin ligase complex, and degraded by the proteasome (Clevers and Nusse 2012). The absence of  $\beta$ -catenin allows the T-cell factor/lymphoid enhancer factor (Tcf/Lef) transcription factors, in particular Tcf3 and Tcf4 (Liu *et al.* 2005), to interact with transducin-like enhancer of split, homolog of *Drosophila* E (spl) (Tle, or groucho). The binding of Tle prevents Wnt target gene transcription (Cadigan and Waterman 2012). When canonical Wnt signaling is active, Wnt ligands bind with the palmitate group to the cysteine-rich domain of their receptor cognate frizzled (Fzd) receptor. Moreover, Wnt ligands bind the Lrp5/6 co-receptor, inducing it to form a complex with Fzd. This results in a conformational change of the receptors inducing the phosphorylation of Lrp5/6. This recruits Axin1 as part of the intact destruction complex leading to the dissociation of  $\beta$ -TrCP. Thus, phosphorylated  $\beta$ -catenin is no longer ubiquitinated and consequently not degraded. This leads to a saturation with phosphorylated  $\beta$ -catenin at the destruction complex and inhibition of the latter (Li *et al.* 2012). Only  $\beta$ -catenin that is newly synthesized after initiation of the Wnt signal is signaling competent (Staal *et al.* 2002). In its active stage  $\beta$ -catenin remains unphosphorylated and accumulates in the cytoplasm resulting in its translocation into the nucleus. In the nucleus active  $\beta$ -catenin can bind to Tcf/Lef transcription factors, in particular Tcf1 and Lef1 (Behrens *et al.* 1996; Molenaar *et al.* 1996; Liu *et al.* 2005). Tcf/Lef transcription factors can directly bind to DNA bearing the motif 5`-CCTTTGATCTT-3` (van de Wetering *et al.* 1997) which is also employed in the *TOP/FOP* reporter system (Korinek *et al.* 1997). When  $\beta$ -catenin binds Tcf/Lef transcriptional activators in a complex containing CREB-binding protein (Cbp), B cell CLL/lymphoma 9 (Bcl9) and pygopus (Pygo) it drives Wnt target genes expression in a tissue- and developmental stage-specific manner. *Axin2* is considered as a general transcriptional target gene of active Wnt/ $\beta$ -catenin signaling and thus serves

an indicator of an active signaling pathway (Lustig *et al.* 2002). In contrast to the proposed model of an intact destruction complex and the dissociation of  $\beta$ -TrCP described above, it is also discussed that the destruction complex is resolved into its compounds as a result of recruitment of Axin to the Fzd receptor. Which model turns out to hold true is an ongoing debate.

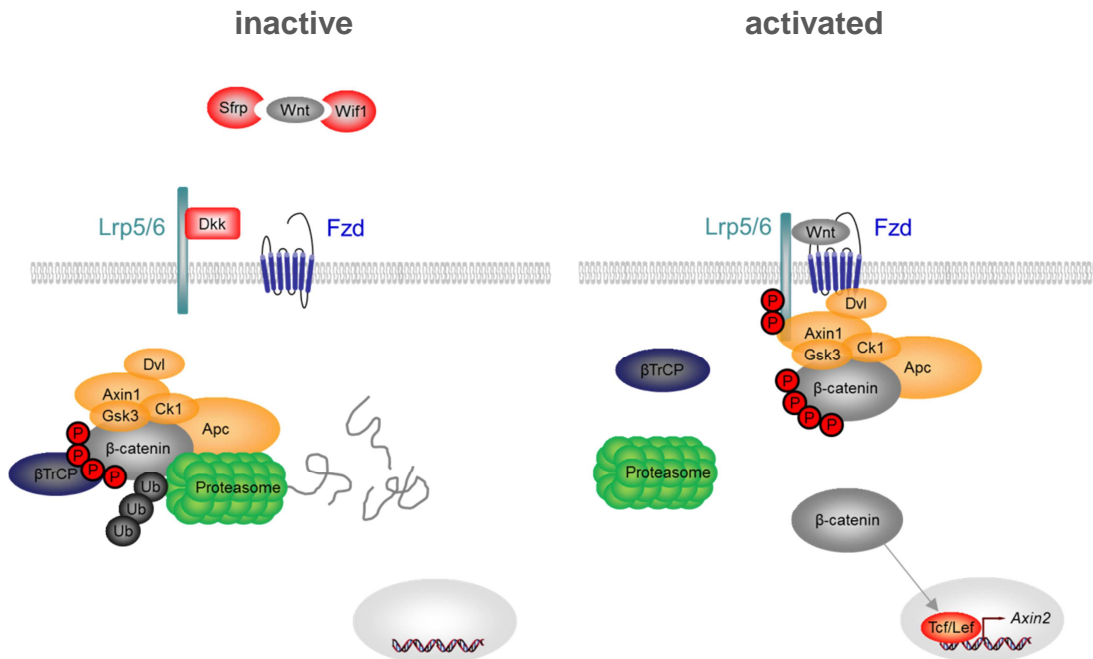


**Fig. 3: canonical Wnt signaling pathway**

Left panel: inactive pathway; proteasome cleaves ubiquitinated  $\beta$ -catenin preventing target gene expression. Right panel: active pathway; Conformational change of the activated receptors result in the dissociation of  $\beta$ TrCP abrogating ubiquitination of  $\beta$ -catenin and thus proteasomal degradation; newly synthesized  $\beta$ -catenin accumulates and translocates into the nucleus triggering target gene expression. Modified from: (Clevers and Nusse 2012).

In contrast to canonical Wnt signaling, the Wnt/PCP pathway is independent from  $\beta$ -catenin. It controls the cell shape, directional migration, asymmetric cell division, and cellular orientation which is required for normal development and function of complex tissues (Kaucka *et al.* 2015). Wnt/PCP signaling is activated by the binding of Wnts to Fzd receptor and the co-receptors receptor tyrosine kinase-like orphan receptor 1 and 2 (Ror1/2), the Ryk, or the protein tyrosine kinase 7 (Ptk7) (Green *et al.* 2014). At the cell surface PCP signaling can be blocked by vang-like (Vangl, or strabismus). The cytoplasmic tail of Vangl binds and recruits prickly (Pk) to the plasma membrane, where Prickle binds and thereby antagonizes the recruitment of Dvl to Fzd resulting in an inhibition of Wnt/PCP signaling (Wang 2009). Activation of the pathway by Wnt ligands results in the recruitment of

cytoplasmic Dvl to the Fzd receptor. When the pathway is active, ankyrin repeat domain (Ankrd, or Diego) binds to Dvl and prevents Pk from binding and inhibiting Dvl (Devenport 2014). At the level of Dvl, two parallel pathways result in the activation of the GTPases Rho and Rac (Habas *et al.* 2003). The first activates Dishevelled associated activator of morphogenesis 1 (Daam1) resulting in the activation of the Rho-associated coiled-coil containing protein kinase (Rock) inducing cytoskeletal reorganization (Kim and Han 2005). Furthermore, Daam1 is a formin-homology protein and a direct nucleator of linear actin filaments (Watanabe and Higashida 2004). The second pathway activates Rac, which in turn stimulates Mapk8 (JNK) activity modulating actin cytoskeleton (Habas *et al.* 2003).

The second  $\beta$ -catenin independent Wnt pathway is Wnt/ $\text{Ca}^{2+}$  signaling (see Fig. 4). This pathway is activated upon binding of specific Wnt ligands to Fzd receptor leading to the activation of phospholipase C (PLC). Activated PLC cleaves membrane bound phospholipid  $\text{PIP}_2$  in  $\text{IP}_3$  and DAG.  $\text{IP}_3$  triggers  $\text{Ca}^{2+}$  influx from the endoplasmic reticulum (ER), which activates several effector proteins including calcium/calmodulin-dependent protein kinase II (CaMKII), PKC and calcineurin (Cn). These kinases regulate and activate a multitude of target proteins including nuclear factor of kappa light polypeptide gene enhancer in B cells (Nf- $\kappa$ B), cAMP responsive element binding protein (Creb), Erk and nuclear factor associated with T cells (Nfat) (Sheldahl *et al.* 1999; Kuhl *et al.* 2000; Hogan *et al.* 2003) that in turn drive the expression various target genes regulating cell survival and proliferation.

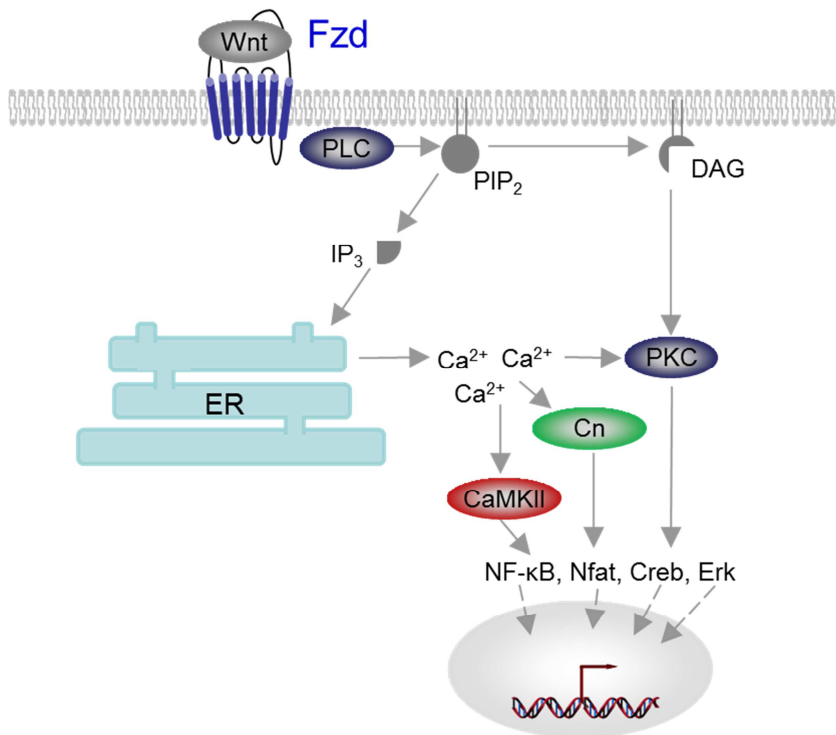


**Fig. 4: Wnt/Ca<sup>2+</sup> signaling pathway**

Wnt binding to the receptor Fzd triggers the activation of PLC. This leads to the cleavage of PIP<sub>2</sub> in DAG and IP<sub>3</sub>. IP<sub>3</sub> induces an efflux of Ca<sup>2+</sup> from the endoplasmic reticulum (ER) into the cytoplasm. Elevated cytoplasmic Ca<sup>2+</sup> levels and DAG induce the activation of CaMKII, Cn and PKC triggering target gene expression by various effector proteins. Modified from: (Lories *et al.* 2013).

Although the canonical and non-canonical pathways are here separately described, they influence and inhibit each other at various interfaces (Weidinger and Moon 2003). In the past, Wnts and their cognate receptors were also classified as either canonical or non-canonical. However, each of the 19 Wnts can bind to several Fzd receptors and each of the 10 Fzd receptors can bind several Wnts, making Wnt signaling highly context specific (van Amerongen and Nusse 2009).

## II.5 Wnt signaling in BCC

Beside Hh signaling Wnt signaling has been shown to be involved in BCC tumorigenesis (Doglioni *et al.* 2003; El-Bahrawy *et al.* 2003). In the *SmoM2* BCC mouse model constitutive Hh signaling induces canonical Wnt target gene expression in tumor cells and in surrounding stromal cells. In the same

context, inhibition of canonical Wnt signaling via Dkk1 results in suppression of tumor formation (Yang *et al.* 2008). Consistently, human BCC samples also exhibit nuclear accumulation of  $\beta$ -catenin and thus active canonical Wnt signaling (Salto-Tellez *et al.* 2006).

Moreover, it has been speculated that canonical Wnt signaling enhances BCC development by modulation of the Hh pathway activity (Yang *et al.* 2008). Indeed, Wnt signaling was shown to alter Hh signaling and *vice versa*. For example Gli3R is capable of inhibiting canonical Wnt signaling by antagonizing  $\beta$ -catenin (Ulloa *et al.* 2007). Interestingly, the generation of Gli3R is triggered by sequential phosphorylation involving Gsk3 which is also part of the destruction complex in canonical Wnt signaling facilitating  $\beta$ -catenin phosphorylation to mark it for proteasomal degradation (see section I.3) (Hui and Angers 2011). Furthermore, Sufu has been shown to bind to  $\beta$ -catenin leading to its nuclear export and to the inhibition of target gene expression. Mutated Sufu lacking this property leads to both active Hh and Wnt signaling (Taylor *et al.* 2004).

In development both Wnt and Hh signaling need to be tightly coordinated to determine the cell fate decision in various organs (Li *et al.* 2009). Thus, it is very likely that Wnt and Hh signaling also influence each other in BCC. Indeed, canonical Wnt signaling induces expression of GLI1 via insulin-like growth factor 2 mRNA binding protein 1 (Igf2bp1). When downregulated, Igf2bp1 suppresses the growth of BCC (Noubissi *et al.* 2014). Furthermore, the expression of constitutively active  $\beta$ -catenin in the absence of vitamin D receptor leads to the formation of BCC-like lesions with up-regulated Ptch expression (Palmer *et al.* 2008).

In contrast, activation of Wnt/Ca<sup>2+</sup> signaling by tumor stroma derived Wnt5a induces the differentiation and regression of BCC in a CaMKII-dependent manner (Nitzki *et al.* 2010).

In conclusion, these studies reflect the significant function of Wnt signaling in BCC development (Lim and Nusse 2013).

## II.6 Wif1

Wif1 was first identified as an expressed sequence tag from human retina. The initial hint that Wif1 affects Wnt signaling was derived from experiments with early *Xenopus* embryos when injection of RNA encoding for human WIF1 caused a partial axis duplication and abnormal somitogenesis which both were known to be controlled by the Wnt signaling pathway (Hsieh *et al.* 1999). Wif1 is highly conserved in human, mouse, *Xenopus* and zebrafish and consists of an N-terminal signal sequence for secretion, five EGF-like repeats, a hydrophilic C-terminus and a WIF domain (WD) which is also present in the Wnt receptors Ryk/Derailed (Drl) (Patthy 2000; Yoshikawa *et al.* 2003) (see Fig. 10).

In the mouse the *Wif1* gene is located on chromosome 10 and in humans on chromosome 12. It encodes for transcripts of 2294 or 2238 bp in length, respectively. For both mouse and human the transcript comprises 10 exons with a protein coding sequence of 1140 bp length which is translated into a ~42 kDa protein consisting of 379 amino acids (according to NCBI CCDS database).

Human WIF1 directly binds eight Wnts (3a, 4, 5a, 7a, 9a, 11 (Surmann-Schmitt *et al.* 2009)), to the *Drosophila* orthologue of Wnt, wingless, and to *Xenopus* Wnt8 (Hsieh *et al.* 1999) by its WD and at least partially by its EGF-like domains (Malinauskas *et al.* 2011). Moreover, the EGF-like domains contain a HSPG-binding site suggesting that Wif1 facilitates the interaction between Wnts and HSPG in the extra cellular space. Other studies showed that the *Drosophila* Wif1 homolog shifted also facilitates interactions of Hh and HSPGs and thereby fosters Hh signaling (Glise *et al.* 2005; Gorfinkiel *et al.* 2005). More recently it was revealed that zebrafish Wif1 affects Hh signaling in *Drosophila*, likewise suggesting a possible role for Wif1 as a modulator of vertebrate Hh signaling (Avanesov *et al.* 2012).

In summary, Wif1 possibly modulates both Wnt and Hh signaling which are dysregulated in a variety of malignancies including BCC.

Wif1 itself also plays a role in tumor development as it suppresses growth of many different tumors. In contrast, also an oncogenic role of Wif1 has been suggested (Huang *et al.* 2014). Thus, Wif1 is upregulated in some adenocarcinoma cell lines and intestinal adenomas of *Apc<sup>min/+</sup>* mice (Cebrat *et al.* 2004). However, Wif1 upregulation could be regarded as a negative feedback loop and therefore a side effect of the constitutive activity of canonical Wnt signaling without any significance for the growth of adenomas. This is due to the fact that *Apc* mutant cells are insensitive towards extracellular Wnt inhibitors with respect to the downregulation of  $\beta$ -catenin driven target gene expression.

As already mentioned, most published data show that reduced levels of Wif1 expression is associated with enhanced tumor growth, whereas Wif1 overexpression is connected with tumor growth inhibition. Thus, disruption of the murine *Wif1* gene results in the development of radiation-induced osteosarcomas (Kansara *et al.* 2009). Promoter methylation induced downregulation of *WIF1* expression is present in numerous human cancers (Mazieres *et al.* 2004; Haqq *et al.* 2005; Taniguchi *et al.* 2005), whereas overexpression of *WIF1* inhibits the growth of lung, bladder cancer and melanoma cells (Kim *et al.* 2007; Lin *et al.* 2007; Tang *et al.* 2009). Recently, a rare missense mutation of *Wif1* in combination with a mutation in *heterogeneous nuclear ribonucleoprotein A0 (HNRNPA0)* has been shown to predispose members of a large family to multiple cancers (Wei *et al.* 2015). These data demonstrate that Wif1 plays a tumor suppressive role in a variety of tumor entities.

Previous experiments of our group showed that Wif1 is highly upregulated in BCC derived from *Ptch<sup>flox/flox</sup>CreERT2<sup>T/-</sup>* mice (König 2012). The same applies to BCC of the *SmoM2* mouse model (Youssef *et al.* 2012). This indicates that Wif1 is also involved in BCC development in these mouse models.

## II.7 Objectives

The aim of this thesis was to analyze the role of Wif1 in BCC. For this purpose, three experimental approaches were pursued.

First, I investigated the Wif1 expression levels in laser microdissected human BCC and compared it with human SCC and melanomas and correlated the expression levels with the degree of malignancy of the respective tumor entity.

Second, I analyzed the function of Wif1 in the BCC cell line ASZ001, which is derived from irradiated *Ptch*<sup>+/-</sup> mice. Since ASZ001 express low levels of Wif1, I have introduced Wif1 by retroviral transduction. This allowed for analyzing the effects of Wif1 on BCC cell growth *in vitro*. The analyses comprised Wif1 related effects on apoptosis, cell viability, proliferation, cell cycle progression, differentiation, migratory capacity and on Wnt, Hh and EGFR pathway activity. Moreover, I transplanted control and Wif1 overexpressing ASZ001 (hereafter ASZ-*pMSCV* and ASZ-*Wif1*, respectively) subcutaneously in nude mice to study the effect of Wif1 on tumor growth *in vivo*. After excision the tumors were subjected to the same analyses as mentioned above. In addition, vascularization, EMT and stromal composition of the tumors were investigated.

Third, *Ptch*<sup>flox/flox</sup>*CreERT2*<sup>T/-</sup> mice (in which BCC can be conditionally induced by injection of tamoxifen) were crossed onto a Wif1-deficient background. After BCC induction in the resulting offspring the tumors were analyzed after 45 and 90 days with respect to size and proliferative capacity.

These investigations allowed us to elucidate the effect of Wif1 on BCC development.

## III Material and methods

### III.1 Software

**Table 1: Software**

Software	Supplier
4D v13 Volume Desktop Version 13.4	4D SAS, Clichy-la-Garenne, France
ABI 3500 XL Data Collection Software v3.0	Applied Biosystems, Darmstadt
BD FACSDiva	Becton Dickinson GmbH, Heidelberg
BioEdit 7.0.9	Ibis Biosciences, Carlsbad, USA
Endnote X5	Thomson ISI Research Soft , California, USA
cellSens Dimension	Olympus, Shinjuku, Japan
CeligoS S software 2.01	Cyntellect, San Diego, USA
Chromas Lite 2.01	Technelysium Pty Ltd, Helensvale, Australia
Fiji	(Schindelin <i>et al.</i> 2012)
FlowJo	Tree Star Inc., Oregon, USA
FluorChemQ SA Version 3.2.2.0	Cell Biosciences Inc., Heidelberg
FreeHand MX	Adobe Systems Incorporated, San Jose, USA
Gen5 1.11	BioTek Instruments, Inc., Bad Friedrichshall
GraphPad Prism 6	GraphPad Software, La Jolla, USA
Intas GDS	Intas Science Imaging Instruments GmbH, Göttingen
Microsoft Office 2007	Microsoft Co., Redmont, USA
MMI CellTools 4.0	Molecular Machines & Industries GmbH, Eching
Photoshop 6.0	Adobe Systems Incorporated, San Jose, USA
SDS 2.2.	Applied Biosystems, Darmstadt
Sequencing Analysis Software v5.4	Applied Biosystems, Darmstadt

### III.2 Databases and web pages

**Table 2: Databases and web pages**

Database or webpage	Uniform Resource Locator
BLAST	<a href="http://blast.ncbi.nlm.nih.gov/Blast.cgi">http://blast.ncbi.nlm.nih.gov/Blast.cgi</a>
Expression Atlas	<a href="http://www.ebi.ac.uk/gxa/home">http://www.ebi.ac.uk/gxa/home</a>
HUGO Gene Nomenclature	<a href="http://www.genenames.org/">http://www.genenames.org/</a>
MGI_3.54-Mouse Genome Informatics	<a href="http://www.informatics.jax.org/">http://www.informatics.jax.org/</a>

National Center for Biotechnology Information (NCBI)	<a href="http://www.ncbi.nlm.nih.gov/">http://www.ncbi.nlm.nih.gov/</a>
Oligo Analyzer	<a href="http://eu.idtdna.com/calc/analyzer">http://eu.idtdna.com/calc/analyzer</a>
RT Primer DB	<a href="http://medgen.ugent.be/rtprimerdb/index.php">http://medgen.ugent.be/rtprimerdb/index.php</a>
The Human Protein Atlas	<a href="http://www.proteinatlas.org">http://www.proteinatlas.org</a>
Ensembl release 64	<a href="http://www.ensembl.org/index.html">http://www.ensembl.org/index.html</a>

### III.3 Equipment

**Table 3: Equipment**

Equipment	Supplier
-80°C Freezer (MDF-U71V)	Sanyo Electric Co. Ltd., Moriguchi, Japan
Accu-jet	Brand GmbH & Co. KG, Wertheim,
Agarose gel electrophoresis chamber	Peqlab Biotechnology GmbH, Erlangen
Arium® 611 VF water purification system	Sartorius, Göttingen
Autoclave (sanoclav)	W. Krannich GmbH & Co. KG, Göttingen
Biophotometer (6131)	Eppendorf AG, Hamburg
Bunsen burner (Gasprofi 2 scs)	WLD-TEC GmbH, Göttingen
(CO <sub>2</sub> -) Incubator (6000, BBD 6220)	Kendro Laboratory Products GmbH, Hanau
Cold light source (KL 200)	Schott Glas, Mainz
Cytometer Celigo S	Cytellect, San Diego, USA
Digital Monochrome Printer P91D	Mitsubishi, Ratingen
Digital Photocamera (PowerShot G2)	Canon Deutschland GmbH, Krefeld
Exposure cassettes	Sigma-Aldrich Chemistry GmbH, Steinheim
FACS Calibur	BD Biosciences GmbH, Heidelberg
FluorChemQ Detection System	Cell Biosciences Inc., Heidelberg
Freezer (-20°C)	Liebherr GmbH, Ochshausen
Fridge (4°C)	Robert Bosch GmbH, Stuttgart
Heating block (Thermomixer)	Eppendorf AG, Hamburg
Heating stirrer (MR 3000/3001)	Heidolph Instruments, Schwabach
High-precision scales (Sartorius Basic plus)	Sartorius AG, Göttingen
Homogenizer (Micra D-1)	ART Prozess- & Labortechnik GmbH & Co. KG, Müllheim
Hybridization oven (HB-1000 Hybridizer)	UVP Inc., Upland, USA
Inverse microscope with fluorescence filter (Axiovert 25, FilterSet 43, 01, 09)	Carl Zeiss Jena GmbH, Jena

Liquid nitrogen tank	L'air liquid S.A., Paris, France
LSR II	BD Biosciences GmbH, Heidelberg
Luminometer (Synergy Mx)	BioTek Instruments, Inc., Bad Friedrichshall
Mastercycler ep gradient S	Eppendorf AG, Hamburg
Mercury-short-arc lamp(HBO 50W/AC)	OSRAM AG, Munich
Microtome (HN 40)	New Brunswick Scientific GmbH, Nürtingen,
Mini centrifuge	Carl Roth GmbH & Co. KG, Karlsruhe
MMI CellCut	Molecular Machines & Industries GmbH, Eching
Mr. Frosty™ Freezing Container	Thermo Fisher Scientific GmbH, Schwerte
Multipette	Eppendorf AG, Hamburg
One-channel pipettes	Eppendorf AG, Hamburg
Paraffin dispenser (Dispenser PAG 12)	MEDITE GmbH, Burgdorf
PCR machine (Primus HT)	MWG AG Biotech, Ebersberg
pH-meter (inoLab pH Level 1)	WTW GmbH, Vienna, Austria
Power supply for electrophoresis	Peqlab Biotechnology GmbH, Erlangen
shaking incubator	New Brunswick Scientific GmbH, Nürtingen
shaking waterbath (1083)	GFL GmbH, Burgwedel
Sequencer (ABI 3500 XL)	Thermo Fisher Scientific Inc., Waltham, USA
Stereo microscope (Stemi 2000)	Carl Zeiss Jena GmbH, Jena
Sterile bench (Euroflow class IIA)	Clean Air Techniek bv, Woerden, Netherlands
TaqMan (ABI Prism 7900HT)	Thermo Fisher Scientific Inc., Waltham, USA
Thermoprinter (DPU-414)	Eppendorf AG, Hamburg
Tissue embedding and rehydrating machine (TP 1020)	Leica Microsystems GmbH, Bensheim
Trans-Blot SD semi-dry transfer cell	Bio-Rad Laboratories GmbH, München
UV transilluminator	Intas Science Imaging Instruments GmbH, Göttingen
Vacuum pump	Schütt Labortechnik, Göttingen
Vortexer-Genie 2	Scientific Industries, Inc., Woburn, USA
Weighing scale (Sartorius Basic plus)	Sartorius AG, Göttingen
XCell4 Surelock Midi-Cell	Invitrogen GmbH, Karlsruhe

### III.4 Consumables

**Table 4: Consumables**

<b>Consumable</b>	<b>Supplier</b>
1.5 ml reaction tubes	Ochs GmbH, Bovenden/Lenglern
1.5 ml Safeseal Microtubes	Sarstedt AG & Co., Nürnberg
13 ml tubes	Sarstedt AG & Co., Nürnberg
15 ml tubes	Greiner Bio-One GmbH, Frickenhausen
2.0 ml reaction tubes	Sarstedt AG & Co., Nürnberg
24-well cell culture plate	Corning Inc., Corning, USA
384-well Optical Reaction Plate	Thermo Fisher Scientific Inc., Waltham, U.S.A.
50 ml tubes	Greiner Bio-One GmbH, Frickenhausen
6-well cell culture plate	Corning Inc., Corning, USA
96-well Assay Plate	Corning Inc., Corning, USA
96-well Optical Reaction Plate	Thermo Fisher Scientific Inc., Waltham, USA.
Balance oeco multi-function paper	inapa tecno, Hamburg
BD Discardit™ II (2,10,20 ml)	BD Biosciences GmbH, Heidelberg
BD Microfine + Demi	BD Biosciences GmbH, Heidelberg
BD Plastipak	BD Biosciences GmbH, Heidelberg
BD Plastipak 1 ml Sub-Q	BD Biosciences GmbH, Heidelberg
Blotting paper (GB 33 B003)	Heinemann Labortechnik GmbH, Duderstadt
Cell culture dishes, 35 mm, 100 mm, (Nunclon Surface)	Nunc GmbH & Co.KG, Wiesbaden
Cell culture inserts, 24 well, 8.0 µm	Corning Inc., Corning, USA
Cell culture inserts, 24 well, 0.4 µm	Corning Inc., Corning, USA
Cell scraper	Sarstedt AG & Co., Nürnberg
Combitips plus (0.2, 0.5, 2.5, 5,10 ml)	Eppendorf AG, Hamburg
Coverslips	Menzel GmbH & Co.KG, Braunschweig
Cryo Pure	Sarstedt AG & Co., Nürnberg
Cuvettes (UVette)	Carl Roth GmbH & Co. KG, Karlsruhe
Filter tips (10 µl)	Sarstedt AG & Co., Nürnberg
Filter tips (100 µl, 200 µl, 1000 µl)	Kisker Biotech GmbH & Co. KG, Steinfurt
Flow cytometry tubes	Sarstedt AG & Co., Nürnberg
Fluted filters	Sartorius AG, Göttingen
Glassware	Schott AG, Mainz
Hyperfilm ECL	Amersham Biosciences Europe GmbH, Freiburg

Microscope slides (SuperFrost Plus)	Menzel GmbH & Co.KG, Braunschweig
MMI MembraneSlides	Molecular Machines & Industries GmbH, Eching
MultiScreen <sub>HTS</sub> -HV plate	Millipore GmbH, Schwalbach am Taunus
Neubauer counting chamber	Brand GmbH & Co KG, Wertheim
Nitrocellulose membrane(Hybond ECL)	GE Healthcare Europe GmbH, Freiburg
NuPAGE Novex 4-12% Bis-Tris Midi Gel	Invitrogen GmbH, Karlsruhe
Pasteur pipettes	Brand GmbH & Co.KG, Wertheim
PCR-Reaction tubes (ThermoFast 96, nonskirted, natural domed cap strips, natural)	Sarstedt AG & Co., Nürnberg
Petri dishes	Ochs GmbH, Bovenden/Lenglern
Pipette tips (10 µl, 200 µl)	Ochs GmbH, Bovenden/Lenglern
Pipette tips (1000 µl)	Sarstedt AG & Co., Nürnberg
Pipette tips (20 µl)	Sarstedt AG & Co., Nürnberg
Protein concentrators, 20 ml, 9k MWKO	Thermo Fisher Scientific Inc., Waltham, USA
QPCR Adhesive Clear Seal	4titude Ltd., Berlin
Scalpel blade #10, #24	Aesculap AG & Co.KG, Tuttlingen
Serological pipettes (5 ml, 10 ml, 25 ml)	Sarstedt AG & Co., Nürnberg
Sterile filter	Omnilab-Krannich, Göttingen
Syringe 30, 50 ml	Terumo Medical Corp., Elkton, USA
Tissue Culture Plate 6-Well	Sarstedt AG & Co., Nürnberg
Tissue Culture Plate 24-Well	Sarstedt AG & Co., Nürnberg

### III.5 Chemicals and reagents

All standard chemicals not listed here were obtained from AppliChem GmbH, Darmstadt, Carl Roth GmbH & Co. KG, Karlsruhe, or from Sigma-Aldrich Chemistry GmbH, Steinheim.

**Table 5: Chemicals and reagents**

Chemicals and reagents	Supplier
100 bp plus and 1 kb DNA Ladder	Fermentas GmbH, St. Leon-Rot
Agarose	Bio-Budget Technologies GmbH, Krefeld
BM Purple	Roche Diagnostics GmbH, Mannheim
Boric acid	MP Biomedicals LLC, Illkirch, France
cOmplete, protease inhibitor cocktail	Roche Diagnostics GmbH, Mannheim

Deoxyribonucleotide triphosphate (dNTP)	Roche Diagnostics GmbH, Mannheim
Dithiotreitol, 100mM (DTT)	Invitrogen GmbH, Karlsruhe
DNase/Rnase-free water	GIBCO Invitrogen GmbH, Karlsruhe
Ethidium bromide (0.07 %)	inna-TRAIN-Diagnostics, Kronberg
EtOH 99 %	J.T. Baker B.V., Deventer, Netherlands
EtOH 99 % denatured	CVH Chemie-Vertrieb GmbH & Co. Hannover KG, Hannover
Formamide	Acros Organics b.v.b.a, Geel, Belgium
Glycergel mounting medium	Dako GmbH, Hamburg
Hematoxylin solution, MAYER	Medite GmbH, Burgdorf
HEPES buffer solution (1M)	GIBCO Invitrogen GmbH, Karlsruhe
I-Block	Tropix, Bedford, USA
Indo-1 AM	Thermo Fisher Scientific Inc., Waltham, USA
ionomycin	Sigma-Aldrich Chemistry GmbH, Steinheim
Matrigel, phenol red free	BD Biosciences GmbH, Heidelberg
NuPAGE MES SDS Running Buffer, 20 x	Invitrogen GmbH, Karlsruhe
PBS-Tablets	GIBCO Invitrogen GmbH, Karlsruhe
Pertex mounting medium	Medite Medizintechnik GmbH, Burgdorf
PhosStop	Roche Diagnostics GmbH, Mannheim
Pluronic F127	Thermo Fisher Scientific Inc., Waltham, USA
SeeBlue® Plus2 Pre-Stained Standard	Invitrogen GmbH, Karlsruhe
illustra Sephadex G-50 DNA Grade F	GE Healthcare Europe GmbH, Freiburg
TRIzol Reagent	Invitrogen GmbH, Karlsruhe
Xylene	J.T. Baker B.V., Deventer, Netherlands

### III.6 Ready-to-use reaction systems

**Table 6: Ready-to-use reaction systems**

Reaction system	Supplier
Amersham ECL Plus™ Western Blotting Detection Reagents	GE Healthcare Europe GmbH, Freiburg
Arcurus Paradise PLUS FFPE RNA Isolation Kit (ABI; KIT0312I)	Thermo Fisher Scientific Inc., Waltham, USA
BigDye Terminator v3.1 Cycle Sequencing Kit	Thermo Fisher Scientific Inc., Waltham, USA
Cell Proliferation ELISA, BrdU	Roche Diagnostics GmbH, Mannheim
Cell Proliferation Reagent WST-1	Roche Diagnostics GmbH, Mannheim

DeadEnd™ Colorimetric TUNEL System	Promega GmbH, Mannheim
Dual-Luciferase Reporter Assay System	Promega GmbH, Mannheim
FITC Annexin V	BD Biosciences GmbH, Heidelberg
HiPure Plasmid DNA Purification Kit	Invitrogen GmbH, Karlsruhe
High Pure PCR Cleanup Micro Kit	Roche Diagnostics GmbH, Mannheim
MicroSpin G50 Columns	Amersham Biosciences Europe GmbH, Freiburg
Pierce BCA Protein Assay Kit	Fisher Scientific GmbH, Schwerte
Platinum SYBR Green qPCR SuperMix-UDG with ROX	Invitrogen GmbH, Karlsruhe
QuantiTect PCR Probe Kit	Qiagen GmbH, Hilden
QuantiTect SYBR Green PCR	Qiagen GmbH, Hilden
Roti-Fect transfection reagent	Carl Roth GmbH & Co. KG, Karlsruhe
RNeasy Fibrous Tissue Kit	Qiagen GmbH, Hilden
SuperScriptII Reverse Transcriptase	Invitrogen GmbH, Karlsruhe
TransIT®-LT1 Transfection Reagent	Mirus Bio LLC., Madison, USA

### III.7 Buffers and solutions

Buffers and solutions were prepared using double-distilled water.

AEC chromogen, pH 5.2

30 mM acetic acid  
70 mM sodium acetate trihydrate  
16 mM 3-amino-9 ethylcarbazole  
(dissolved in dimethyl formamide)

Blotting buffer

6 % (w/v) Tris base  
3 % (w/v) glycine  
0.075 % SDS  
20 % (v/v) methanol

Boric acid, pH 5.1

0.2 M Boric acid

## III

## Material and methods

BSA/sodium azide solution	0.1 % (v/v) Tween-20 0.02 % (w/v) sodium azide 3 % (w/v) BSA in 1 x TBS
Citrate buffer, pH 3.0	10 mM sodium citrate
Citrate buffer, pH 6.0	10 mM sodium citrate
Cresol solution	0.1 % (w/v) Cresol in saturated sucrose-solution
Deoxyribonukleotidtriphosphate (dNTP)-mix	10 mM dATP 10 mM dTTP 10 mM dGTP 10 mM dCTP
DNase I buffer	40 mM Tris-HCl (pH 7.9) 10 mM NaCl 6 mM MgCl <sub>2</sub> 10 mM CaCl <sub>2</sub>
Eosin	1 % (w/v) eosin y (water soluble) 80 % (v/v) ethanol
Krebs Ringer solution	10 mM HEPES (pH 7.0) 140 mM NaCl 4 mM KCl 1 mM MgCl <sub>2</sub> 1 mM CaCl <sub>2</sub> 10 mM glucose

## III

## Material and methods

Krebs Ringer solution (Ca <sup>2+</sup> -free)	10 mM HEPES (pH 7.0) 140 mM NaCl 4 mM KCl 1 mM MgCl <sub>2</sub> 0.5 mM EGTA 10 mM glucose
Modified RIPA buffer	50 mM Tris/HCl pH 7.4 1% NP-40 0.25 % Na-Deoxycholat 150 mM NaCl 1 mM EDTA 1 protease inhibitor cocktail tablet per 10ml 1 PhosSTOP tablet per 10ml
Paraformaldehyde solution (PFA)	4 % (w/v) Paraformaldehyde in 1 x PBS
Phosphate-buffered sodium chloride-solution (PBS), 10 x, pH 7.4	1.4 M NaCl 27 mM KCl 15 mM KH <sub>2</sub> PO <sub>4</sub> 65 mM Na <sub>2</sub> HPO <sub>4</sub>
PBST (washing buffer)	0.1 % (v/v) Tween-20 in 1x PBS
Proteinase K buffer	50 mM Tris/HCl pH 8.0 5 mM EDTA
SDS loading buffer, 6 x in upper gel buffer	35 % (v/v) glycerol 9 % (w/v) SDS 8.5 % (w/v) DTT 0.1 % (w/v) bromophenol blue

STE-buffer	50 mM Tris/HCl pH 8.0 100 mM NaCl 1 mM EDTA 1 % (w/v) SDS
Tris-EDTA buffer pH 9,0 (TE)	10 mM Tris 1 mM EDTA
Tris-boric acid-EDTA-solution, 10 x (TBE)	890 mM Tris/HCl pH 8.0 730 mM boric acid 12.5 mM EDTA
Tris-buffered sodium chloride-solution, 10 x (TBS)	0.5 M Tris/HCl pH 7.4 1.5 M NaCl
TBST	0.1 % (v/v) Tween-20 in 1 x TBS
Upper gel buffer	6 % (w/v) Tris base pH 6.8 4 % (v/v) SDS

## III.8 Media

### III.8.1 Media for bacteria culture

For cultivation of bacteria (*E. coli* DH5 $\alpha$ , Invitrogen GmbH, Karlsruhe) lysogeny broth-medium ((LB-medium; 1 % (w/v) tryptone, 0.5 % (w/v) yeast extract, 1 % (w/v), NaCl; pH 7.0)) was used. LB-medium was prepared with double-distilled water, autoclaved and stored at 4°C. Selection for adequate resistance genes was achieved by addition of 100  $\mu$ g/ml ampicillin (stock concentration: 100 mg/ml; Carl Roth GmbH & Co. KG, Karlsruhe) or 50  $\mu$ g/ml kanamycin (stock concentration: 10 mg/ml, Sigma-Aldrich Chemistry GmbH, Steinheim)

### III.8.2 Agar plates

For preparation of LB-agar plates 1.5 % (w/v) agar was added to LB-medium and autoclaved. After cooling down to 55°C the adequate antibiotic (100 µg/ml ampicillin or 50 µg/ml kanamycin) was added and LB-agar was plated in 10 cm Petri dishes. Agar plates were stored at 4°C in sterile plastic bags.

### III.8.3 Media and reagents for cultivation of eukaryotic cell lines

All Media and supplements including antibiotics used for selection of resistant clones that were used for cultivation of eukaryotic cell lines are listed in Table 7. For the preparation of Ca<sup>2+</sup>-chelexed and heat-inactivated FCS, 50 ml FCS were heat-inactivated by incubation for 30 min at 56°C. Afterwards, 10 g Chelex 100 were added and stirred for 60 min at room temperature (RT) on a magnetic stirrer to eliminate Ca<sup>2+</sup>-ions. Subsequently, the FCS was sterile filtered with an UV-sterilized fluted filter and additionally with a 0.2 µm sterile filter and stored at -20°C.

**Table 7: Cell culture media and supplements for eukaryotic cell lines**

Medium or reagent	Supplier
154CF Medium	Gibco, Invitrogen GmbH, Karlsruhe
Accutase	PAA Laboratories GmbH, Pasching
Chelex 100 Resin Chelating Ion Exchanger Resin	BioRad Laboratories Inc., Hercules, USA
Dulbecco's Modified Eagle Medium (DMEM)	Gibco, Invitrogen GmbH, Karlsruhe
Fetal calf serum (FCS)	Gibco, Invitrogen GmbH, Karlsruhe
G 418 disulfate salt solution (50 mg/ml)	Sigma-Aldrich Chemistry GmbH, Steinheim
HEPES (1M)	Gibco, Invitrogen GmbH, Karlsruhe
Horse serum	Gibco, Invitrogen GmbH, Karlsruhe
RPMI 1640 Medium	Gibco, Invitrogen GmbH, Karlsruhe
Penicillin (10.000 U/ml)/Streptomycin (10 mg/ml) (P/S)	PAN Biotech GmbH, Aidenbach
Puromycin dihydrochloride (10 mg/ml)	Sigma-Aldrich Chemistry GmbH, Steinheim
S.O.C. medium	Invitrogen GmbH, Karlsruhe

Trypsin/EDTA and TrypLE Express	Gibco, Invitrogen GmbH, Karlsruhe
---------------------------------	-----------------------------------

## III.9 Biological material

### III.9.1 Bacterial strain

For transformation and amplification of plasmid DNA the *E. coli* strain DH5 $\alpha$  was used.

### III.9.2 Eukaryotic cell lines

Eukaryotic cell lines B9, C5N, NIH/3T3, NIH/3T3-Wnt5a, HEK-293 and Wnt-3A L and L cells were cultured in Dulbecco's Modified Eagle Medium (DMEM) supplemented with 10 % FCS and 1 % penicillin/streptomycin (P/S). The cell line ASZ001 was cultured in medium 154CF containing 0.05 M CaCl<sub>2</sub>, 2 % heat-inactivated and Ca<sup>2+</sup>-chelexed FCS and 1 % P/S. The respective stably transfected cell lines were cultured in the presence of an adequate antibiotic (see Table 8).

**Table 8: Eukaryotic cell lines**

1: Designation of cell line; 2: Origin of cell line; 3: Culture medium; 4: Source of cell line/reference; Abbreviations: BCC: basal cell carcinoma; FCS: fetal calf serum; P/S: penicillin/streptomycin; DMEM: Dulbecco's Modified Eagle Medium; Wnt3a: wingless-related MMTV integration site 3A;

1	2	3	4
ASZ001	murine BCC	154CF, 2 % chelexed FCS, 1 % P/S	(So <i>et al.</i> 2006)
B9	murine adult fibroblasts	DMEM, 10% FCS, 1 % P/S	F. Nitzki, dissertation, 2008
C5N	murine keratinocytes	DMEM (lacking pyruvate), 10% FCS, 1 % P/S	(Kulesz-Martin <i>et al.</i> 1983)
HEK-293	human embryonic kidney	DMEM, 10% FCS, 1 % P/S	ATCC LGC Promochem, Wesel; CRL-1573
L929	murine fibroblast	RPMI 1640 10% FCS, 1 % P/S	85011425, Sigma Aldrich Chemistry GmbH, Steinheim

## III

## Material and methods

L cells	murine fibroblasts	DMEM, 10% FCS, 1 % P/S	ATCC® CRL-2648™
Wnt-3A L cells	murine fibroblasts stably overexpressing Wnt3a	DMEM, 10% FCS, 1 % P/S, 0.4 µg/ml G418	ATCC® CRL-2647™
NIH/3T3	murine embryonic fibroblasts	DMEM, 10% FCS, 1 % P/S	ATCC LGC Promochem, Wesel; CRL-1658
NIH/3T3-Wnt5a	see above, stably overexpressing Wnt5a	DMEM, 10% FCS, 1 % P/S, 0.4 µg/ml G418	(Kispert <i>et al.</i> 1998)
Platenium-E	retroviral packaging cell line	DMEM, 10% FCS), 1 µg/mL puromycin, 10µg/mL blasticidin, 1% P/S	RV-101, cell biolabs, Inc.

### III.9.3 Mouse lines

**Table 9: Mouse lines**

1: Designation of mouse line; 2: strain background; 3: Genetic modification and use; 4: Source

1	2	3	4
nude mice	outbred	athymic; allograft	animal keeping
<i>Ptch<sup>flax</sup></i>	C57BL/6N, 129/Sv	Floxed exons 8 and 9 of the murine <i>Ptch</i> gene; for conditional <i>Ptch</i> gene deletion	(Uhmann <i>et al.</i> 2007)
<i>ROSA26-CreERT2</i>	129Sv	ubiquitous tamoxifen-inducible CreERT2-recombinase expression under control of ROSA26 promoter	generous gift from A. Berns, Netherlands
<i>Wif1<sup>-/-</sup></i>	C57BL/6, 129/Sv	Tau-LacZ reporter cassette integrated in Exon 1 causes a frameshift and thereby abrogates Wif1 expression	(Kansara <i>et al.</i> 2009)

All experiments using animals were performed in compliance with all legal and ethical requirements.

### III.10 Plasmids

Plasmids listed in Table 9 were either used for transfection, nucleofection or transduction of eukaryotic cell lines.

**Table 10: Plasmids**

1: Designation of vector; 2: Purpose; 3: Designation of vector backbone if different from 1; 4: Supplier of vector backbone or reference (if applicable);

1	2	3	4
<i>pCR3.1</i>	Dual-Luciferase assay		Invitrogen GmbH, Karlsruhe
<i>pCI-neo-<math>\beta</math>-cateninS33Y</i>	Dual-Luciferase assay	<i>pCI-neo</i>	(Morin <i>et al.</i> 1997)
<i>pcDNA3-Wif1</i>	Wif1 overexpression	pcDNA3	(Becker 2011)
<i>pGFPmax</i>	Nucleofection control		Lonza Group AG, Basel, Switzerland
<i>pMSCVpuro</i>	Wif1 overexpression control plasmid		Clontech Laboratories, Inc.
<i>pMSCVpuro-Wif1</i>	Wif1 overexpression	<i>pMSCVpuro</i>	this thesis
<i>pRL-CMV</i>	Dual-Luciferase assay		Promega GmbH, Mannheim
<i>SuperTOPFlash</i>	Dual-Luciferase assay	<i>pTA-Luc</i>	(Korinek <i>et al.</i> 1997)
<i>SuperFOPFlash</i>	Dual-Luciferase assay	<i>pTA-Luc</i>	(Korinek <i>et al.</i> 1997)
<i>pEGFP-N1</i>	Transfection efficiency control		Takara Bio Europe/Clontech, Saint-Germain-en-Laye, France

### III.11 Synthetic oligonucleotides

Synthetic DNA-oligonucleotides were ordered from Eurofins MWG Operon, Ebersberg. The stock concentration of DNA-oligonucleotides was set to 100  $\mu$ M using RNase- and DNase-free water. For all PCR reactions a 10  $\mu$ M solution was used.

#### III.11.1 Synthetic DNA-oligonucleotides for qRT-PCR

Since embryos express of a broad range of genes, cDNAs made from mouse embryos of different ages (see Table 11) were used a) to establish the qRT-PCR assay for the expression analysis of a specific gene and b) to set up the standard curve to calculate the expression level of the respective gene. The age of an embryo used for the synthesis of cDNA was chosen according to the expression profile of respective mRNA reported in the database MGI and Expression Atlas.

**Table 11: Oligonucleotides for qRT-PCR analyses**

1: Designation of analysed transcript; 2: Designation of oligonucleotides; 3: Oligonucleotide sequence (5'→3'); 4: control cDNAs, 10.5, 12.5, 13.5: Age of mouse embryos in days post coitum (dpc) for generation of control cDNA, BCC: Basal Cell Carcinoma, HEK LiCl: HEK-293 treated for 12 h with 50 nM LiCl; 5: References; 6: Supplier of utilized SYBR Green (determining program used, see. III.14.2.3).

1	2	3	4	5	6
18S	18S forw 18S rev2	CGCAAATTACCCACTCCCG TTCCAATTACAGGGCCTCGAA	13.5	(Nitzki <i>et al.</i> 2010)	Invitrogen, Qiagen
Axin2	mAxin2-F mAxin2-R	TGTGAGATCCACGGAAACAGCT TGTCCTCATGGACATGGAATC	12.5	(Nitzki <i>et al.</i> 2010)	Qiagen
AXIN2	hAXIN2-F hAXIN2-R	GCCAACGACAGTGAGATATCC CTCGAGATCAGCTCAGCTGCA	HEK LiCl	this thesis	Invitrogen
Cdh1	mCdh1-F3 mCdh1-R3	AGGAGCTGGAGCCTGAGTC CGAAAAGAAGGCTGTCTTG	13.5	this thesis	Invitrogen
Cdh2	Cdh2-F Cdh2-R	TTACAGCGCAGTCTTACCGA CGTCCACCTTGAAATCTGCT	10.5	this thesis	Invitrogen
c-Myc	mc-MycF mc-MycR	TAGTGCTGCATGAGGAGAC CTCCACAGACACCACATCA	12.5	working group Hahn, F. Nitzki	Qiagen
Fn1	Fn1-F Fn1-R	GGTCAGTCCTACAAGATTGGC TCCAATCCTATAGGATGTCCG	10.5	this thesis	Invitrogen
Gli1	mGli1-tq-f mGli1-tq-r	TACATGCTGGTGGTGACATG ACCGAAGGTGCGTCTTGAGG	12.5	working group Hahn, F. Nitzki	Qiagen
Hprt	mHprt-Fw-Q mHprt-Rev-Q	AGCCCCAAAATGGTTAAGGTTGC TTGCAGATTCAACTTGCGCTCAT	13.5	working group Hahn, B. Linder	Invitrogen, Qiagen
Ivl	Ivl-1-F1 Ivl-1-R1	CCTCCTGTGAGTTTGTGGTCT CTGAGGATATGATCTGGAGAAC	BCC	working group Hahn, B. Linder	Invitrogen
K1	K1-F K1-R	TCAACGTTGAGGTTGACCCTC ACCTTCCTTCTGAGGATGCTG	BCC	(Nitzki <i>et al.</i> 2010)	Qiagen
K10	K10-F K10-R	GGATGCTGAAGAGTGGTTCAA TCTGTTTCTGCCAAGGAGGCT	BCC	(Nitzki <i>et al.</i> 2010)	Qiagen
Lor	Lor-F1 Lor-R1	CACTCATCTTCCCTGGTGCTTC GTCTTTCCACAACCCACAGGAG	BCC	working group Hahn, B. Linder	Invitrogen
Tbp	mTBP-Q-Fwd mTBP-Q-Rev	CACCAATGACTCCTATGACCCCTA CAGTTGTCCGTGGCTCTCTTATTC	13.5	working group Hahn, B. Linder	Invitrogen, Qiagen
Tgm	Tgm1-F Tgm1-R	GCAGTGGTGTAATGCAGCTGG ATGAGGAGCTCAAGGGCAATGC	BCC	working group Hahn, S. König	Qiagen
Wif1	mWif1-F mWif1-R	TCCTGTCAATATCCAATCCATGAA CTGATGCCTTGTGAGGCACT	12.5	working group Hahn, S. König	Invitrogen
WIF1	hWIF1-F2 hWIF1-R2	ACAACCCTGTGCAATGGAG GTGTCTTCCATGCCAACCTT	Colo 320 HSR	this thesis	Qiagen

### III.11.2 Synthetic DNA-oligonucleotides for cloning

The DNA-oligonucleotides listed in Table 12 were used for the cloning of a *mWif1* expression vector.

**Table 12: Oligonucleotides for cloning**

1: Designation of synthetic DNA-oligonucleotide; 2: nucleotide sequence of oligonucleotides (5'→3'); 3: Reference.

1	2	3
mWif1-BgIII-F	AGTGCCAGATCTGCCGCCACCATGGCTCGG AGAAGAGCCT	this thesis
mWif1-HpaI-R	CGTAACTCACCAGATGTAATTGGATTC	this thesis

### III.11.3 Synthetic DNA-oligonucleotides for sequencing

The primers listed in Table 13 were used for sequencing of the *mWif1* insert cloned into *pMSCVpuro* expression vector.

**Table 13: Oligonucleotides for sequencing of *mWif1***

1: Designation of oligonucleotide; 2: Nucleotide sequence of oligonucleotides; 3:Reference.

1	2	3
<i>mWif1-F</i>	TCCTGTCAATATCCACTCCATGAA	König 2012
<i>mWif1-intraF1</i>	AAGGAGACCTGTGCTCTAAGC	this thesis
<i>mWif1-R</i>	CTGATGCCTTGTGAGGCACT	König 2012
<i>mWif1-seq-rv1</i>	CCTCCATTTCCGGCAGGGTTGG	this thesis
<i>mWif1-tq-F</i>	CGCCCATCAGGCTAGAGTGC	Ecke 2008
<i>mWif1-tq-R</i>	GACAGGAATGGCTGGCATTCT	Ecke 2008

### III.11.4 Synthetic DNA-oligonucleotides for genotyping

**Table 14: Oligonucleotides for genotyping**

1: Designation of analyzed allele; 2: Designation of oligonucleotide nucleotide; 3: Sequence of oligonucleotides; 4: Reference.

1	2	3	4
<i>Ptch wt</i>	mPTCNx_f mPTCwt_r.2	TGGTAATTCTGGGCTCCCGT ACACAACAGGGTGGAGACCACT	(Uhmann <i>et al.</i> 2007)
<i>Ptch flox</i>	mPTCNx_f mPTCNx_r	TGGTAATTCTGGGCTCCCGT CCGGTAGAATTAGCTTGAAGTTCCT	(Uhmann <i>et al.</i> 2007)

<i>Ptch del</i>	Exon7-F neo-R	AGGAAGTATATGCATTGGCAGGAG GCATCAGAGCAGCCGATTGTCTG	(Uhmann <i>et al.</i> 2007)
<i>CreERT2</i>	Ella-Cre-F Ella-Cre-R	CCAGGCTAAGTGCCCTTCTCTACA AATGCTTCTGTCCGTTTGCCGGT	(Uhmann <i>et al.</i> 2007)
<i>Wif1 wt</i>	mWif1-geno-F mWif1-wt-R	CGAGAACTTCACAAGCAGCACAGG CCTGTTACAAATCTGCAGTCAGGA	(Kansara <i>et al.</i> 2009)
<i>Wif1 knockout allele</i>	mWif1-geno-F mWif1-TauR2	CGAGAACTTCACAAGCAGCACAGG CTGGAATCCGGGTGGCGTTGGC	(Kansara <i>et al.</i> 2009)

### III.12 Enzymes

All enzymes were used with appropriate buffers and according to manufacturer`s protocol.

**Table 15: Enzymes**

Enzyme	Supplier
<i>Bgl</i> II	Invitrogen GmbH, Karlsruhe
<i>Hind</i> III	Invitrogen GmbH, Karlsruhe
DNase I	Qiagen GmbH, Hilden
Phusion DNA Polymerase	New England Biolabs GmbH, Frankfurt am Main
Proteinase K	Carl Roth GmbH & Co. KG, Karlsruhe
RNase A	Carl Roth GmbH & Co. KG, Karlsruhe
RQ1-DNase	Promega GmbH, Mannheim
SuperScriptII Reverse Transcriptase	Invitrogen GmbH, Karlsruhe
T4 DNA Ligase	Invitrogen GmbH, Karlsruhe
Taq DNA Polymerase	Molzym GmbH Co.KG, Bremen

## III.13 Antibodies

### III.13.1 Primary antibodies

**Table 16: Primary antibodies for immunohistochemistry**

1: Designation; 2: Source; 3: Dilution; 4: Antigen retrieval; 5: Supplier.

1	2	3	4	5
$\beta$ -catenin (610153)	mouse, polyclonal	1:100	TE, pH 9.0, microwave	Becton Dickinson GmbH, Heidelberg
CD34 antibody (MEC14.7)	rat, polyclonal	1:1000	boric acid, pH 5.1, 30 min 60°C	Bio-Rad Laboratories GmbH, München
E-cadherin (610181)	mouse, polyclonal	1:200	TE, pH 9.0, microwave	Becton Dickinson GmbH, Heidelberg
F4/80 antibody Cl:A3-1	rat, monoclonal	1:100	-	Bio-Rad Laboratories GmbH, München
Ki67 antibody (556003)	rabbit monoclonal	1:50	Citrate, pH 6.0, microwave	Becton Dickinson GmbH, Heidelberg
p53 Protein (CM5) Antibody	rabbit, polyclonal	1:500	TE, pH 9.0, microwave	Leica Biosystems Nussloch GmbH, Nussloch
Anti-Acta2 1A4 (Sma)	mouse, monoclonal	1:50	-	mous, monoclonal
Anti-WIF1 antibody [EPR9385] (ab155101)	rabbit, polyclonal	1:400	TE, pH 9.0, microwave	Abcam plc., Cambridge, UK

**Table 17: Primary antibodies for Western blot**

Designation	Source	Dilution	Supplier
Akt (610861)	mouse, polyclonal	1:1000	Becton Dickinson GmbH, Heidelberg
Phospho-Akt (Ser473) Antibody	rabbit, polyclonal	1:1000	New England Biolabs GmbH, Frankfurt am Main
anti-Bcl-2, Clone: 6C8	rabbit, polyclonal	1:200	Becton Dickinson GmbH, Heidelberg
$\beta$ -catenin (610153)	mouse, polyclonal	1:1000	Becton Dickinson GmbH, Heidelberg
Phospho-CaMKII (Thr286) Antibody	rabbit, polyclonal	1:1000	New England Biolabs GmbH, Frankfurt am Main
Caspase-3	rabbit, polyclonal	1:1000	New England Biolabs GmbH, Frankfurt am Main
cyclin E (M20)	rabbit, polyclonal	1:200	Santa Cruz Biotechnology, Inc. Heidelberg

E-cadherin	mouse, polyclonal	1:2500	Becton Dickinson GmbH, Heidelberg
Phospho-SAPK/JNK (Thr183/Tyr185) Antibody	rabbit, polyclonal	1:1000	New England Biolabs GmbH, Frankfurt am Main
Phospho-c-Jun (Ser63) II Antibody	rabbit, polyclonal	1:1000	New England Biolabs GmbH, Frankfurt am Main
Anti MAP Kinase (ERK1, ERK2) antibody	rabbit, polyclonal	1:1000	Sigma Aldrich Chemistry GmbH, Steinheim
p44/42 MAPK (Erk1/2) Antibody	rabbit, polyclonal	1:1000	New England Biolabs GmbH, Frankfurt am Main
HSC 70 (B-6): sc-7298	mouse, monoclonal	1:10000	Santa Cruz Biotechnology, Inc. Heidelberg
Phospho-PKC (pan) ( $\beta$ II Ser660) Antibody	rabbit, polyclonal	1:1000	New England Biolabs GmbH, Frankfurt am Main
S6 Ribosomal Protein (54D2)	mouse, monoclonal	1:1000	New England Biolabs GmbH, Frankfurt am Main
Phospho-S6 Ribosomal Protein (Ser240/244)	rabbit, monoclonal	1:1000	New England Biolabs GmbH, Frankfurt am Main
Anti-Acta2 1A4 (Sma)	mouse, monoclonal	1:50	Beckman Coulter Inc., Brea, USA
Syndecan 2 antibody	rabbit, polyclonal	1:100	Biorbyt Ltd., Cambridge, UK
Anti-WIF1 antibody [EPR9385] (ab155101)	rabbit, polyclonal	1:1000	Abcam plc., Cambridge, UK

### III.13.2 Secondary antibodies

**Table 18: Secondary antibodies**

1: Designation; 2: Source; 3: Specificity; 4: Application; 5: Supplier.

1	2	3	4	5
ECL Anti-Mouse IgG, Horseradish Peroxidase- Linked Species-Specific Whole Antibody	sheep	mouse	Western blot	Amersham Biosciences Europe GmbH, Freiburg
Anti-rabbit IgG (whole molecule) peroxidase conjugate	goat	rabbit	Western blot	Sigma Aldrich Chemistry GmbH, Steinheim
EnVision™/HRP, Rabbit/Mouse (ENV)	goat	rabbit, mouse	IHC	Dako GmbH, Hamburg

Anti-Rabbit Immunoglobulins/AP (D 0487)	goat	rabbit	IHC	Dako GmbH, Hamburg
donkey anti-goat IgG (H+L) (clone: pAK)-HRPO	donkey	goat	IHC	Dianova GmbH, Hamburg
Biotinylated Rabbit Anti-Rat IgG Antibody (BA-4001)	rabbit	rat	IHC	Biozol Diagnostica Vertrieb GmbH, Eching
Streptavidin/HRP (P0397)			IHC	Dako GmbH, Hamburg

### III.14 Molecular biological methods

All subsequently described methods are standard procedures that have been described elsewhere.

#### III.14.1 Isolation of nucleic acids

##### III.14.1.1 Isolation of plasmid DNA from bacteria

For small- and medium-scale isolation of plasmid DNA from bacteria the HiPure Plasmid DNA Purification Kit was used according to manufacturer's instructions.

##### III.14.1.2 Isopropanol/ethanol precipitation of nucleic acids

2 volumes of 100% ethanol or alternatively an equal volume of isopropanol were added to the nucleic acid solution, thoroughly mixed and precipitated overnight at -20°C. Then, solution was centrifuged for 30 min at 16000 x g and 4°C. The pellet was washed twice with 70 % EtOH for 10 min, 4°C and 16000 x g, air dried and dissolved in DNase/RNase-free water and the DNA/RNA concentration was measured via photometer (Eppendorf).

### **III.14.1.3 Isolation of total RNA from embryonic tissue**

To isolate total RNA from embryos tissue was minced with a scalpel blade, homogenized 60 sec in 1 ml Trizol on ice, incubated for 5 min at room temperature (RT) and mixed with 200  $\mu$ l chloroform. The mixtures were vortexed, incubated for 3 min at RT and centrifuged for 10 min at 4°C and 800 x g. Afterwards, the upper phase was precipitated with 500  $\mu$ l isopropanol overnight at -20°C and centrifuged for 30 min at 16000 x g and 4°C. The pellet was washed twice with 70 % EtOH for 10 min, 4°C and 16000 x g, air dried and dissolved in RNase-free water and the RNA concentration was measured via photometer (Eppendorf).

### **III.14.1.4 Isolation of total RNA from murine tissue**

RNA from skin samples was isolated using the RNeasy Fibrous Tissue Kit (Qiagen) following the manufacturer's instructions. Subsequently, the samples were incubated with DNase I (Qiagen). For this purpose, 10 % (v/v) RDD-buffer (supplied with DNase I) and 0.14 U/ $\mu$ l DNase I were added to the RNA, incubated 1 h at 37°C and then for 5 min at 65°C. RNA was precipitated using 99% EtOH overnight at -20°C, centrifuged at 16000 x g for 35 min and washed with 70 % EtOH. The pellet was dissolved in 20  $\mu$ l RNase-free water and the RNA concentration was measured using a photometer (Eppendorf).

### **III.14.1.5 Isolation of total RNA from cell culture**

Cells were rinsed with 1 x PBS and detached in 1 ml TRIzol by pipetting. To avoid RNA degradation the subsequent steps were performed on ice, unless stated otherwise. Samples were vortexed for 2 min and then incubated for 5 min at RT. Subsequently, 200  $\mu$ l of chloroform were added followed by vortexing for 15 sec and an incubation step for 3 min at RT. Afterwards, the mixture was centrifuged for 10 min at 6000 x g and 4°C. The upper phase

containing the RNA was transferred into a new 1.5 ml E-cup containing 1 ml isopropyl alcohol, inverted and precipitated overnight at -20°C. Subsequently, the mixture was centrifuged for 30 min at 10000 x g and 4°C. The supernatant was discarded and the remaining pellet was washed with 1 ml 70 % EtOH (-20°C) by centrifugation for 10 min at 10000 x g and 4°C. Afterwards, supernatant was removed and the pellet was air-dried at RT. Subsequently, the pellet was dissolved in 20 µl RNase-free H<sub>2</sub>O for 5-10 min at 56°C. The RNA concentration was measured using a photometer (Eppendorf).

#### **III.14.1.6 Laser microdissection**

For the microdissection 10 µm paraffin sections were cut using a microtome, transferred to MMI membrane slides, dried for 30 min at 37°C and frozen at -80°C. After thawing, sections were deparaffinized with xylene and rehydrated using descending ethanol series. To stain the nuclei the sections were incubated in hemalaun solution and 0.1% NaHCO<sub>3</sub> solution was added. After the staining reaction sections were dehydrated by ascending ethanol series and transferred in xylene. Laser microdissection was subsequently performed using MMI CellCut and MMI CellTools software and RNA was isolated with Arcturus Paradise PLUS FFPE RNA Isolation Kit according to the manufacturer`s protocol.

#### **III.14.1.7 Photometric quantification of nucleic acids**

1 µl of sample DNA or RNA was dissolved in 99 µl water (1:100 dilution) and transferred into a cuvette. The concentration of nucleic acids was measured using a photometer at a wavelength of 260nm to quantify the DNA/RNA and at a wavelength of 280 nm to determine the purity of the sample. Pure DNA or RNA sample have a 260/280 ratio of 1.8 and 2.0, respectively, and are relatively free from protein contamination. DNA or RNA concentrations can be estimated by measuring the absorbance at 260nm ( $A_{260}$ ), adjusting the

$A_{260}$  measurement for turbidity (measured by absorbance at 320nm), multiplying by the dilution factor, and using the relationship that an  $A_{260}$  of 1.0 equates 50  $\mu\text{g/ml}$  pure DNA or  $A_{260}$  of 1.0 equates 40  $\mu\text{g/ml}$  pure RNA. The concentration thus can be calculated according to the following formula:

concentration ( $\mu\text{g/ml}$ ) = ( $A_{260}$  reading –  $A_{320}$  reading)  $\times$  dilution factor  $\times$  50 (or 40)  $\mu\text{g/ml}$ .

### **III.14.2 Polymerase chain reaction**

#### **III.14.2.1 Reverse transcription**

Reverse transcription of RNA was performed in a final volume of 20  $\mu\text{l}$ . 250 ng hexamers were added to 2  $\mu\text{g}$  total RNA and the mixture was incubated for 10 min at 70°C. Afterwards, 1  $\times$  1<sup>st</sup> strand buffer (Invitrogen), 10mM DTT (Invitrogen) and 0.5mM dNTPs were added and the mixture was incubated at 25°C for 10 min and at 42°C for 2 min. Subsequently, 1  $\mu\text{l}$  (200 U/ $\mu\text{l}$ ) SuperScript II Reverse Transcriptase (Invitrogen) was added and mixtures were incubated for 1 h at 42°C, followed by incubation at 70°C for 10 min. The efficiency of the reverse transcription is empirically 50%, thus resulting in 1  $\mu\text{g}$  cDNA when 2  $\mu\text{g}$  RNA is reversely transcribed.

#### **III.14.2.2 Polymerase chain reaction of cDNA**

The amplification of cDNA in reaction volumes of 10-20  $\mu\text{l}$  was performed with the following reagents and final concentrations:

10-100 ng template-cDNA  
 0.5  $\mu$ M sequence-specific forward-DNA-oligonucleotides  
 0.5  $\mu$ M sequence-specific reverse-DNA-oligonucleotides  
 0.2 mM dNTP-mix  
 1 % (v/v) N.N.-dimethyl sulfoxide (DMSO)  
 10 % (v/v) cresol solution  
 1 x polymerase-buffer  
 0.1 U Taq-polymerase (Molzym)

PCR-conditions varied depending on utilized DNA-oligonucleotides and amplified fragment sizes. Usually the following conditions were applied:

5 min	95°C	} 27 cycles
30 sec	95°C	
1 min	58°C	
1 min	72°C	
5 min	72°C	
$\infty$	8°C	

The results were visualized by agarose gel electrophoresis.

### III.14.2.3 Quantitative real-time PCR (qRT-PCR)

The expression levels of different genes in allografts and BCCs were measured by means of qRT-PCR using SYBR Green (SYBR Green I, Invitrogen or QuantiTect SYBR Green, Qiagen). Genes analyzed were *Axin2*, c-myelocytomatosis oncogene (*c-Myc*), *cadherin 1* and *2* (*Cdh1* and *2*), *fibronectin 1* (*Fn1*), Glioma-associated oncogene family member *1* (*Gli1*), *keratin 1* and *10* (*K1* and *K10*), *involucrin* (*Ivl*), *loricrin* (*Lor*), and *Wnt inhibitory factor-1* (*Wif1*). The expression of these genes was measured using 5 ng cDNA derived from allografts and human or murine BCC samples. For normalization the expression of the *hypoxanthine guanine phosphoribosyl transferase* (*Hprt*) and *TATA box binding protein* (*Tbp*) was measured in 5 ng cDNA. Alternatively, the expression of *18S rRNA* in 16 pg cDNA of each sample was measured. All oligonucleotides used are listed in

Table 11. For qRT-PCR analyses SYBR Green from Invitrogen or Qiagen was used at the following conditions.

Qiagen:      50°C for 2 min  
              95°C for 15 min  
              95°C for 15 sec } 40 cycles  
              60°C for 30 sec }  
              72°C for 30 sec }

Invitrogen: 50°C for 2 min  
              94°C for 2 min  
              94°C for 15 sec } 40 cycles  
              60°C for 1 min }

For both reactions the following reagents were used in a total volume of 10 µl:

2.5 ng template-cDNA  
0.4 µM sequence-specific forward-DNA-oligonucleotides  
0.4 µM sequence-specific reverse-DNA-oligonucleotides  
1 x SYBR Green master mix (containing HotStar*Taq* DNA Polymerase [Qiagen] or Platinum *Taq* DNA Polymerase [Invitrogen], SYBR Green PCR Buffer, dNTP mix, SYBR Green dye and ROX dye)

As data were analyzed by the standard curve method a standard curve with cDNA was compiled for each measurement. For this purpose, a series of seven 1:5 dilutions (S1-S7) was set up and amplified for each analysis. cDNA with a concentration of 10 ng/µl for S1 from mouse BCCs, embryos isolated at either 13.5, 12.5 or 10.5 days post coitum (dpc) or HEK-293 cells treated with LiCl was used (see Table 11). The ABI Prism 7900HT Sequence Detection System was used for all qRT-PCR analyses. Each sample was measured in a reaction volume of 10 µl in triplicates.

### **III.14.2.3.1 Data analysis using the standard curve method**

The results were analyzed using SDS 2.2.1 (Applied Biosystems) and Microsoft EXCEL (Microsoft Co) softwares. The standard was set up by a serial 1:5 dilution. For correct analysis the amplification curve ought to be in the exponential phase of the reaction when the Ct was achieved. Based on the determined values of the standard curve a standard line was compiled by plotting the logarithm of the quantity of cDNA against the Ct-value for each dilution. Thus, the standard line follows the equation  $y = mx + b$ . With this equation the expression level of each analyzed gene was determined in each sample. Each sample was normalized to the endogenous control (*Hprt*, *Tbp*, or *18S rRNA*, respectively).

### **III.14.3 Cloning techniques**

#### **III.14.3.1 Restriction hydrolysis**

Restriction hydrolyses of DNA were performed in volumes of 10 µl at 37°C for 2 h. 1 µg DNA was hydrolyzed with 3 units (U) of adequate restriction endonuclease. If possible, simultaneous hydrolysis of a DNA sample with two different enzymes was performed using a buffer ensuring optimal conditions for both enzymes. Alternatively, a serial restriction hydrolysis was performed. For this purpose, the DNA sample was first hydrolyzed for 1h at 37°C using the first restriction endonuclease that has the lowest salt concentration in its recommended buffer. Subsequently, salt concentration was adjusted for the second reaction. Then, the second restriction endonuclease was added and incubated for 1h at 37°C. Restriction hydrolysis was stopped by heat-inactivation if applicable.

### III.14.3.2 Isolation of DNA fragments from agarose gels

DNA fragments from agarose gels were excised under UV-light using a sterile scalpel blade and were extracted from the gel using the High Pure PCR Cleanup Micro Kit according to the manufacturer's instructions.

### III.14.3.3 Ligation

Ligation of DNA fragments was performed using T4 DNA Ligase as it is capable of catalyzing the ligation of two DNA double-strands in the presence of ATP between the 5'-phosphate and the 3'-hydroxyl groups of adjacent nucleotides in either a cohesive-ended or blunt-ended configuration. Ligation was conducted using 1 x ligation buffer and 4 U T4 DNA ligase (Invitrogen) in a total reaction volume of 20  $\mu$ l. The amount of insert per ng of vector used was estimated from the gel and calculated according to the formula:

$$\text{ng of insert} \approx \frac{(\text{length of insert}) \times (\text{ng of vector})}{(\text{length of vector})} \times \text{molar ratio} \left( \frac{\text{insert}}{\text{vector}} \right)$$

The molar ratio of insert to vector (100-200 ng) was set 3 to 1.

### III.14.3.4 DNA-sequencing

For cycle-sequencing of *pMSCVpuro-mWif1* 500 ng of the plasmid, 1  $\mu$ M primer (see Table 13), 1 x Sequencing Buffer, 1  $\mu$ l BigDye® Terminator v3.1 Ready Reaction Mix were used in a total reaction volume of 10  $\mu$ l. The following cycler program was used:

1 min	95°C	
30 sec	95°C	} 30 x
2.5 min	60°C	
5 min	60°C	
$\infty$	10°C	

Amplificates were purified using Sephadex G-50 in a MultiScreen<sub>HTS</sub>-HV plate and the analysis of the sequence was performed on a ABI 3500 XL

genetic analyzer and ABI 3500 data collection software. Further analysis was performed with the Sequencing Analysis Software v5.4 and BioEdit software.

### III.14.3.5 Cloning of a Wif1 expression plasmid

A Wif1 expression plasmid was generated by inserting the *mWif1* cDNA amplified from *pcDNA3-mWif1* (Becker 2011) in the vector backbone *pMSCVpuro*.

At first, the *mWif1* insert was generated by means of PCR using a forward primer containing a *Bgl*II recognition sequence and a Kozak consensus sequence, and a reverse primer containing an *Hpa*I recognition sequence (see Table 12). Integrity of the amplicon was determined by gel electrophoresis. A band of 1156 bp was generated as expected and purified from the agarose gel (see section III.14.3.2 and Fig. 5).

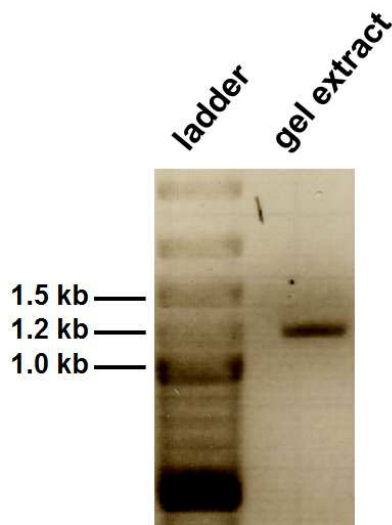


**Fig. 5: Gel electrophoresis of amplified and purified Wif1 insert**

Insert is 1156 bp long containing *Bgl*II recognition sequence, a Kozak consensus sequence, the 1140 bp coding sequence and an *Hpa*I recognition sequence.

Then, insert and *pMSCVpuro* were hydrolyzed with restriction endonucleases *Bgl*II and *Hpa*I, purified by ethanol precipitation (see II.14.X) and dissolved in 20  $\mu$ l ddH<sub>2</sub>O. 2  $\mu$ l of each 20  $\mu$ l DNA solution was analyzed by gel electrophoresis (see Fig. 6). The concentration of DNA solutions was estimated by comparing the respective band intensity with band intensity of neighboring DNA ladder having a known DNA concentration.

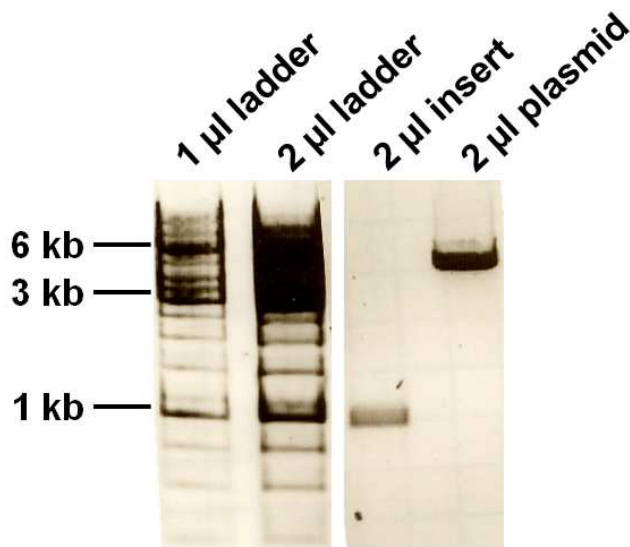


**Fig. 6: Gel electrophoresis of hydrolyzed *Wif1* insert and *pMSCV* vector backbone**

Insert is 1156 bp long containing *Bgl*II recognition sequence, a Kozak consensus sequence, the 1140 bp coding sequence and an *Hpa*I recognition sequence. *pMSCV* vector backbone has a given size of 6.3 kb.

Subsequently, a 3:1 ratio of the insert to vector DNA was used for ligation (see III.14.3.3) and transformed into *E. coli* (see III.14.4.1). Single cell clones were picked for small-scale isolation of plasmid DNA from bacteria culture (see III.14.1.1). A total number of 18 clones were isolated. Successful cloning of *pMSCVpuro-Wif1* was verified by restriction hydrolyses (see III.14.3.1) and DNA sequencing (see III.14.3.4) (see Fig.7 and data not shown). By using *Bgl*II and *Hpa*I only plasmids containing the full-length insert are hydrolyzed resulting in a 1.2 kb (*mWif1*-insert) and a 6.3 kb (*pMSCVpuro*) fragment (top panel). Using *Hind*III and *Bam*HI the orientation of the inserts was determined. In a 5'→3' orientation two fragments of 560 bp and 6.9 kb length were generated. When inserts were in 3'→5' orientation restriction hydrolysis would result in fragments of 1.6 and 5.7 kb length (bottom panel).

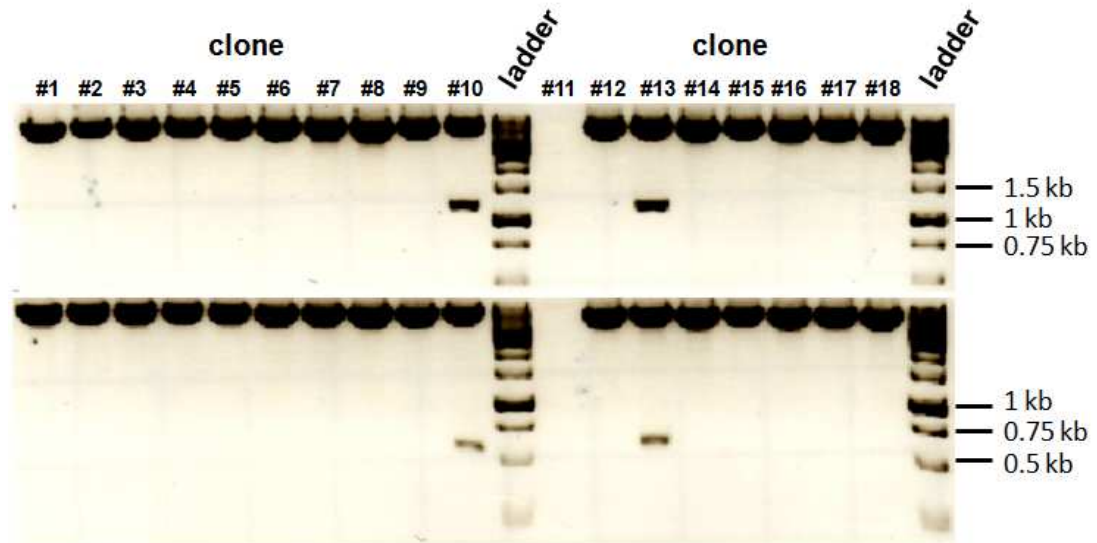


**Fig. 7: Gel electrophoresis of restriction hydrolyzed *pMSCV-Wif1***

18 clones were picked from agar plates for downstream analysis. Top: Use of restriction enzymes *Bgl*I and *Hpa*I result in the generation of a 1.2 kb and a 6.3 bp fragment. Bottom: An insertion in 5'→3' orientation resulted in two fragments of 560 bp and 6.9 kb length when hydrolyzed with *Hind*III and *Bam*HI. A 3'→5' orientation would result in fragments of 1.6 and 5.7 kb length.

The 2 clones #10 and #13 were shown to have the insert in the correct orientation. All following experiments were performed with plasmid derived from clone #10. The plasmid *pMSCVpuro-mWif1* (hereafter *pMSCV-Wif1*) was transfected in the packaging cell line Platinum-E for the production of retroviral particles (see III.14.4.8).

### III.14.4 Cell biological techniques

#### III.14.4.1 Transformation of bacteria

100 ng plasmid was added to 50  $\mu$ l competent cells (DH5 $\alpha$ ) and incubated for 20 min on ice. Afterwards, bacteria were transformed by heat-shock for 45 sec at 42°C and chilled on ice for 2 min. Subsequently, 500  $\mu$ l SOC-medium were added and cells were incubated for 1 h at 37°C and 900 rpm on a heating block. 50  $\mu$ l of the bacterial solution were plated on an agarose plate containing adequate antibiotics (1  $\mu$ g/ml) and incubated overnight (O/N) at 37°C.

### **III.14.4.2 Culture of eukaryotic cells**

Cells were cultured in an incubator at 5% CO<sub>2</sub>, 90% humidity and 37°C. Medium was changed every three days and cells were subcultured by splitting them 1:10 upon reaching 70-80% confluence. Culture of cells was performed using media listed in Table 8.

### **III.14.4.3 Isolation and cultivation of BMDMs**

To isolate bone marrow-derived macrophages (BMDMs) the femur of a wt mouse was excised and the attached connective and muscle tissue was removed. Both ends of the femur were cut by scissors and macrophages of the bone marrow were expelled in a petri dish using a syringe and 10 ml Pluznik medium (DMEM/10 % FCS/5 % horse serum/30 % L929 CM/1 % P/S/0.0002 % β-mercaptoethanol). L929 CM was prepared as described in section II.14.4.4.2. Afterwards, cells were incubated O/N at 37°C, 5 % CO<sub>2</sub> and 95 % humidity. The Supernatant containing the unattached macrophages was centrifuged for 10 min at 800 x g, the cell pellet was dissolved in 40 ml Pluznik medium, split and subcultivated in 4 uncoated petri dishes. The culture medium was changed every third day. 7 days after the isolation of BMDMs, cells were detached from petri dishes using Accutase and used for coculture proliferation assay (see section III. 14.4.10.2)

### **III.14.4.4 Conditioned media (CM)**

#### **III.14.4.4.1 Generation and use of Wnt3a and Wnt5a CM**

NIH/3T3 Wnt5a, NIH/3T3, L Wnt-3A and L cells were cultured as described in section III.14.4.2. Cells that were 70 % confluent were subcultured by splitting them 1:10 in media without selective antibiotics. After 4 days the first fraction of the conditioned medium was collected and new medium was added for additional 3 days for the production of the second fraction. The 2 conditioned media fractions were combined and centrifuged at 1000 x g for 5

min to eliminate remaining cells and the supernatant was subsequently sterile filtered through 0.2 µm filters and stored at 4°C.

#### **III.14.4.4.2 Generation and use of L929 CM**

L929 conditioned medium was prepared from L929 cells having an initial 50% confluency and which were cultured 5 days in RPMI/10 % FCS/1 % PS. Subsequently, the medium was collected and sterile filtered with a 0.2 µm filter and stored at -20°C. L929 conditioned medium was used as indicated in section III.14.4.3

#### **III.14.4.5 Concentration of Wif1-containing media**

ASZ-*pMSCV* and ASZ-*Wif1* cells were split 1:10 after reaching 70-80 % confluency and transferred in fresh culture medium without puromycin. After 5 days the medium was removed and replaced with fresh culture medium for 5 additional days. Both supernatants were subsequently centrifuged at 4500 x g for 10 min to remove all cells and debris. Afterwards, the supernatants were transferred to a protein concentrator tube (Thermo Fisher Scientific). Concentrator was used according to manufacturers` protocol generating a 75-fold concentrated supernatant.

#### **III.14.4.6 Transfection of eukaryotic cells**

HEK-293 cells were seeded in 6-well plates ( $10^5$  cells/well) in 1 ml of the respective culture medium (see Table 8). 24 h later 1 - 2.2 µg plasmid DNA and Roti-Fect (Carl Roth) transfection reagent (5 µl per 1 µg DNA) were added to 100 µl DMEM and incubated for 40 min at RT to allow for nucleic acid-lipid complex formation. Subsequently, the mixture was added to the cells cultured in 1 ml of fresh culture medium without P/S for 3 h. Thereafter, the cells were washed and incubated with the respective culture medium for 24 h.

### III.14.4.7 Nucleofection of eukaryotic cells

For nucleofection  $2 \cdot 10^6$  ASZ001 cells were centrifuged at  $90 \times g$  for 10 min. 2.5  $\mu\text{g}$  total plasmid (see scheme below) or 1  $\mu\text{g}$  nucleofection control plasmid (*pGFPmax*) in 100  $\mu\text{l}$  Nucleofector solution was added to the cell pellet and cells were resuspended. Then, cells were transferred into an electroporation cuvette and nucleofected using program T-029 in the electroporation device Amaxa Nucleofector 2b (Lonza). Afterwards, 100  $\mu\text{l}$  of nucleofected cells were directly plated in 96-well plates for downstream analysis via *TOP/FOP* reporter assay (see III.14.4.9).

**Table 19: Scheme of plasmid combinations for nucleofection**

1: 1<sup>st</sup> plasmid (200 ng) ; 2: 2<sup>nd</sup> plasmid (1  $\mu\text{g}$ ); 3: 3<sup>rd</sup> plasmid (1  $\mu\text{g}$ )

1	2	3
<i>pRL-CMV</i>	<i>SuperTOPFlash (TOP)</i>	<i>pCl-neo-<math>\beta</math>-catS33Y</i>
<i>pRL-CMV</i>	<i>SuperTOPFlash (TOP)</i>	<i>pCR3.1</i>
<i>pRL-CMV</i>	<i>SuperFOPFlash (FOP)</i>	<i>pCl-neo-<math>\beta</math>-catS33Y</i>
<i>pRL-CMV</i>	<i>SuperFOPFlash (FOP)</i>	<i>pCR3.1</i>
-	<i>pGFP-max</i>	-

### III.14.4.8 Retroviral transduction of eukaryotic cells

For preparation of virus particles used for transduction of ASZ001 cells Platinum-E cells were used as packaging cell line. Platinum-E cells were seeded at a confluency of 70 % in 5 cm culture dishes one day before transfection with the retroviral vectors. For the transfection the following reagents were used:

400  $\mu\text{l}$  serum free medium (154 CF)

9  $\mu\text{l}$  TransIT®-LT1 Transfection Reagent

3  $\mu\text{g}$  retroviral expression vector

(*pMSCVpuro* or *pMSCVpuro-Wif1*, respectively)

The reagents were mixed and incubated at RT for 30 min. Afterwards, the Platinum-E cells were washed and the medium was replaced with 4 ml fresh culture medium (154CF, 2% FCS, 1% P/S). The transfection mixture was added drop wise onto the plates and mixed by swirling. After 48 h the cell supernatants containing the viruses were sterile-filtered using a 0.45 µm pore sterile filter. 3 ml supernatant was mixed with 3 ml fresh medium containing 3 µg/ml polybrene and applied to a 5 cm culture dish containing 50 % confluent ASZ001 cells. After 24 h the cells were washed and supplied with fresh medium. After additional 24 h the culture media were supplemented with puromycin.

#### **III.14.4.9 TOP/FOP reporter assay**

The  $\beta$ -catenin dependent activity of Wnt signaling was analyzed using a dual luciferase reporter assay. HEK-293 cells were seeded at a density of  $1.5 \cdot 10^5$  cells/well in a 6-well plate. 24 h later cells were transfected with 1 µg of either *SuperTOPFlash* (*TOP*) plasmid containing multiple T cell-specific transcription factor/lymphoid enhancer-binding factor (TCF/LEF)-binding sites or its negative control vector *SuperFOPFlash* (*FOP*) containing mutated and thereby inoperable binding sites (1 µg). 200 ng of the renilla-luciferase encoding plasmid *pRL-CMV* was cotransfected for normalization. Cotransfection with 1 µg *pCl-neo- $\beta$ -catS33Y* encoding for a constitutively active  $\beta$ -catenin served as positive control. In all settings, the final amount of DNA was increased to a total of 2.2 µg with *pCR3.1* vector DNA. 24 h after transfection (see section III.14.4.6) cells were trypsinized and 6000 cells were subcultured in 96 well plates with Wnt3a CM or control medium. To block Wnt3a, Wnt3a CM was supplemented with 600 ng/ml Dkk1 or was preincubated with an equal volume of 75 x concentrated ASZ-*Wif1*, ASZ-*pMSCV* (control) conditioned medium or with 30 µg/ml rWnt3a, respectively, for 5 h at RT and 450 rpm and then added to the transfected HEK-293 cells. After additional 48 h, cells were lysed and renilla- and firefly-luciferase activity was measured using the Dual-Luciferase Reporter Assay

System kit (Promega) according to manufacturer's protocol in a luminometer (Synergy Mx).

### **III.14.4.10 Proliferation assay**

#### **III.14.4.10.1 5-Bromo-2`-deoxyuridine assay**

8000 cells were seeded in a 96 well plate 24 h before BrdU labeling. The BrdU labeling was performed for 24 h according to manufacturer's protocol (Roche).

The measurement was conducted by means of a plate reader (Synergy MX).

#### **III.14.4.10.2 Coculture proliferation assay**

On the first day  $4 \times 10^4$  cells of the cell lines *ASZ-pMSCV* or *ASZ-Wif1* were seeded in each well of a 24-well plate and  $5 \times 10^4$  bone marrow derived macrophages (BMDMs), B9, NIH/3T3, NIH3T3-Wnt5a, Wnt-3A or L cells were seeded in 24-well inserts (0.2  $\mu\text{m}$  pore size) placed in 24-well plates for coculture proliferation measurement. On each of 5 consecutive days the total cell number per well was counted using Celigo S device and software.

#### **III.14.4.11 Cell cycle analysis**

For cell cycle analysis  $1 \cdot 10^6$  cells were subcultivated in 10 mm culture dishes. After 48 h the cells were detached using Accutase and transferred into a 15 ml tube containing 5 ml Medium. Then, cells were washed by centrifugation for 5 min at  $300 \times g$  and  $4^\circ\text{C}$  and resuspended in 1ml PBS. Subsequently, the cell suspension was mixed with 10 ml  $-80^\circ\text{C}$  100 % ethanol. Afterwards, the cells were fixed for 2 h at  $-20^\circ\text{C}$ . Then, cells were centrifuged for 5 min at  $1000 \times g$  and  $4^\circ\text{C}$  and washed with 2 ml 100 % Ethanol by additional centrifugation for 5 min at  $1000 \times g$  and  $4^\circ\text{C}$ . Subsequently, the cell pellet was resuspended in 500 $\mu\text{l}$  propidium iodide

solution (10 µg/ml propidium iodide and 100 µg/ml RNaseA in PBS) and incubated for 30 min at 37°C. Afterwards, cells were analyzed using the flow cytometer LSR II (BD Biosciences) and FACS Diva™ (BD Biosciences) and FlowJo softwares (Tristar, Inc.), respectively.

#### **III.14.4.12 Cell viability assay**

8000 cells were seeded in a 96 well plate 24 h before adding WST-1. WST-1 was added for 4h. 200 mM H<sub>2</sub>O<sub>2</sub> was added as negative control. The measurement was conducted by means of a plate reader (Synergy MX). Protocol and measurement was conducted according to manufacturer's protocol (Roche).

#### **III.14.4.13 Annexin V assay**

When in the early phase of apoptosis the integrity of the plasma membrane gets lost, phosphatidylserine translocates from the inner side of the plasma membrane to the cell surface. Annexin V is a Ca<sup>2+</sup>-dependent protein that can bind to PS. FITC coupled Annexin V was used to detect apoptosis and propidium iodide (PI) was used to identify necrotic cells.

Cells were detached using 1 ml Accutase and washed with 1 x PBS by centrifugation at 300 x g for 5 min. Afterwards, the cell pellet was resuspended in 100 µl 1 x Annexin V-binding buffer containing 2 µl Annexin V-FITC for 10 min. Subsequently, 2 µl of a 100 µg/ml PI solution was added and cells were incubated in the dark at RT for 5 min. Then, 400 µl of 1 x Annexin V-binding buffer were added and cells were analyzed using FACS Calibur (BD) and FlowJo software.

#### **III.14.4.14 Transwell migration assay**

75000 cells were seeded in 24-well inserts (8.0 µm pore size) and placed in a 24-well plate containing 500 µl complete cell culture medium, Wnt3a CM or

control CM. After 24 h migrated cells were stained with 5  $\mu\text{M}$  calcein for 1 h. Subsequently, all cells that have not been migrated were removed and 5 consecutive pictures at 100 fold magnification were taken for each well. Cell number was counted using FIJI software.

#### **III.14.4.15 $\text{Ca}^{2+}$ -flux assay**

For measuring the intracellular levels of  $\text{Ca}^{2+}$ ,  $5 \times 10^6$  cells were incubated in 700  $\mu\text{L}$  RPMI 1640 medium supplemented with 5 % FCS, 1 mM Indo-1-AM (Thermo Fisher Scientific), and 0.015 % Pluronic F127 (Thermo Fisher Scientific) at 30°C for 25 min. The cell suspension was diluted with 700  $\mu\text{L}$  RPMI 1640 containing 10 % FCS and incubated for additional 10 min at 37°C. Subsequently, cells were washed twice with 600  $\mu\text{L}$  Krebs Ringer solution. Prior to measurements cells were resuspended in 600  $\mu\text{L}$   $\text{Ca}^{2+}$ -free Krebs Ringer solution supplemented with 0.5 mM EGTA. Flow cytometric analysis was performed on an LSR II cytometer configured with a 488 nm and a 355 nm laser (BD Biosciences). After monitoring the basal  $\text{Ca}^{2+}$  level for 30 s, cells were stimulated with 1  $\mu\text{l}$  ionomycin. The emission fluorescence intensities of Indo-1-AM were recorded at wavelengths of 405 nm and 530 nm to determine changes in the ratios of  $\text{Ca}^{2+}$ -unbound versus  $\text{Ca}^{2+}$ -bound Indo-1-AM. Data acquisition and analysis was performed with BD FACS Diva™ (BD Biosciences) and FlowJo software (Tristar, Inc.), respectively.

#### **III.14.5 Western blot (WB)**

##### **III.14.5.1 Isolation of proteins from cell culture**

Cells were harvested in 1 ml PBS using a cell scraper. Afterwards, cells were centrifuged for 5 min at 1000 x g and 4°C. The pellet was resuspended in 700  $\mu\text{l}$  PBS, centrifuged for 5 min at 1000 x g and 4°C and immediately shock-frozen in liquid nitrogen for cell lysis. Subsequently, the pellet was thawed on ice and resuspended in 50  $\mu\text{l}$  of modified RIPA buffer. After 30 min the lysate was centrifuged at 16000 x g and 4°C for 25 min. The

supernatant containing the proteins was stored at  $-80^{\circ}\text{C}$  and the protein concentration was measured with Pierce BCA Protein Assay Kit according to manufacturer's instructions.

### **III.14.5.2 Isolation of proteins from tissue samples**

30mg of tissue was cut with scalpel and added to 300 $\mu\text{l}$  modified RIPA buffer containing protease inhibitors in a 2 ml reaction tube. Subsequently, the tissue was homogenized for 1 min at level B of homogenizer. Afterwards, homogenate was shock frozen in liquid nitrogen to disrupt cell membranes, thawed on ice and centrifuged at 10.000 x g for 10 min at  $4^{\circ}\text{C}$ . Subsequently, the supernatant was transferred in a new 1.5 ml reaction tube and the protein concentration was measured.

### **III.14.5.3 Western blot**

For sample preparation 1 x sample buffer was added to 35  $\mu\text{g}$  protein lysate and samples were filled up to equal volumes with lysis buffer. Proteins were denatured for 5 min at  $96^{\circ}\text{C}$  and 450 rpm on a heating block. Proteins were separated using NuPAGE Novex Midi Gels in 1 x running buffer (NuPAGE MES SDS buffer, 20 x) for 1.5-2 h at 160 mA. For the determination of the molecular weight 4  $\mu\text{l}$  SeeBlue Plus2 Prestained Standard were run in parallel. Proteins were transferred to a nitrocellulose membrane (GE Healthcare) using a semi-dry blotting device at 120 mA per gel for 80 min. After blocking with 5 % (w/v) milk powder/TBST for 1.5 h at RT and washing three times for 10 min in TBST the primary antibody (see Table 17) was added in a dilution of 1:1000 in 0.02 % (w/v) sodium azide/3 % (w/v) BSA in TBST. The membrane was incubated overnight on an orbital shaker at  $4^{\circ}\text{C}$ . Subsequently, the membrane was washed 3 x 10 min in TBST and the secondary antibody 1:5000 in 5 % (w/v) milk powder/TBST was added for 1 h at RT on orbital shaker. After three washing steps in TBST 1.5 ml the detection reagent (Amersham ECL Plus Western Blotting Detection

Reagents) per membrane was added for 3 min. For visualization the FluorchemQ device and AlphaView Software was used.

### **III.14.6 Animal experiments**

#### **III.14.6.1 Mouse keeping**

All used mouse lines were kept within the institutes' own mouse facility at 12 h day-night-rhythm at 20±2°C and 50±10% humidity. Mice had ad libitum access to pelleted dry food and tap water. All experiments were performed in compliance with all relevant legal and ethical requirements. Immune deficient nude mice were kept in individually ventilated and sealed cages supplying ad libitum autoclaved pelletized dry food and tap water.

#### **III.14.6.2 Genotyping PCR**

Ear marks to identify each mouse and tail tip biopsies at the age of 3 weeks were performed by animal caretakers. Biopsies were digested using 0.5 mg/ml proteinase K in 400 µl STE buffer over night at 56°C followed by ethanol precipitation to isolate genomic DNA (gDNA). 1 µl of gDNA was used as template for genotyping PCR utilizing appropriate DNA-oligonucleotides listed in Table 14.

#### **III.14.6.3 Intramuscular tamoxifen injection**

Tamoxifen (Sigma-Aldrich Chemie GmbH, Steinheim) was solved in 96% ethanol to obtain a 100mg/ml tamoxifen solution which was diluted 1:10 in sterile sun flower oil (Sigma-Aldrich Chemie GmbH, Steinheim). This emulsion (10mg/ml) was stored at -20°C. For inducing the activity of Cre-recombinase in the mouse lines *Ptch<sup>flox/flox</sup>CreERT2<sup>T/-</sup>Wif1<sup>-/-</sup>*, *Ptch<sup>flox/flox</sup>Wif1<sup>-/-</sup>* and *Ptch<sup>flox/flox</sup>CreERT2<sup>T/-</sup>* 10µl of the tamoxifen emulsion

was injected in the *musculus soleus* of 8 week old mice using BD microfine + Demi syringes (Zibat *et al.* 2009).

#### III.14.6.4 BCC mouse model and *Wif1* knockout

The analysis of BCC development was conducted using *Ptch<sup>flox/flox</sup>ROSA26-CreERT2<sup>T/-</sup>* mouse model (hereafter *Ptch<sup>flox/flox</sup>CreERT2<sup>T/-</sup>*). In these mice tamoxifen injection can trigger the nuclear translocation of the ubiquitously expressed fusion protein consisting of a Cre-recombinase domain and a mutated estrogen receptor domain (CreERT2). Subsequently, nuclear CreERT2 can cause deletions at floxed sequences of host DNA.

To analyze the effect of *Wif1* on BCC formation, development and regression *Ptch<sup>flox/flox</sup>* mice were crossed to *Wif1<sup>-/-</sup>* mice (see Table 9). The resulting *Ptch<sup>flox/+</sup>Wif1<sup>+/-</sup>* were mated with to mice of the same genotype to generate *Ptch<sup>flox/flox</sup>Wif1<sup>-/-</sup>* mice. These mice in turn were crossed with *Ptch<sup>flox/flox</sup>CreERT2<sup>T/-</sup>* mice.

Resulting *Ptch<sup>flox/flox</sup>CreERT2<sup>T/-</sup>Wif1<sup>+/-</sup>* and *Ptch<sup>flox/flox</sup>Wif1<sup>+/-</sup>* were mated to generate *Ptch<sup>flox/flox</sup>CreERT2<sup>T/-</sup>Wif1<sup>-/-</sup>*, *Ptch<sup>flox/flox</sup>Wif1<sup>-/-</sup>* and *Ptch<sup>flox/flox</sup>CreERT2<sup>T/-</sup>* which were injected with a single dose of 100 µl tamoxifen emulsion (10 mg/ml, Sigma-Aldrich Chemie GmbH, Steinheim) i.m. at an age of 8 weeks. For the genotypes *Ptch<sup>flox/flox</sup>CreERT2<sup>T/-</sup>Wif1<sup>-/-</sup>* and *Ptch<sup>flox/flox</sup>CreERT2<sup>T/-</sup>* 20 animals were injected with tamoxifen. After 45 days and 90 days 10 animals each were euthanized for further analyses. For the genotype *Ptch<sup>flox/flox</sup>Wif1<sup>-/-</sup>* 10 animals were injected with tamoxifen. After 45 days and 90 days 5 animals each were euthanized for further analyses.

#### III.14.6.5 Allograft

Cells were suspended in a 200 µl solution of 50% matrigel in complete cell culture medium without puromycin. Cell suspension was subsequently injected subcutaneously into the flanks of nude mice using 1 ml Sub-Q

syringes (BD) which were precooled on ice to prevent hardening of the matrigel. Each nude mouse was injected bilaterally on one flank with ASZ-*pMSCV* cell suspension and on the other flank with ASZ-*Wif1* cell suspension to exclude mouse effects. After 2 weeks when the tumors reached a diameter of 5mm the width (b) and length (a) of each tumor was measured by caliper 3 times a week and tumor volume (V) was calculation by use of the modified ellipsoid formula:  $V = \frac{1}{2} a \cdot b^2$  (Euhus *et al.* 1986; Tomayko and Reynolds 1989).

When the tumors reached a maximal diameter of 20 mm mice were euthanized and tumors were removed, weighed and measured. For RNA and protein isolation (see III.14.1.4 and III.14.6.2) portions of the tumors were snap-frozen on dry ice and for antibody stainings tumor portions were fixed in 4% PFA for 1 week in embedding cassettes.

### **III.14.7 Histological stainings**

For all histological stainings, PFA-preserved tissue was embedded in paraffin, cut into 5µm sections and mounted onto glass slides. All samples were examined by a pathologist.

#### **III.14.7.1 Hematoxylin and eosin (H&E) staining**

Sections were deparaffinized with xylene for 20 min and subsequently rehydrated using descending ethanol solutions. After washing with ddH<sub>2</sub>O, slides were placed in hematoxylin solution for 15 min. The staining reaction was done in warm tap water for at least 5 min. Samples were then quickly dipped in 1% eosin solution containing 0.5% (v/v) glacial acetic acid. Subsequently, slides were washed with ddH<sub>2</sub>O and dehydrated using ascending ethanol solutions. Slides were placed again in xylene and afterwards mounted in Pertex. Then, slides were dried at 55°C for 15 min.

### **III.14.7.2 Immunohistochemistry (IHC)**

Sections were deparaffinized with xylene and rehydrated in descending ethanol series. Whenever necessary, antigen retrieval was done performed according to Table 16. Sections were blocked with 3% H<sub>2</sub>O<sub>2</sub> to inhibit endogenous peroxidases and blocked with 0.2% casein to prevent non-specific antibody binding. Afterwards, the sections were incubated with a primary antibody over night at 4°C and on the next day with the appropriate secondary antibody (see Table 16 and Table 18) in a humid chamber. Antibody binding was visualized using DAB+ (Envision+ system-HRP, Dako) or aminoethylcarbazol as chromogen. To stop the reaction, slides were rinsed with distilled water. All sections were counterstained with hematoxylin.

### **III.14.7.3 TdT-mediated dUTP-biotin nick end labeling (TUNEL)**

Tissue sections were deparaffinized with xylene and rehydrated with descending ethanol series. Afterwards, slides were first washed in 0.85% NaCl and then in 1 x PBS. Subsequently, slides were fixated in 4% PFA for 15 minutes at RT and washed twice in 1 x PBS. Then, 20µg/ml proteinase K solution was applied on each tissue section and incubated for 10 minutes at RT. Afterwards, slides were washed with 1 x PBS. Tissue sections which were treated with a solution of 10 unit/ml RQ1 RNase-free DNase I in DNase I buffer served as positive controls. Then, sections were again fixated in 4% PFA for 5 min at RT and washed twice in 1x PBS. The labeling reaction was performed using the DeadEnd Colorimetric TUNEL System (Promega) according to the manufacturer`s protocol. Subsequently, sections were counterstained with Hematoxylin and mounted using glycer gel (Dako).

**III.14.7.4 Ladewig staining**

To stain for extra cellular matrix Ladewig staining was performed by the technical assistants in the department of neuropathology following standard protocols. Analysis was performed by means of FIJI software.

## IV Results

### IV.1 WIF1 expression in human BCC

The relevance of WIF1 in human BCC was first tested by protein expression analysis of WIF1 on paraffin sections derived from 10 human BCC samples. As shown in Fig. 8 all analyzed human BCC samples showed WIF1 expression (10/10). In all samples WIF1 was homogeneously expressed by tumor cells (see Fig. 8, arrow head). It also was expressed by tumor-associated inflammatory cells (see Fig. 8, asterisk). Moreover, WIF1 expression in fibroblasts of the tumor stroma was detectable (see Fig. 8, arrows). Together, these data show that WIF1 is highly expressed in BCC. Basically all tumor cells express this protein. WIF1 is also expressed in the tumor stroma, however to a variable extent.

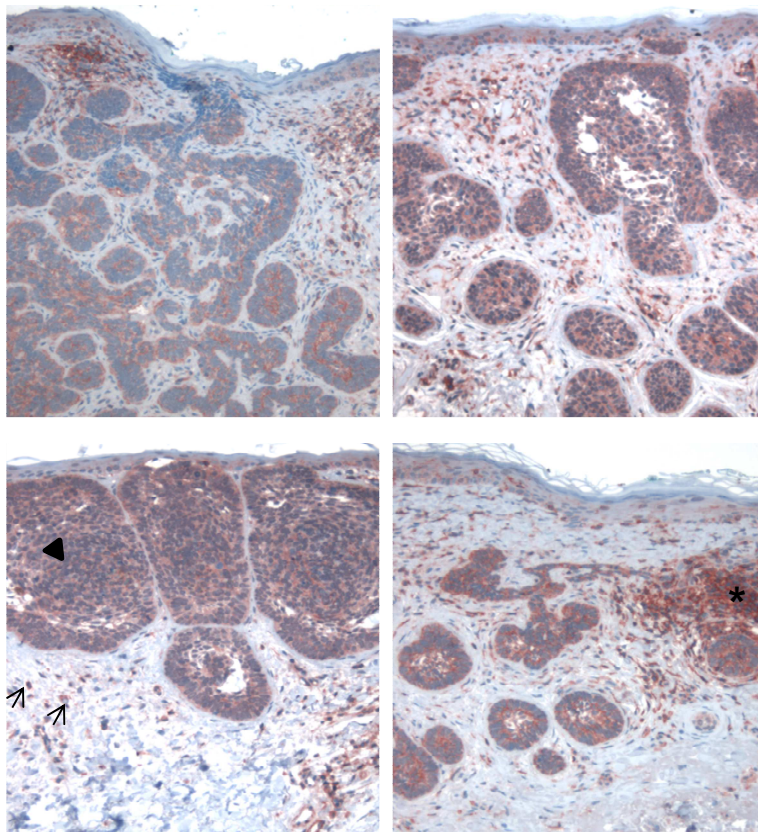


**Fig. 8: Antibody staining of WIF1 in human BCC**

Four representative stainings of paraffin sections derived from human BCC using an anti-WIF1 antibody. Staining reaction was performed using AEC. WIF1 expression is detectable in cells of inflammatory infiltrate (asterisk), tumor cells (arrow head), and stromal fibroblasts (arrows).

As *WIF1* is a well-known tumor suppressor we hypothesized that *WIF1* expression might be absent or reduced in more aggressive skin tumors such as SCC and melanoma. In addition, we wanted to know whether there is any difference in *WIF1* expression in subtypes of BCC. To test this, tumor tissue was separated from stromal cells by laser microdissection and *WIF1* expression was analyzed in the tumor tissue by means of qRT-PCR. The analysis included 3 superficial, 3 nodular and 3 infiltrative BCC, 3 SCC and 3 melanomas. *WIF1* was detectable in all samples (see Fig. 9). The weakest expression levels were detectable in superficial and nodular subtypes of BCC, the highest in infiltrative BCC, SCC and melanomas. No significant differences between infiltrative BCC, SCC and melanomas were noticeable. Moreover, the differences between BCC subtypes were also not statistically significant. However, superficial and nodular BCC expressed significantly lower levels of *WIF1* in comparison with SCC and melanomas.

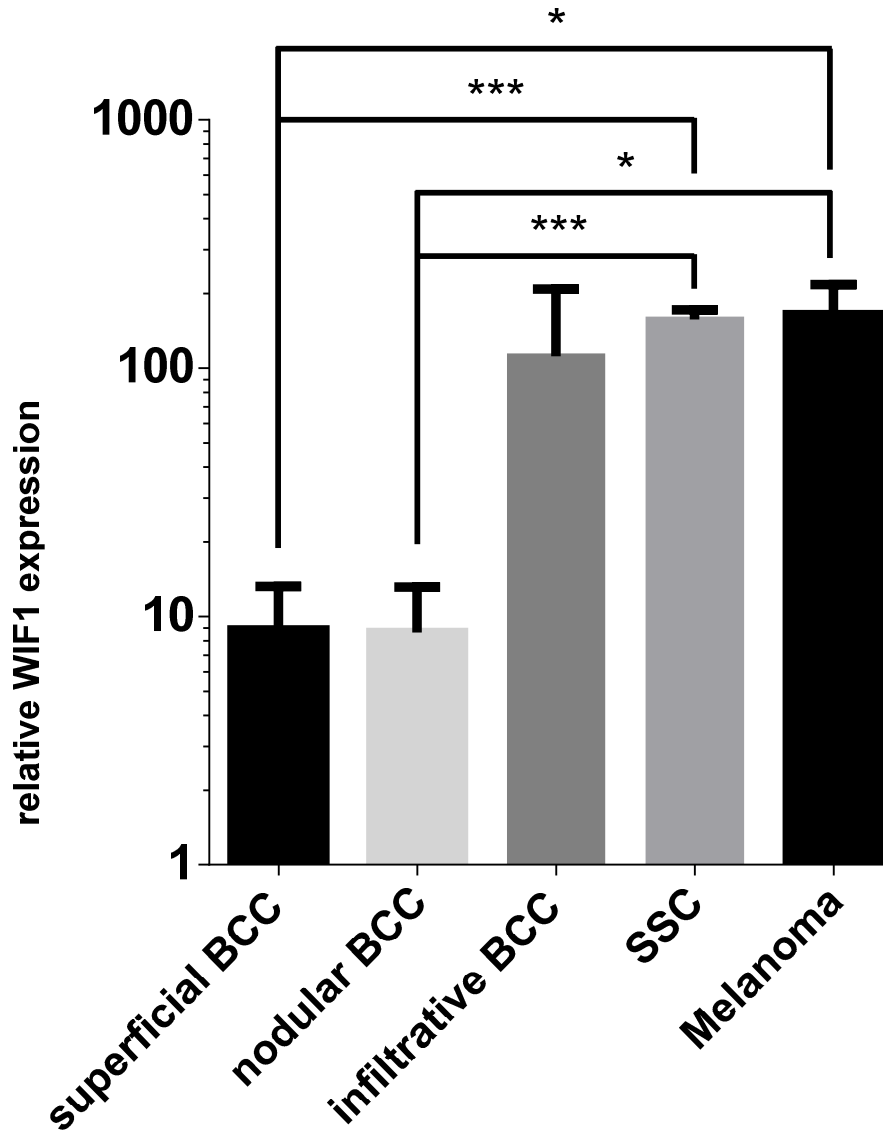


**Fig. 9: Evaluation of *WIF1* qRT-PCR of microdissected BCC subtypes, SCC and melanomas**

3 skin samples each were analyzed. Tumor tissue was excised using laser microdissection. All data are represented as mean + SEM. Statistical significance was tested using unpaired t test with Welch's correction. \*  $p < 0.05$ , \*\*\*  $p < 0.001$ .

Because these results seemed to be contradictory to the reported tumor suppressive function of WIF1, we analyzed the role of WIF1 in BCC in more detail.

## IV.2 Generation of a *Wif1* expression vector

### IV.2.1 Cloning strategy

According to CCDS database only one protein-coding *Wif1* transcript is known. However, Ensemble database describes two distinct transcripts. These are a 1140 bp transcript encoding for a 379 aa protein (see Fig. 10) and a transcript variant of 1098 bp length encoding for a 365 aa protein lacking roughly the second half of exon 8. Nevertheless, all investigations, at least to our knowledge, focused on the first one. To analyze the role of *Wif1* in BCC formation and development we therefore also focused on this isoform.

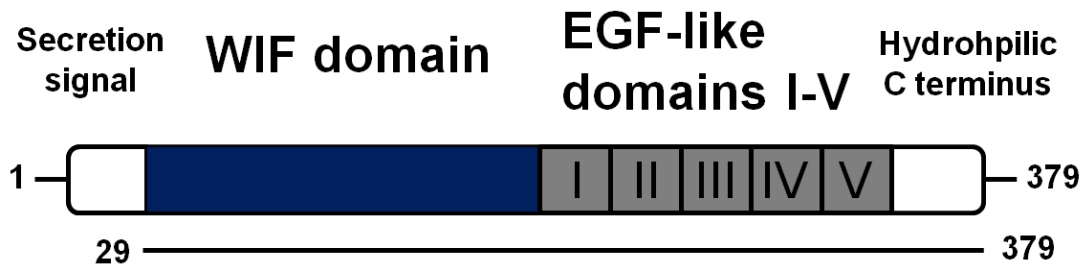


**Fig. 10: Functional structure *Wif1***

*Wif1* consists of a 28 amino acids long N-terminal secretion signal sequence which is cleaved off upon secretion, the WIF domain (WD, 143 amino acid residues), five EGF-like domains (31–33 residues each) and a hydrophilic C-terminus.

During my master thesis I cloned a *Wif1* expression vector (*pcDNA3-mWif1*) containing the complete coding sequence of murine *Wif1* together with a Kozak consensus sequence. However, as the BCC cell line ASZ001 is hard to transfect, the overexpression of *Wif1* by means of conventional transfection of *pcDNA3-mWif1* was unsuccessful. Therefore, the insert was subcloned into *pMSCVpuro* to generate the retroviral expression vector *pMSCV-Wif1* as described in III.14.3.5.

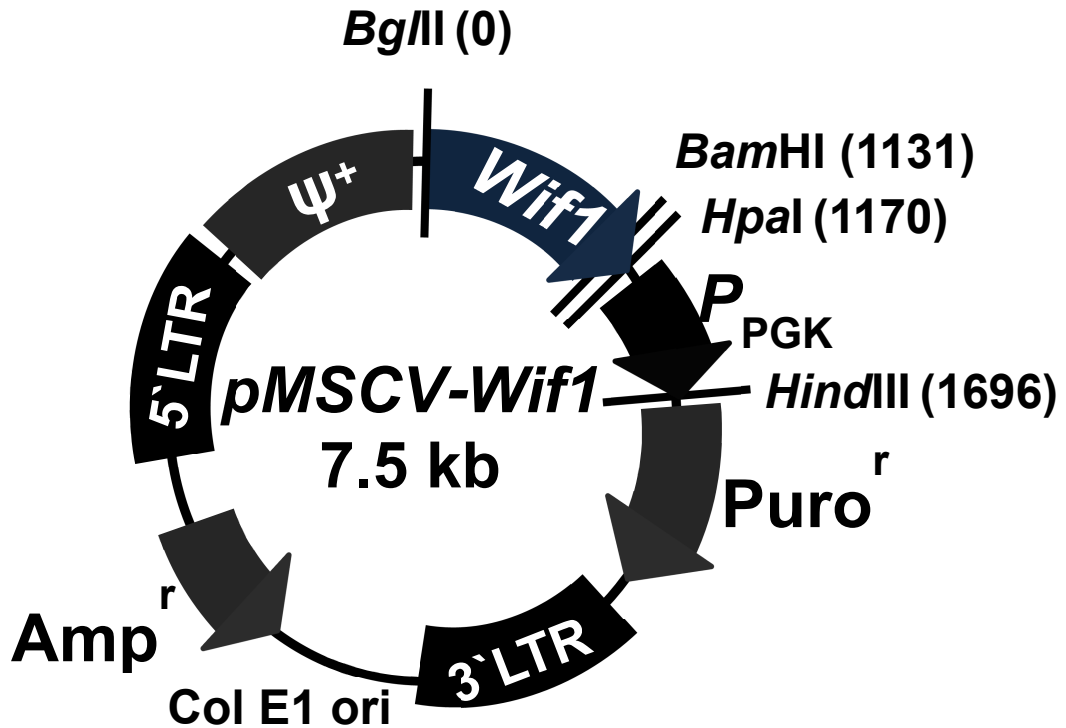


**Fig. 11: Schematic of *pMSCV-Wif1***

Retroviral expression vector containing murine *Wif1* ORF. *Bgl*II(0), *Bam*HI(1131), *Hpa*I(1170), *Hind*III(1696): restriction sites for respective endonucleases. Puro<sup>r</sup>: puromycin resistance cassette for stable selection in eukaryotic expression systems. Amp<sup>r</sup>: Ampicillin resistance cassette for selection in prokaryotic expression systems. 3' and 5'LTR: 3' and 5' long terminal repeats, sequences allowing for stable integration into target cell genome. Ψ<sup>+</sup>: packaging signal for retrovirus production in Platinum-E packaging cell line. P<sub>PGK</sub>: promoter for puromycin expression in eukaryotic cells. Col E1 ori: origin of replication.

The correct orientation of the insert was assessed by restriction hydrolysis and sequencing. As described in III.14.4.8 the supernatants from Platinum-E cells with retroviral particles containing *pMSCV* (control) or *pMSCV-Wif1*, respectively, were used for transduction of ASZ001.

#### **IV.2.2 Selection of stably transfected cells and verification of *Wif1* expression**

2 days after transduction of ASZ001 with either *pMSCV* control vector or the *pMSCV-Wif1* overexpression plasmid, cells were treated with 2 μg/ml puromycin to select stably transduced cells. Moreover, single cell clones

were isolated by limited dilution. RNA was isolated, reversely transcribed and a *Wif1* specific PCR was performed (see Fig. 12)

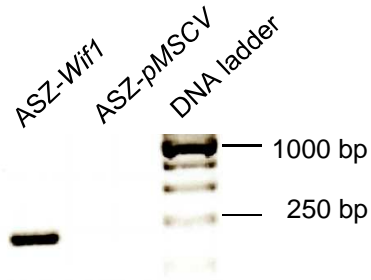


**Fig. 12: PCR detecting *Wif1* of *pMSCV* and *pMSCV-Wif1* transduced ASZ001 cells**  
PCR product of 220 bp length was generated as expected.

Moreover, in order to confirm the translation of the *Wif1* mRNA a Western blot was performed (see Fig. 13).

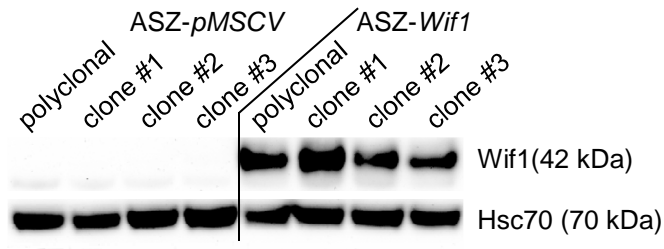


**Fig. 13: Western blot detecting *Wif1* of *pMSCV* and *pMSCV-Wif1* transduced ASZ001 cells**  
Antibody detecting Hsc70 served as loading control. Single cell clones and a polyclonal cell population (no single cell clone selection) were analyzed regarding *Wif1* expression.

As shown in Fig. 13 protein samples from *pMSCV* transduced ASZ001 cells (hereafter ASZ-*pMSCV*) do not express detectable levels of *Wif1*. In contrast, in the samples isolated from *pMSCV-Wif1* transduced ASZ001 cells (hereafter ASZ-*Wif1*) the *Wif1* protein was detected at the expected size of 42 kDa. This confirmed the successful transduction and operability of the retroviral expression plasmid *pMSCV-Wif1* to induce *Wif1* overexpression.

For the analysis of successful *Wif1* production and secretion the supernatant of ASZ-*Wif1* was 75-fold concentrated (see III.14.4.5) and analyzed by Western blot. As shown in Fig. 14, *Wif1* is not only expressed by ASZ-*Wif1* but also secreted.

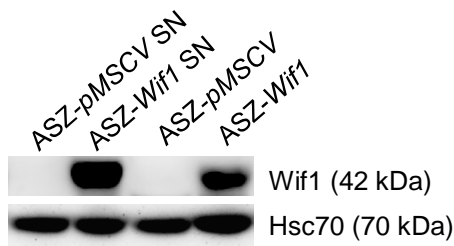


**Fig. 14: Western blot detecting Wif1 in supernatant and cellular extracts of ASZ-pMSCV and ASZ-Wif1**

Antibody detecting the housekeeper protein Hsc70 was used as loading control. Abbreviation: SN: concentrated supernatant.

### IV.3 Functional analysis of Wif1 *in vitro*

Wif1 is a well-known inhibitor of Wnt signaling due to sequestration of Wnt ligands in the extra cellular space. Orthologs of human WIF1 have also been shown to interact with Hh thereby promoting its activity. In addition, the Wnt and Hh signaling pathways can influence each other at several interfaces. To investigate whether Wif1 can modulate the activity of the latter signaling cascades, I employed functional assays and analyzed target gene expression of the respective pathways. To analyze the function of Wif1 *in vitro* on Wnt and Hh signaling, I analysed the expression of *Axin2* and *Gli1*, respectively. I also tried to establish the *TOP/FOP* reporter assay, which is useful to analyze the activity of the Wnt signaling pathway after its induction with Wnt ligands.

#### IV.3.1 *TOP/FOP* reporter assay for assessment of Wif1 activity

In order to analyze the inhibitory capability of Wif1 on Wnt ligands and thus on Wnt signaling activity, the *TOP/FOP* reporter assay was used as described in III.14.4.9.

As mentioned above ASZ001 are hard to transfect using lipid based transfection systems. However, nucleofection improved the plasmid transfer in ASZ001 resulting in ~50 % eGFP positive cells when using the reporter

plasmid *pGFPmax* (data not shown). Unfortunately, this method significantly reduced ASZ001 cell viability (data not shown).

Nevertheless, ASZ001 were transfected with the *TOP* plasmid. Cotransfection with *pCl-neo- $\beta$ -cateninS33Y* encoding for a mutationally, constitutively activated  $\beta$ -catenin (S33Y) served as positive control. *TOP* transfected cells were incubated with Wnt3a conditioned medium derived from stably transfected L cells (Wnt3a CM). Conditioned medium from untransfected L cells (L CM) served as control medium. As negative control, ASZ001 were transfected with the *FOP* and S33Y plasmids (data not shown).

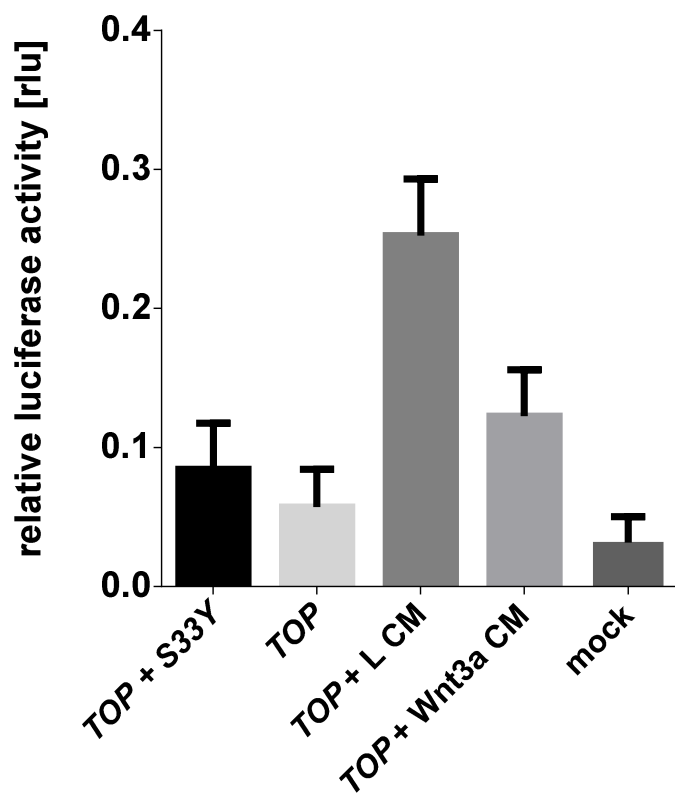


**Fig. 15: *TOP/FOP* reporter assay of Wnt signaling in ASZ001 cells incubated with Wnt3a**

As positive control ASZ001 cells were co-nucleofected with *SuperTOPFlash* (*TOP*) and *pCl-neo- $\beta$ -cateninS33Y* (S33Y). As negative control ASZ001 were co-nucleofected with *SuperFOPFlash* (*FOP*) and S33Y. ASZ001 cells only nucleofected with *TOP* or *TOP* transfected cells incubated with conditioned medium of untransfected L cells (L CM) were used as further controls. In addition, *TOP* nucleofected cells were incubated with Wnt3a conditioned medium from L cells stably expressing and secreting Wnt3a in order to activate canonical Wnt signaling driving luciferase expression (Wnt3a CM). Firefly luciferase activity was normalized to *Renilla* luciferase activity, which is under CMV promoter control. All data are represented as mean + SEM. Statistical significance was tested using Mann-Whitney *U* test. rlu: relative light units.

However, neither the positive control *TOP* + *S33Y* nor *Wnt3a* CM did induce luciferase activity in this assay. Therefore, we decided to change the experimental setup and employed the easy-to-transfect cell line HEK-293 for further experiments. For activation of Wnt signaling *Wnt3a* CM was used. The 75-fold concentrated supernatant of ASZ-*Wif1* cells (*Wif1* conc. SN, see Fig. 16) was employed and 75-fold concentrated supernatant of ASZ-*pMSCV* (*pMSCV* conc. SN) served as control. As additional controls of successful Wnt signaling inhibition, I used recombinant dickkopf1 (rDkk1) at a concentration of 750 ng/ml and recombinant *Wif1* (rWif1) protein at a concentration of 30 µg/ml. In HEK-293 cells, all negative controls (i.e. *TOP*, *FOP* or *FOP* + *S33Y*) did not induce luciferase activity. In contrast, transfection with *TOP* + *S33Y* highly induced luciferase activity. Cells that were transfected with *TOP* in combination with a 24 h incubation with a 1:1 mixture of *Wnt3a* CM and *pMSCV* conc. SN moderately induced luciferase activity (24 h incubation with *Wnt3a* CM alone resulted in an equal induction of luciferase activity, data not shown). This induction was significantly reduced by *Wif1* conc. SN comparable with 30 µg/ml rWif1 and to a lesser extent compared with 750 ng/ml rDkk1.

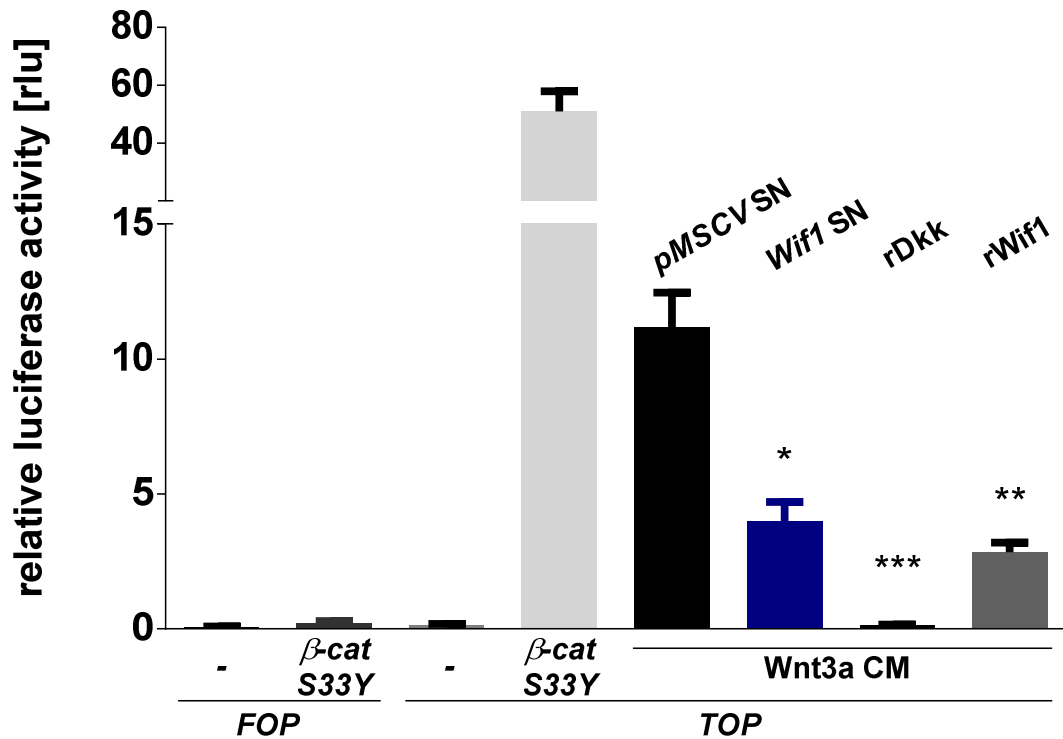


**Fig. 16: TOP/FOP reporter assay in HEK-293 cells incubated with Wnt3a and Wif1-concentrated supernatant**  
 As positive control HEK-293 cells were co-nucleofected with *SuperTOPFlash* (TOP) and *pCl-neo- $\beta$ -cateninS33Y* ( $\beta$ -cat S33Y). As negative control HEK-293 were co-nucleofected with *SuperFOPFlash* (FOP) and S33Y. HEK-293 cells only nucleofected with TOP or TOP transfected cells incubated with conditioned medium of untransfected L cells (L CM) were used as further controls. In addition, TOP nucleofected cells were incubated with Wnt3a conditioned medium from L cells stably expressing and secreting Wnt3a in order to activate canonical Wnt signaling driving luciferase expression (Wnt3a CM). Moreover, cells were incubated with concentrated supernatant from ASZ-pMSCV (pMSCV SN) and from ASZ-Wif1 (Wif1 SN), respectively. Firefly luciferase activity was normalized to *Renilla* luciferase activity, which is under CMV promoter control. As a control for efficient Wnt inhibition recombinant dickkopf1 protein (rDkk1) (750 ng/ml) and recombinant Wif1 protein (rWif1) (30  $\mu$ g/ml) were used. Firefly luciferase activity was normalized to *Renilla* luciferase activity. rlu: relative light units. All data are represented as mean + SEM. Statistical significance was tested using Mann-Whitney *U* test. \*  $p < 0.05$ , \*\*  $p < 0.005$ , \*\*\*  $p < 0.001$ .

Together, these data demonstrate that ASZ-Wif1 cells express and secrete functionally active Wif1.

### IV.3.2 Analysis of Hh and Wnt pathway activity and $\text{Ca}^{2+}$ measurement

*Axin2* and *Gli1* are considered as the most general and common target genes of active Wnt and Hh signaling, respectively. Analysis of ASZ-pMSCV

and ASZ-*Wif1* by means of qRT-PCRs showed no significant differences in expression levels of both genes (see Fig. 17).

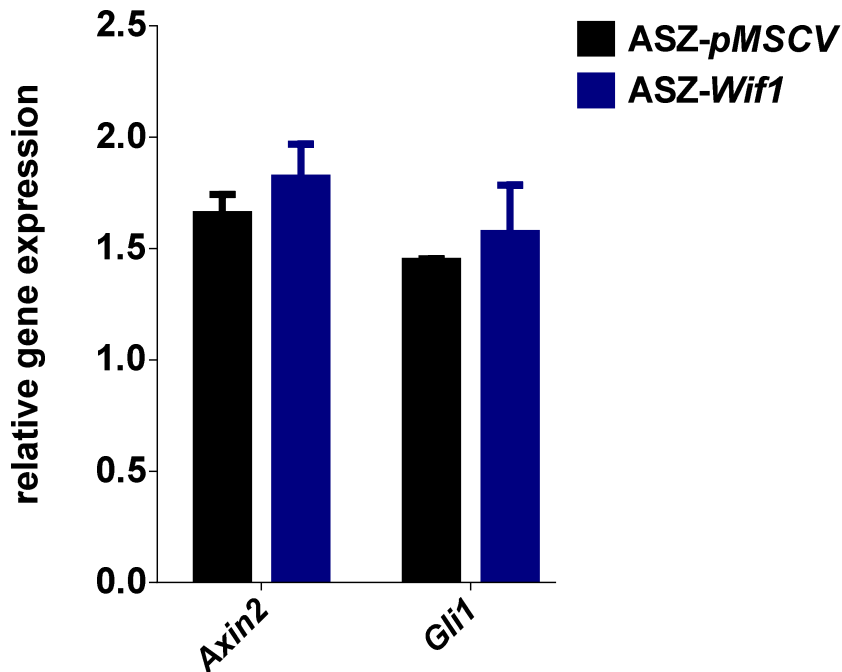
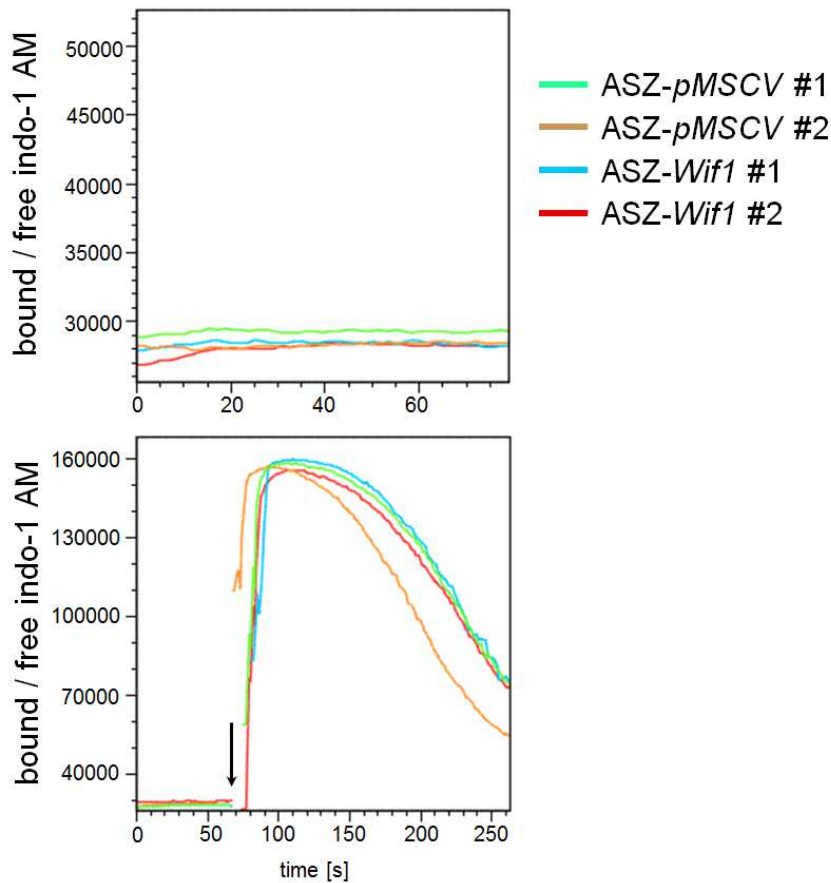


Fig. 17: qRT-PCR of *Axin2* and *Gli1* in ASZ-pMSCV and -*Wif1*

Relative *Axin2* and *Gli1* expression in ASZ-pMSCV and -*Wif1*. Values were normalized to *Hprt* expression. All data are represented as mean + SEM. Statistical significance was tested using Mann-Whitney *U* test.

However, as both cell lines do not feature *a priori* activated Wnt signaling, it cannot be ruled out that *Wif1* might have affected *Axin2* expression in an activated status of Wnt signaling. Unfortunately, Wnt3a transfected L cells do not secrete Wnt3a when cultured in 154 CF medium that is used to propagate ASZ001. *Vice versa*, ASZ001 differentiate in DMEM based medium due to high  $\text{Ca}^{2+}$  concentrations, biasing Wnt target gene expression analysis.

Next, the cytoplasmic  $\text{Ca}^{2+}$  concentrations as an indicator for active Wnt/ $\text{Ca}^{2+}$  signaling were examined. In addition the  $\text{Ca}^{2+}$  influx from ER into the cytoplasm was analyzed by  $\text{Ca}^{2+}$ -influx assay (see Fig. 18).



**Fig. 18: Ca<sup>2+</sup>-influx assay of ASZ-pMSCV and -Wif1**

Ratio of bound and free indo-1 AM was measured for 60 s to determine the basal Ca<sup>2+</sup> levels (top). After 60 s 1 µg/ml ionomycin was added (arrow) to establish a maximum Calcium flux ratio for each cell line (bottom).

However, neither the basal cytoplasmic Ca<sup>2+</sup> concentrations nor the maximum Ca<sup>2+</sup> flux ratio was altered in ASZ-Wif1 compared to ASZ-pMSCV.

#### **IV.4 Effect of Wif1 overexpression on various cellular processes of ASZ001 *in vitro***

Wif1 has been implicated in various cellular processes including the regulation of cell viability, apoptosis, migration, epithelial-to-mesenchymal transition (EMT), differentiation, cell cycle progression and proliferation. The impact of Wif1 on these processes was analyzed *in vitro* in ASZ-Wif1 and ASZ-pMSCV control cells.

#### IV.4.1 Effect of *Wif1* on cell viability *in vitro*

Cell viability was analyzed by WST-1 assay. 5.000 cells/well were seeded in 96-well plates and cultured for 48 h in total. Incubation for the last 24 h with 200 mM H<sub>2</sub>O<sub>2</sub> served as a control for reduced cell viability. WST-1 assay was performed 3 times in triplicates. As expected, incubation with 200 mM H<sub>2</sub>O<sub>2</sub> significantly reduced cell viability compared to untreated cells. However, no significant difference between the cell lines were detected, neither after incubation with H<sub>2</sub>O<sub>2</sub> nor between untreated ASZ-*pMSCV* and ASZ-*Wif1* cells (see Fig. 19; shown is a representative experiment).

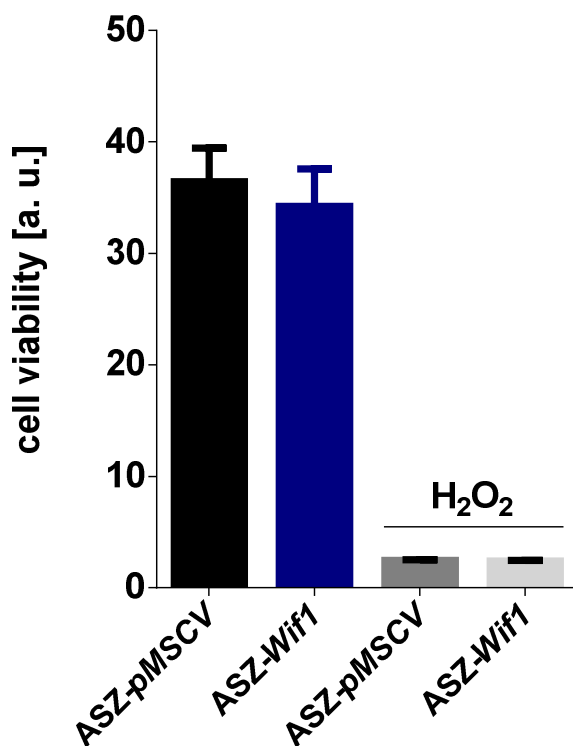


Fig. 19: WST-1 assay of ASZ-*pMSCV* and -*Wif1*

ASZ-*pMSCV* and -*Wif1* cells were cultured untreated in 154 CF supplemented with 2 % chelexed FCS and 1 % P/S for 48 h in total or treated for the last 24 h with 200 mM H<sub>2</sub>O<sub>2</sub> (H<sub>2</sub>O<sub>2</sub>). All data are represented as mean + SEM. [a. u.]: arbitrary units. Statistical significance was tested using Mann-Whitney *U* test.

#### IV.4.2 Effect of *Wif1* on apoptosis *in vitro*

In order to investigate the effect of *Wif1* on apoptosis *in vitro* we used an Annexin V assay as described in III.14.4.13. Shown is a representative experiment performed in duplicates. As a positive control 1 μM of the protein kinase inhibitor staurosporine (stauro) was applied for 24 h. Staurosporine

significantly induced apoptosis in both cell lines. However, no significant difference between ASZ-*pMSCV* and ASZ-*Wif1* cell lines was detected. The difference was also not significant when the values of untreated ASZ-*pMSCV* and ASZ-*Wif1* were compared (see Fig. 20).

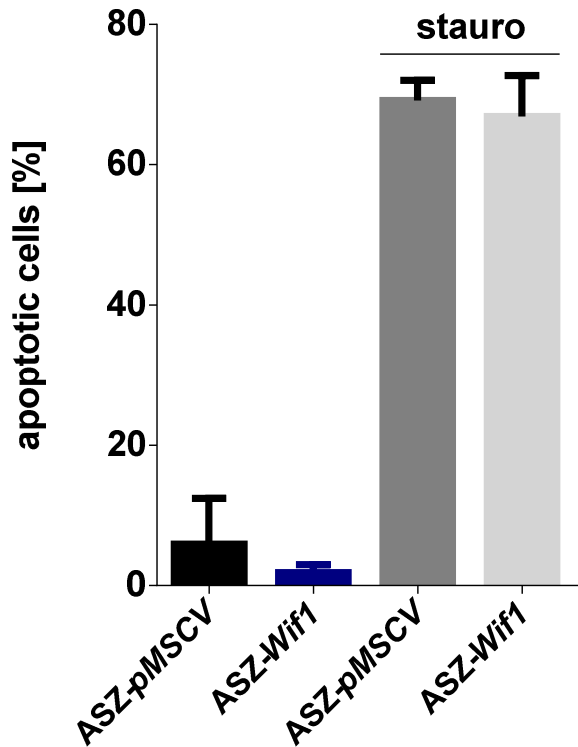


**Fig. 20: Annexin V assay of uninduced and staurosporine induced ASZ-*pMSCV* and -*Wif1***

Annexin V negative, propidium iodide (PI) positive cells were considered as necrotic (not shown). Annexin V negative, propidium iodide (PI) negative cells were considered as living cells (not shown). Annexin V positive cells were considered as apoptotic. Cells were treated either with DMSO or 1  $\mu$ M staurosporine (stauro) for 24 h. Respective proportion of cells that are apoptotic is given in percent. All data are represented as mean + SEM. Statistical significance was tested using Mann-Whitney *U* test.

#### IV.4.3 Effect of Wif1 on cell cycle regulation and proliferation *in vitro*

To analyze the effect of Wif1 on cell cycle regulation a PI staining was performed. Compared to ASZ-*pMSCV* the cell line ASZ-*Wif1* showed a tendency to accumulate in the G1 phase of the cell cycle. This resulted in a reduced proportion of cells in the G2/M phase (see Fig. 21), which, however, was statistically not significant.

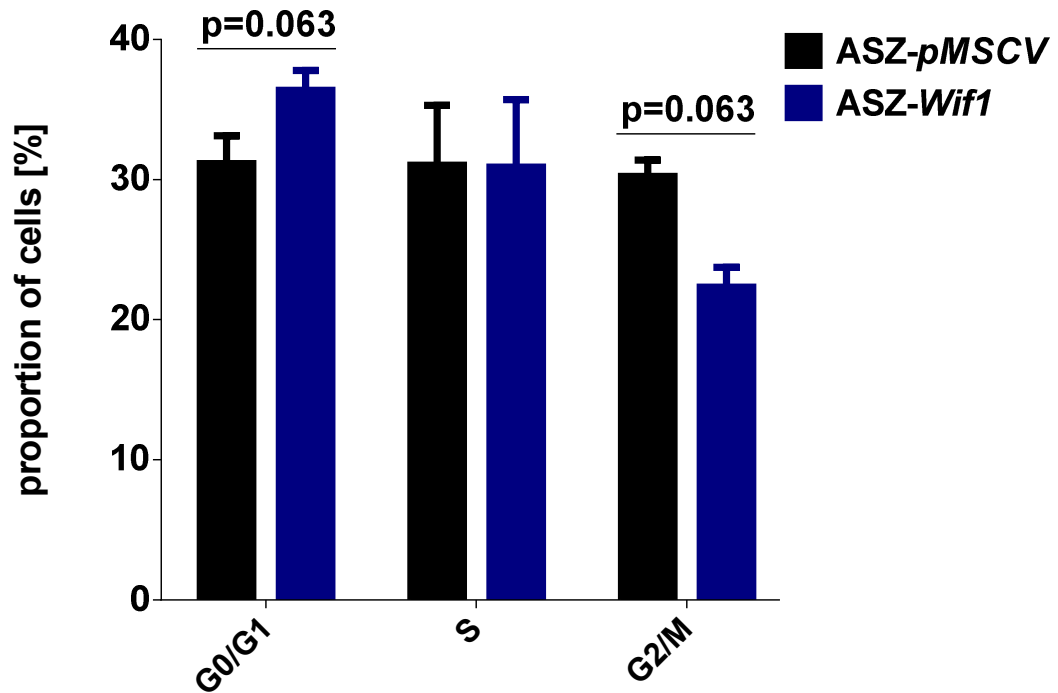


**Fig. 21: Distribution of ASZ-pMSCV and -Wif1 in respective phases of cell cycle**

All values represent the mean + SEM of 2 independent experiments performed in duplicates in G0/G1, S and G2/M phase of cell cycle. Statistical significance was tested using Wilcoxon test.

In order to investigate whether the accumulation of the cells in G1 was associated with changes in DNA replication, a BrdU assay was performed. The cells were cultured for 72 h and labelled with BrdU for the last 24 h. The analysis was conducted 3 times in sextuplicates. Shown is a representative experiment (see Fig. 22). However, there was no significant difference in cellular proliferation when comparing the values for ASZ-pMSCV and ASZ-Wif1.

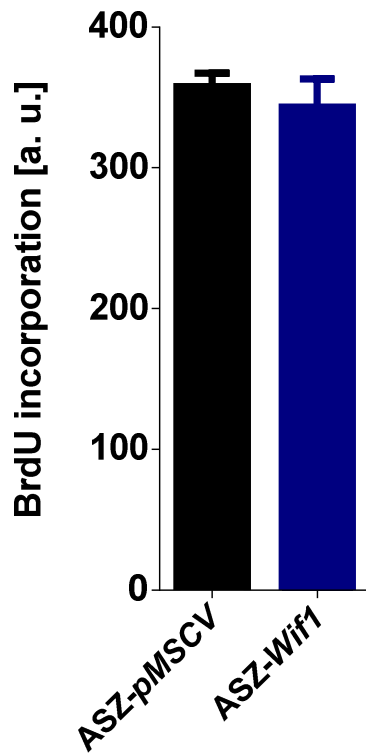


**Fig. 22: BrdU assay of ASZ-pMSCV and -Wif1**

ASZ-pMSCV and -Wif1 cells were cultured untreated in regular culture medium for 72 h. BrdU was added for the last 24 h. All data are represented as mean + SEM. Statistical significance was tested using unpaired t test with Welch's correction.

Moreover, ASZ-pMSCV and ASZ-Wif1 cells were cocultivated with Wnt3A L and L cells, with Wnt5a-NIH/3T3 and NIH/3T3 cells, with B9 (murine fibroblasts) and murine bone marrow derived macrophages (BMDMs). This allowed for examination of potential effects of Wif1 on cellular proliferation in response to cues derived from adjacent fibroblasts or macrophages. For this purpose, ASZ-pMSCV and ASZ-Wif1 were seeded in a 24-well plate. On the same day, the cell lines used for coculture were seeded in 24-well plate inserts and the inserts were placed in the 24-well plate. On each day of 5 consecutive days the cell numbers were counted using the CeligoS device and corresponding software, taking 24 serial images of each well (see Fig. 23).

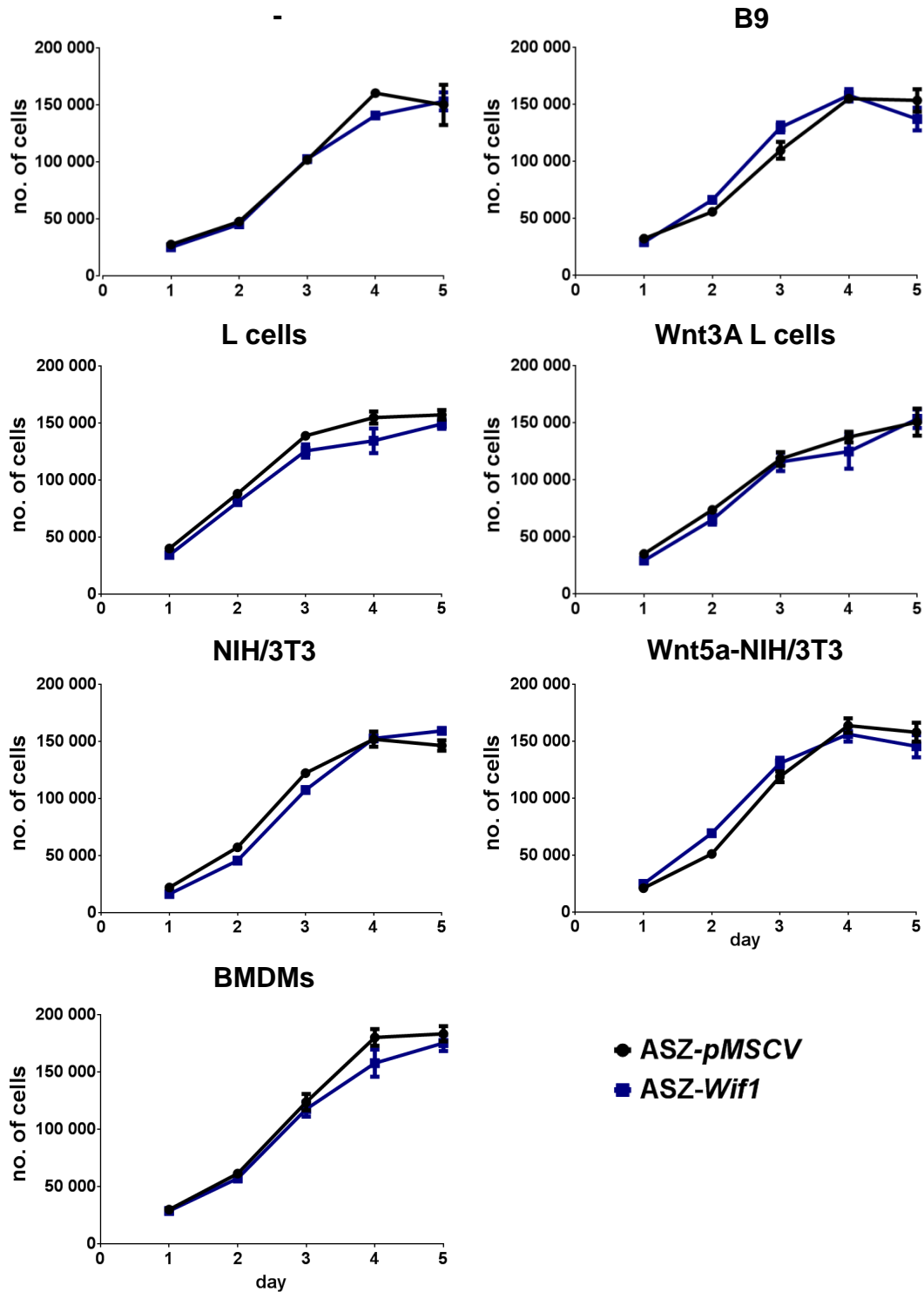


**Fig. 23: Cell proliferation assay of ASZ-*pMSCV* and ASZ-*Wif1* cocultured with B9, L cells, Wnt3A L cells, NIH/3T3, Wnt5a-NIH/3T3 or BMDMs**

ASZ-*pMSCV*, ASZ-*Wif1* and cocultured cells were seeded on day 0 in 24-well plates or 24-well plates inserts, respectively. Cells were counted each day of 5 consecutive days. All data are represented as mean  $\pm$  SEM.

ASZ-*pMSCV* and ASZ-*Wif1* cells showed an exponential growth and reached the plateau phase between day 4 and day 5. This was seen in all settings.

None of the cocultured cells elevated or decreased the proliferation of ASZ-*Wif1* when compared to ASZ-*pMSCV*.

In summary, these data suggest that *Wif1* does not alter the proliferative capacity of ASZ001 *in vitro*.

#### IV.4.4 Effect of *Wif1* on migration *in vitro*

As *Wif1* has also been shown to inhibit migration of several cancer cell lines (Yee *et al.* 2010; Vassallo *et al.* 2015), the migratory capacity of ASZ-*pMSCV* and ASZ-*Wif1* was investigated in a transwell migration assay (see Fig. 24). However, the migratory capacity of ASZ-*Wif1* cells did not show any significant difference compared to ASZ-*pMSCV* cells.

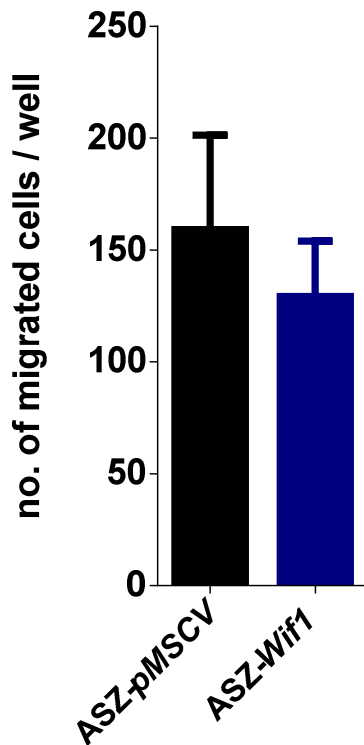


Fig. 24: Transwell migration assay of ASZ-*pMSCV* and -*Wif1*

Cells were seeded in 24-well plate inserts. 16 h later cells that had migrated through 8.0  $\mu\text{m}$  pores were counted. All data are represented as mean + SEM. Statistical significance was tested using Wilcoxon test.

#### IV.4.5 Effect of *Wif1* on differentiation *in vitro*

The cellular morphology of ASZ-*Wif1* and ASZ-*pMSCV* cells was examined microscopically. No obvious alterations in cell morphology were observed. Next, the expression of the differentiation markers *Krt1* and *Krt10* were

analyzed by means of qRT-PCR. *Krt1* was not expressed and *Krt10* expression was not changed significantly in ASZ-*Wif1* compared to ASZ-*pMSCV*.

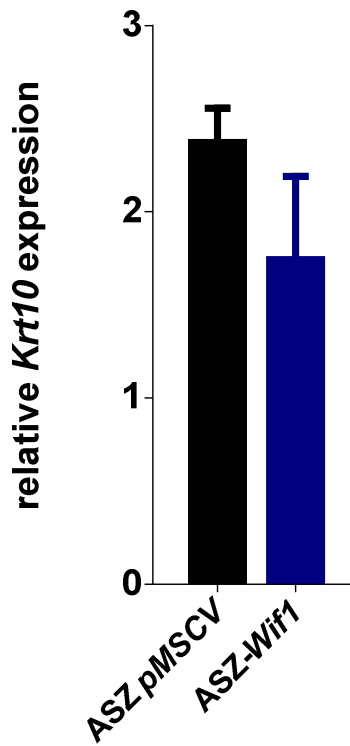


Fig. 25: qRT-PCR of *Krt10* in ASZ-*pMSCV* and -*Wif1*

Relative *Krt10* expression in ASZ-*pMSCV* and -*Wif1*. Values were normalized to *Hprt* expression. All data are represented as mean + SEM. Statistical significance was tested using Mann-Whitney *U* test.

## IV.5 Effect of *Wif1* *in vivo*

In order to investigate the influence of *Wif1* on BCC growth in mice,  $1 \cdot 10^6$  cells of both cell lines suspended in matrigel were subcutaneously transplanted in the flanks of nude mice. In order to exclude individual mouse effects, each mouse was injected with 200  $\mu$ l of ASZ-*pMSCV* and ASZ-*Wif1* cell suspension in matrigel on the left and right flank, respectively. When reaching a size of 5 mm, tumor size was measured every second day using a caliper. Measurement was conducted until general health conditions or tumor size required the termination of the experiment. The age of the 17 mice upon transplantation was 10 weeks.

As demonstrated in Fig. 26, the minimum size of the tumors (i.e. 5 mm) was generally reached at day 17 after transplantation. Then the tumors showed an approximately exponential growth until day 33 after injection. Tumors that arose from transplanted ASZ-*pMSCV* cells grew significantly faster compared to tumors that originated from ASZ-*Wif1* cells (see Fig. 26). Indeed, the size of ASZ-*pMSCV*-derived tumors was significantly larger at any time point during measurement.

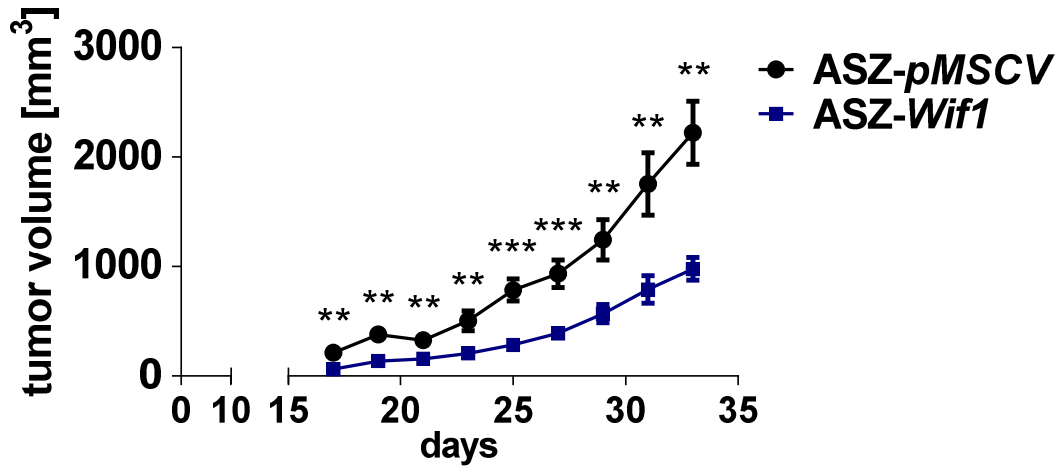


**Fig. 26: Growth curve of ASZ-*pMSCV* and ASZ-*Wif1* allografts in nude mice**

$1 \cdot 10^6$  cells in a 200  $\mu$ l cell suspensions in matrigel of either ASZ-*pMSCV* or ASZ-*Wif1* were injected in the left or right flank, respectively, in 17 nude mice. After the tumors reached a minimum diameter of 5 mm the tumor size were measured every other day. All data are represented as mean  $\pm$  SEM. Statistical significance was tested using Wilcoxon test. \*\*  $p < 0.005$ , \*\*\*  $p < 0.001$ .

The significant difference in tumor sizes was also reflected by a significantly reduced tumor weight of tumors originating from transplanted ASZ-*Wif1* cells. (see Fig. 27).

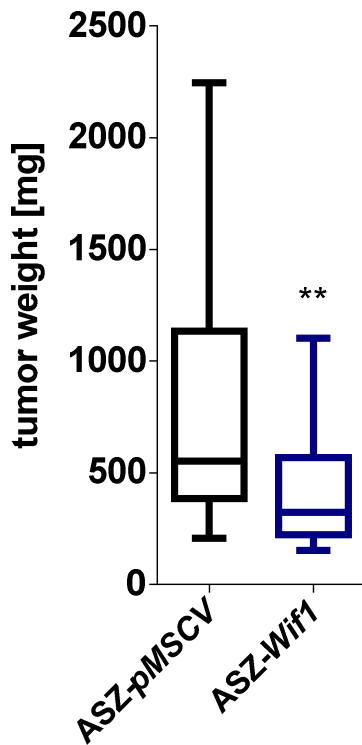


**Fig. 27: Tumor weight of ASZ-*pMSCV* and ASZ-*Wif1* allografts after dissection**

$1 \cdot 10^6$  cells in a 200  $\mu$ l cell suspensions in matrigel of either ASZ-*pMSCV* or ASZ-*Wif1* were injected in the left or right flank, respectively, in 17 nude mice. After the termination of the experiment, tumors were removed and weighed. All data are represented as a box-whisker plot: median (horizontal line), 25-75 percentile (box), 5-95 percentile (whiskers). Statistical significance was tested using Wilcoxon test. \*\*  $p < 0.005$ .

Similar results were obtained when  $1 \cdot 10^6$  cells originating from 3 different single cell clones of both cell lines (see section IV.2.2 and Fig. 13) were transplanted (data not shown).

In Fig. 28 representative images of H&E stainings of ASZ-*pMSCV* and ASZ-*Wif1* derived allografts are depicted. Both groups of allografts show growth of tumor nodules surrounded by stroma, spots of differentiation in form of keratinization (arrows) and areas of necrosis (asterisks) (see Fig. 28).

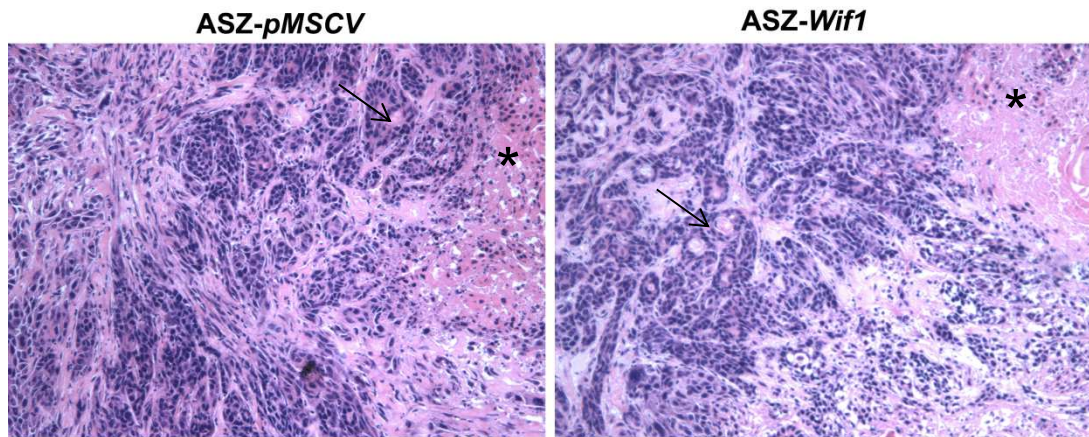


**Fig. 28: H&E stainings of ASZ-pMSCV and ASZ-Wif1 allografts**

Arrows indicate spots of keratinization. Asterisks indicate necrotic areas.

In order to rule out that the difference in tumor size between ASZ-pMSCV and ASZ-Wif1 derived tumors was not simply caused by swelling of ASZ-pMSCV allografts due to increased keratinization and necrosis, the areas which were clearly necrotic or keratinous were subtracted from the total tumor area. This was done on serial images using the software cellSens. Fig. 29 shows two examples of the total tumor (overlay of serial images). The red lines indicate the borders of vital tumor tissue and necrotic/keratinous areas.

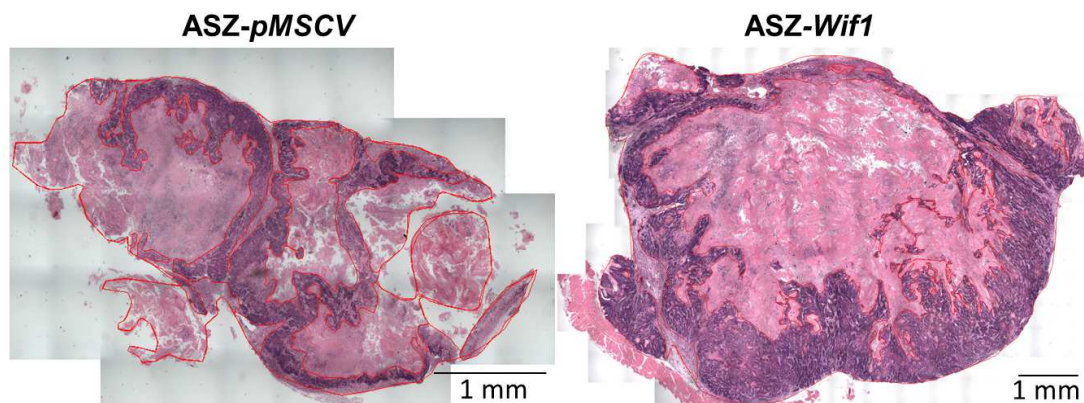


**Fig. 29: Total sections of ASZ-pMSCV and ASZ-Wif1 allografts**

Necrotic and keratinous areas were encircled and separated from the total tumor areas by red lines. Image acquisition, image overlay and area demarcation were performed using cellSens software.

The proportion of necrotic and keratinous areas in ASZ-pMSCV allografts was moderately decreased compared to ASZ-Wif1 allografts. However, this difference was statistically not significant (see Fig. 30).

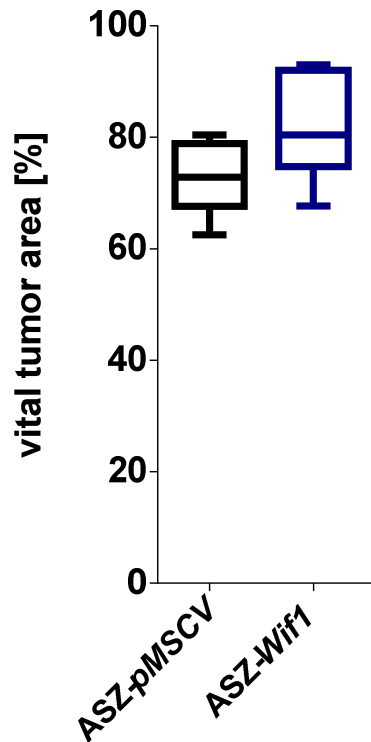


**Fig. 30: Vital tumor area of ASZ-pMSCV and ASZ-Wif1 allografts**

Necrotic and keratinous areas were measured and subtracted from total tumor area of 7 different ASZ-pMSCV and ASZ-Wif1 derived tumors. Image acquisition and area calculation was performed using cellSens software. All data are represented as a box-whisker plot: median (horizontal line), 25-75 percentile (box), 5-95 percentile (whiskers). Statistical significance was tested using Wilcoxon test.

#### **IV.5.1 Effect of Wif1 on Hh, Wnt and Akt signaling pathways *in vivo***

In order to analyze the effect of Wif1 overexpression on Wnt and Hh signaling, target gene expression analysis of both pathways was performed. Ten tumor samples from each group (i.e. ASZ-pMSCV and ASZ-Wif1 derived tumors) were analyzed.

When the Hh target *Gli1* was measured, the tumors did not show different levels of *Gli1* expression indicating comparable Hh signaling activity in ASZ-pMSCV and ASZ-Wif1 allografts (see Fig. 31).

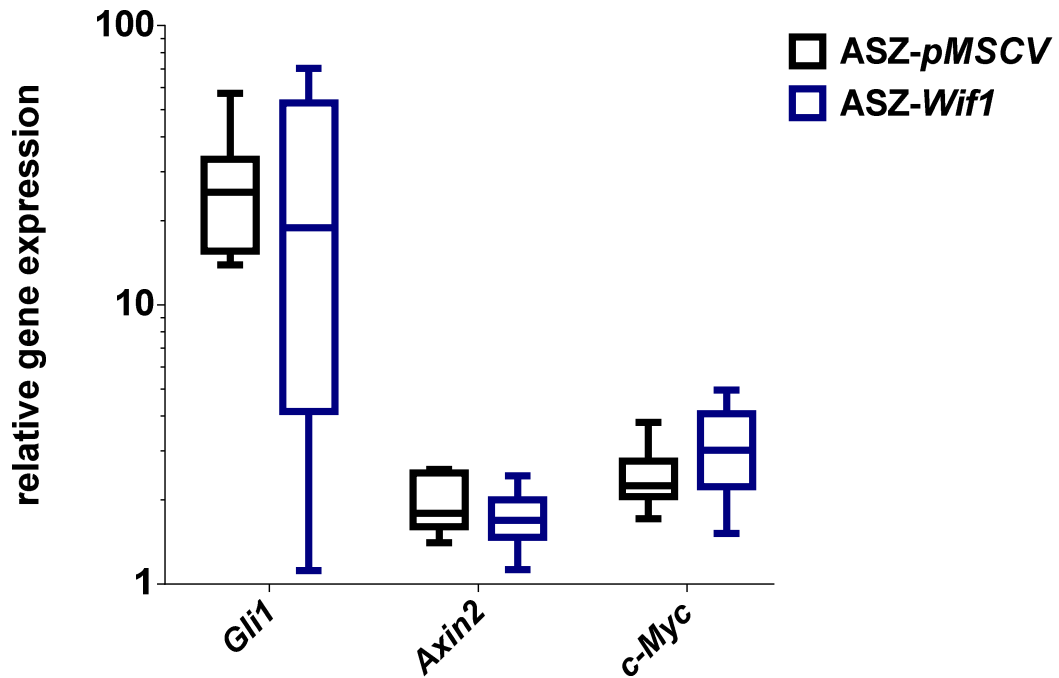


**Fig. 31: qRT-PCR of *Gli1*, *Axin2* and *c-Myc* expression in ASZ-pMSCV and ASZ-Wif1 allografts**

Each bar summarizes data of 10 individual ASZ-pMSCV or ASZ-Wif1 derived tumors. Values were normalized to *Hprt* expression. Statistical significance was tested using Wilcoxon test. All data are represented as a box-whisker plot: median (horizontal line), 25-75 percentile (box), 5-95 percentile (whiskers). Statistical significance was tested using Wilcoxon test.

Similarly, Wif1 overexpression did not influence the expression of *c-Myc* and *Axin2*. This indicates that canonical Wnt signaling was not affected (see Fig. 31). Moreover, translocation of  $\beta$ -catenin into the nucleus, which is a hallmark of active canonical Wnt signaling, was investigated. For this purpose, antibody staining of  $\beta$ -catenin was performed.

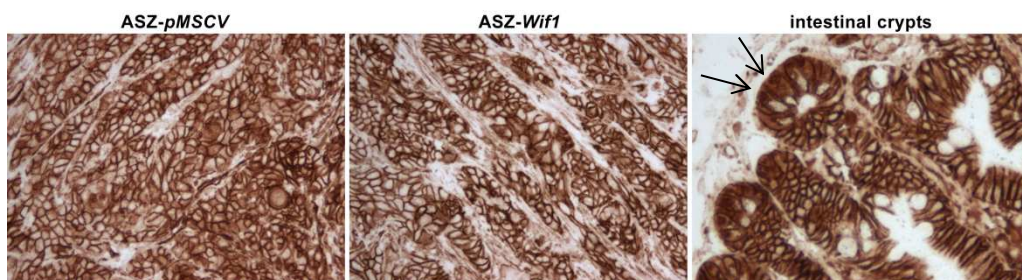


**Fig. 32: Antibody staining of  $\beta$ -catenin in ASZ-pMSCV and ASZ-Wif1 allografts**

Anti- $\beta$ -catenin antibody staining of paraffin sections derived from ASZ-pMSCV and ASZ-Wif1 allografts. Images were taken at 100-fold magnification. Intestinal crypts served as positive control for nuclear staining of  $\beta$ -catenin (arrows). Staining reaction was performed using DAB+.

As shown in Fig 32, Wif1 also did not affect  $\beta$ -catenin translocation. Together, absent nuclear  $\beta$ -catenin staining and unchanged target gene expressions in ASZ-*pMSCV* and ASZ-*Wif1* derived allografts indicate that Wif1 does not affect canonical Wnt signaling.

Next, the phosphorylation status of JNK and CaMKII was examined, which are targets of the  $\beta$ -catenin-independent (i.e. non-canonical) Wnt/PCP and Wnt/Ca<sup>2+</sup> signaling pathways, respectively. Besides allografts I also analyzed the phosphorylation status of the proteins in the respective parental cell lines. Neither JNK nor CaMKII showed significant phosphorylation compared to the positive controls indicating that both kinases are inactive both *in vitro* and *in vivo* in allografts.

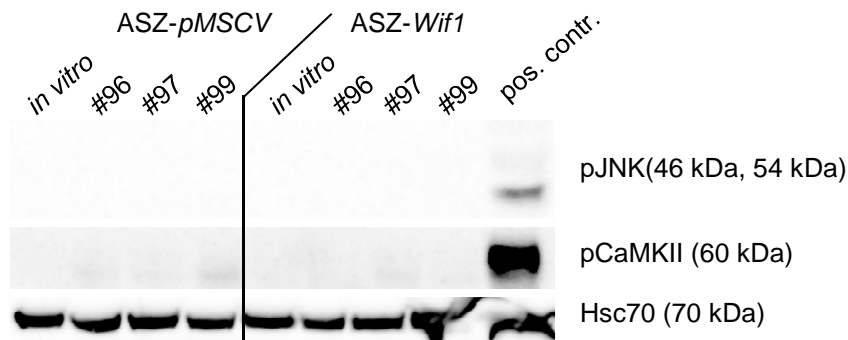


**Fig. 33: Western blot of pJNK and pCaMKII in ASZ-*pMSCV* and ASZ-*Wif1* allografts**

Protein samples from ASZ-*pMSCV* and ASZ-*Wif1* *in vitro* cultures (*in vitro*) and from allografts of the three mice #96, 97 and 99 (#96, 97 and 99) were analyzed. pJNK antibody detects phosphorylated SAPK/JNK (Mapk8/9) protein with the size of 46 kDa and 54 kDa. pCaMKII antibody detects phosphorylated CaMKII protein with the size of 50 kDa (data not shown) and 60 kDa. Hsc70 served as loading control.

As discussed later Wif1 was described to bind several EGF receptors. For this reason, the phosphorylation status of several proteins involved in EGFR signaling was analyzed. Fig. 34 shows the phosphorylation status of Akt and of S6. S6 is a target of mTOR which in turn can be activated by Akt. As shown in Fig. 34 Akt is unphosphorylated in ASZ-*pMSCV* and ASZ-*Wif1* *in vitro* samples. In contrast, the individual allograft samples showed elevated phosphorylation levels compared with *in vitro* samples. However, they exhibit a very heterogeneous protein expression and protein phosphorylation pattern, which was not clearly different between ASZ-*pMSCV* and ASZ-*Wif1* derived allografts. The same was true for the Akt/mTOR downstream target

S6. Therefore, the data suggest that Wif1 overexpression does not significantly alter Akt/mTOR signaling activity.

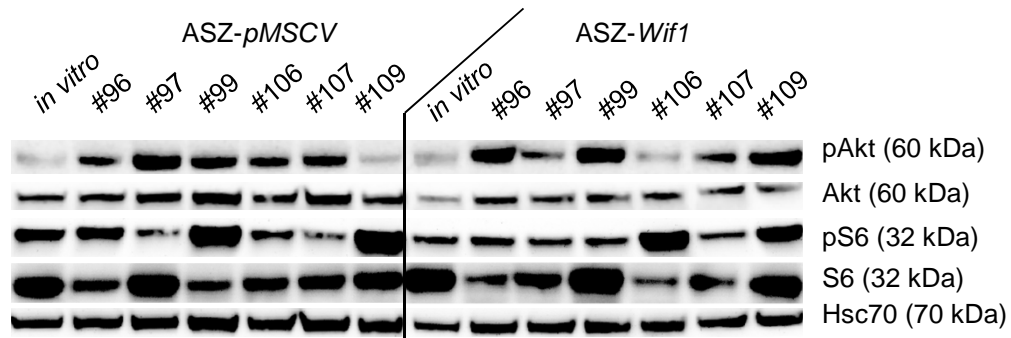


**Fig. 34: Western blot of pAkt, Akt, pS6 and S6 in ASZ-pMSCV and ASZ-Wif1 allografts**

Protein samples from ASZ-pMSCV and ASZ-Wif1 *in vitro* cultures (*in vitro*) and from allografts of the six mice #96, 97, 99, 106, 107 and 109 (#96, 97, 99, 106, 107 and 109) were analyzed. pAkt antibody detects phosphorylated Akt and Akt antibody detects total Akt protein with a size of 60 kDa. pS6 antibody detects phosphorylated S6 and S6 antibody detects total S6 protein with a size of 32 kDa. Hsc70 served as loading control. Please note that Hsc70 loading control in this Figure is identical with that in Fig. 36 and Fig. 46 as all proteins were detected using the same membrane.

Beside S6 and Akt, the additional downstream effectors of EGFR signaling PKC and Erk1/2 were examined regarding their phosphorylation status. The ASZ-Wif1 cell line (*in vitro*; see Fig. 35) showed an elevated phosphorylation level of PKC compared with the ASZ-pMSCV cell line. Moreover, PKC phosphorylation was maintained in ASZ-Wif1 derived allografts. In ASZ-pMSCV allografts the phosphorylation status remained at low levels comparable with the *in vitro* sample (see Fig. 35).

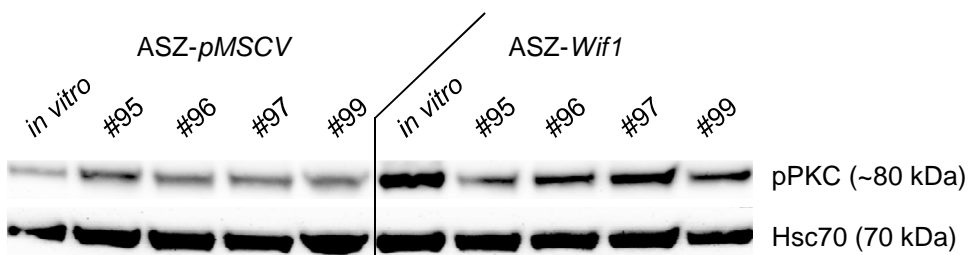


**Fig. 35: Western blot of pPKC in ASZ-pMSCV and ASZ-Wif1**

Protein samples from ASZ-pMSCV and ASZ-Wif1 *in vitro* cultures (*in vitro*) and from allografts of the four mice #95, 96, 97 and 99 (#95, 96, 97 and 99) were analyzed. Pan pPKC antibody detects phosphorylated forms of PKC protein with a size of 78-82 kDa. pErk1 and 2 antibody detects phosphorylated Erk1 and 2 protein with a size of 44 and 42 kDa, respectively. Erk1 and 2 antibody detects total Erk1 and 2 protein with a size of 44 and 42 kDa, respectively. Hsc70 served as loading control.

The total amounts of Erk1 and Erk2 were at comparable levels in all analyzed *in vitro* and *in vivo* samples, except for ASZ-*pMSCV* and ASZ-*Wif1* allografts from mouse #109 showing relatively low total Erk1 and Erk2 expression levels (see Fig. 36). Moreover, the total expression of Erk2 seemed to be higher than total expression of Erk1 in all samples, provided that the antibody has equal binding affinities to both proteins. The phosphorylation of Erk2 in both *in vitro* samples was at comparable levels. In the allografts, the phosphorylation of Erk2 seemed to be slightly increased in most ASZ-*Wif1* derived samples (#96, 99, 106, 107 and 109) compared with ASZ-*pMSCV* allografts. Interestingly, the phosphorylation of Erk1 was slightly increased in the ASZ-*Wif1* cell line compared to the ASZ-*pMSCV* cell line. When the cell lines were transplanted Erk1 phosphorylation was reduced in ASZ-*pMSCV* allografts but was maintained in ASZ-*Wif1* allografts.

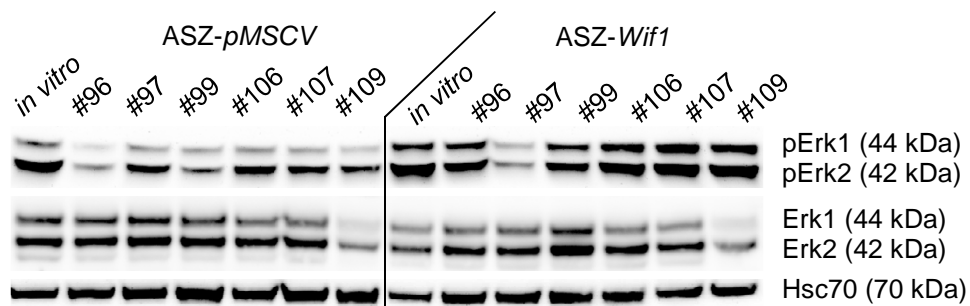


**Fig. 36: Western blot of pErk1 and 2 and Erk1 and 2 in ASZ-*pMSCV* and ASZ-*Wif1* allografts**

Protein samples from *in vitro* cultures and from allografts (#96-109) were analyzed. pPKC antibody detects phosphorylated forms of PKC protein with a size of 78-82 kDa. pErk1 and 2 antibody detects phosphorylated Erk1 and 2 protein with a size of 44 and 42 kDa, respectively. Erk1 and 2 antibody detects total Erk1 and 2 protein with a size of 44 and 42 kDa, respectively. Hsc70 served as loading control. Please note that Hsc70 loading control in this Figure is identical with that in Fig. 34 and with that in Fig.46 as all proteins were detected using the same membrane.

Together, these results suggest that *Wif1* overexpression in ASZ001 cells results in the maintenance of PKC and Erk1/2 phosphorylation after transplantation in nude mice.

#### IV.5.2 Cellular response on *Wif1 in vivo*

As *Wif1* reduced the growth of ASZ derived allografts (see Fig. 26), the differentiation status, apoptosis, the deposition of extracellular matrix, vascularization and proliferation of the tumors were analyzed.

### IV.5.2.1 Effect of *Wif1* on differentiation *in vivo*

The expression of early and late markers for differentiation of keratinocytes was analyzed by qRT-PCR and the proportion of keratin in the allografts was measured using the cellSens software.

The markers for early differentiation, *loricrin* (*Lor*) and *involucrin* (*Ivl*), as well as the markers for late differentiation, *keratin 1* and *10* (*Krt1* and *Krt10*), did not show any significant differences in expression levels when the data of 10 individual ASZ-*pMSCV* or ASZ-*Wif1* allografts were compared (see Fig. 37).

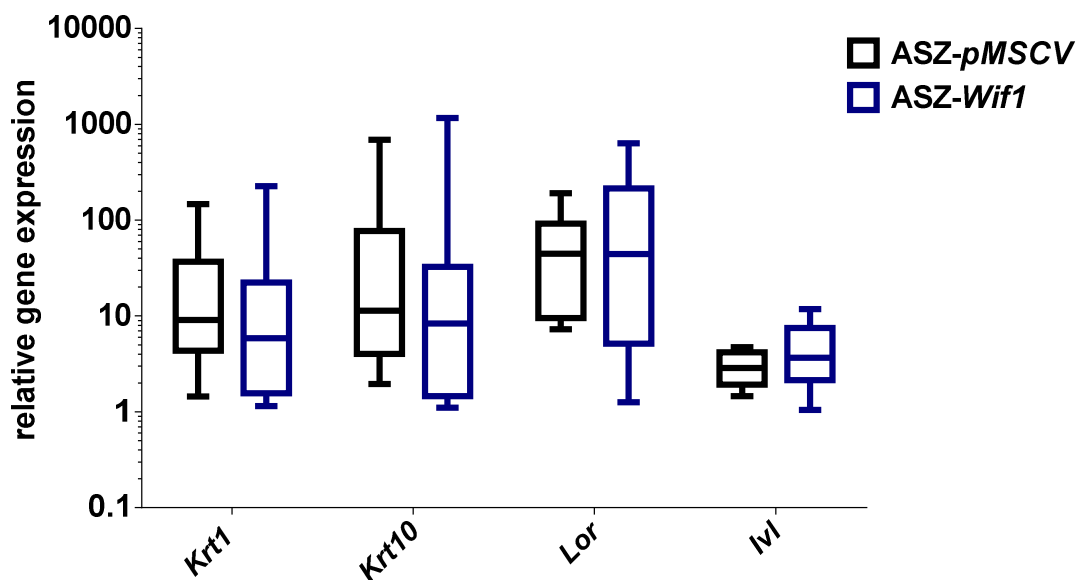
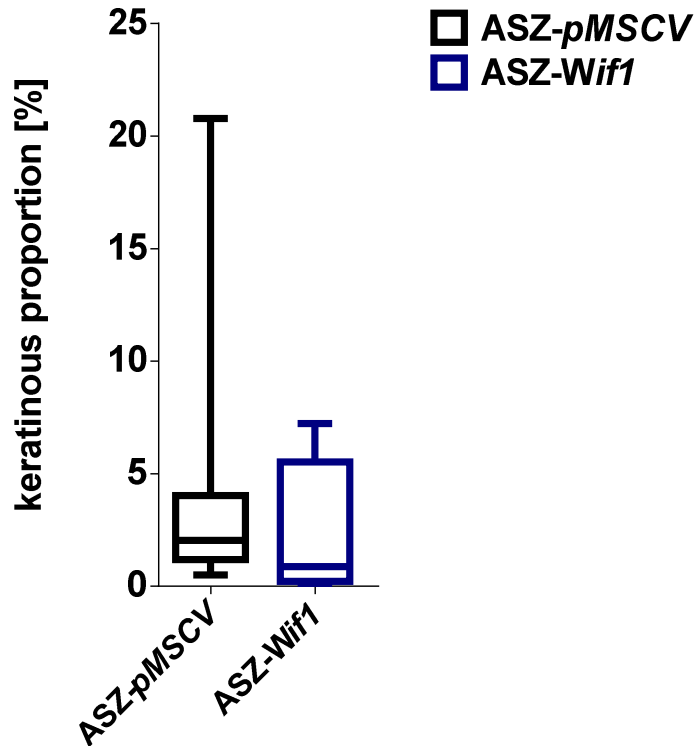


Fig. 37: qRT-PCRs of early and late keratinocyte differentiation markers in ASZ-*pMSCV* and ASZ-*Wif1* allografts

Each bar summarizes data of 10 individual ASZ-*pMSCV* or ASZ-*Wif1* derived tumors. Statistical significance was tested using Wilcoxon test. All data are represented as a box-whisker plot: median (horizontal line), 25-75 percentile (box), 5-95 percentile (whiskers). Statistical significance was tested using Wilcoxon test.

In order to determine the proportion of keratin in the allografts, keratinous areas were subtracted from vital tumor area of H&E stained paraffin sections using cellSens software. For this purpose, 3 pictures each derived from either 16 ASZ-*pMSCV* or 16 ASZ-*Wif1* tumors were analyzed. However no significant difference between allografts was detected (see Fig. 38).



**Fig. 38: Proportion of keratinous tissue in ASZ-pMSCV and ASZ-Wif1 allografts**

Proportion of keratin in % was measured in H&E stained paraffin sections by means of cell sense software. Each plot summarizes values from 3 images each derived from 16 individual tumors. Statistical significance was tested using Mann-Whitney *U* test. All data are represented as a box-whisker plot: median (horizontal line), 25-75 percentile (box), 5-95 percentile (whiskers). Statistical significance was tested using Wilcoxon test.

#### IV.5.2.2 Effect of Wif1 on EMT marker gene expression *in vivo*

Since Wif1 can induce a reversal of EMT in prostate cancer cells (Yee *et al.* 2010), the expression of *Cdh1*, *Cdh2* and *Fn1* was analyzed by means of qRT-PCR. While upregulation of *Cdh1* is indicative for the induction of epithelial cell fate, *Cdh2* and *Fn1* expressions are associated with EMT. However, as demonstrated in Fig. 39, none of the examined transcripts was differentially expressed in ASZ-pMSCV or ASZ-Wif1 derived allografts.

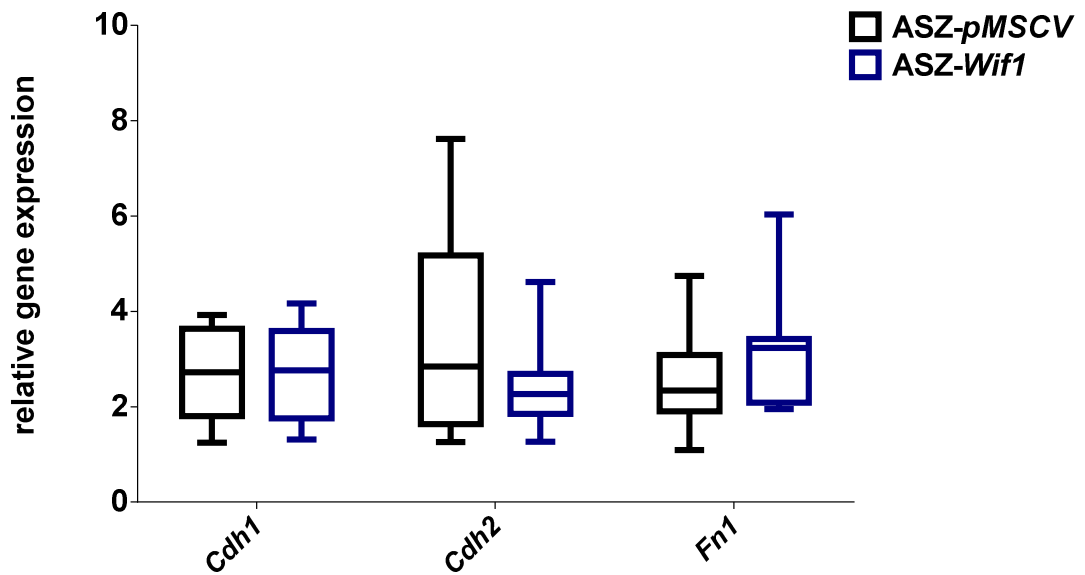


**Fig. 39: qRT-PCRs of EMT markers in ASZ-pMSCV and ASZ-Wif1 allografts**

Each plot summarizes values from 10 individual ASZ-pMSCV and ASZ-Wif1 allografts each. Statistical significance was tested using Wilcoxon test. All data are represented as a box-whisker plot: median (horizontal line), 25-75 percentile (box), minimum and maximum values (whiskers). Statistical significance was tested using Wilcoxon test.

### IV.5.2.3 Effect of Wif1 on vascularization

Vascularization can restrict growth and size of tumors as it limits the supply with nutrients. To investigate whether Wif1 alters the vascularization of the tumors, paraffin sections were stained with an antibody against CD34, which is a marker for vascular endothelial cells. Counting the vessels per vision field revealed no significant difference between ASZ-pMSCV and ASZ-Wif1 allografts (see Fig. 40).

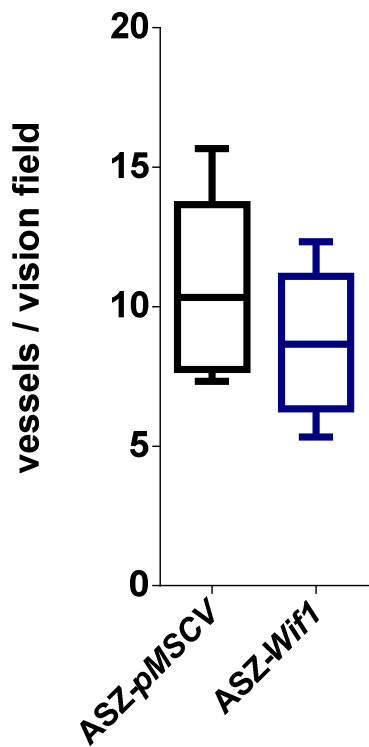


**Fig. 40: Number of CD34 positive blood vessels in ASZ-pMSCV and ASZ-Wif1 allografts**

Number of blood vessels was counted on paraffin sections stained with an anti CD34 antibody. Analyzed were 3 images of 8 allograft samples each. Statistical significance was tested using Mann-Whitney test. All data are represented as a box-whisker plot: median (horizontal line), 25-75 percentile (box), minimum and maximum values (whiskers). Statistical significance was tested using Wilcoxon test.

#### IV.5.2.4 Effect of Wif1 on cell death *in vivo*

Since apoptosis could have been causative for reduced growth of ASZ-Wif1 derived allografts, Western blot detecting cleaved Caspase 3 in protein lysates and TUNEL and p53 staining using paraffin sections from ASZ-pMSCV and ASZ-Wif1 allografts were performed. Cleavage of Caspase 3 and nuclear localization of p53 indicate the induction of apoptosis. Moreover, when cells undergo apoptosis, fragmentation of DNA occurs, which can be visualized by TUNEL.

When the cleavage of Caspase 3 was analyzed, no obvious differences between ASZ-pMSCV and ASZ-Wif1 allografts could be detected (see Fig. 41). Furthermore, neither the percentage of cells positive for nuclear p53 (see Fig. 42) nor TUNEL (see Fig. 43) revealed significant differences between ASZ-pMSCV and ASZ-Wif1 derived allografts.

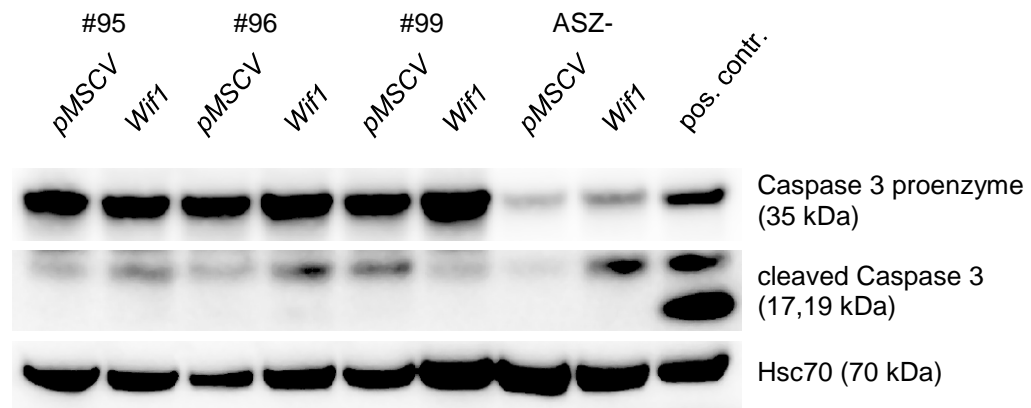


**Fig. 41: Western blot of Caspase 3 in ASZ-pMSCV and ASZ-Wif1 allografts**

Protein samples from *in vitro* cultures and from allografts (#95, 96, and 99) were analyzed. Caspase 3 antibody detects total Caspase 3 proenzyme protein with a size of 35 kDa and the cleaved Caspase 3 at a size of 17 and 19 kDa. Hsc70 served as loading control.

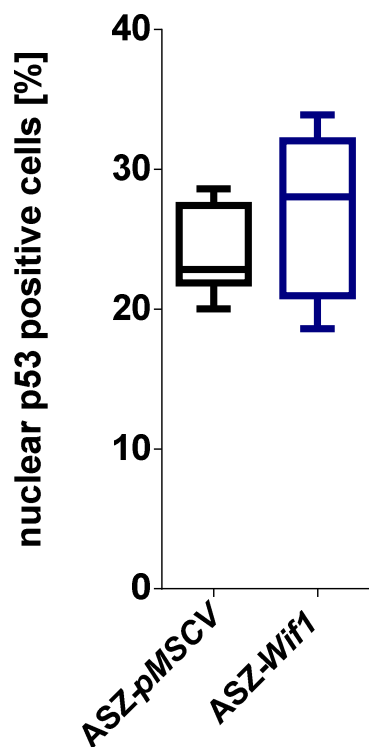


**Fig. 42: Nuclear p53 staining of ASZ-pMSCV and ASZ-Wif1 allografts.**

Proportion of nuclear p53 staining was calculated using the FIJI software. Analyzed were 3 images of 7 allograft samples each. All data are represented as a box-whisker plot: median (horizontal line), 25-75 percentile (box), 5-95 percentile (whiskers). Statistical significance was tested using Wilcoxon test.

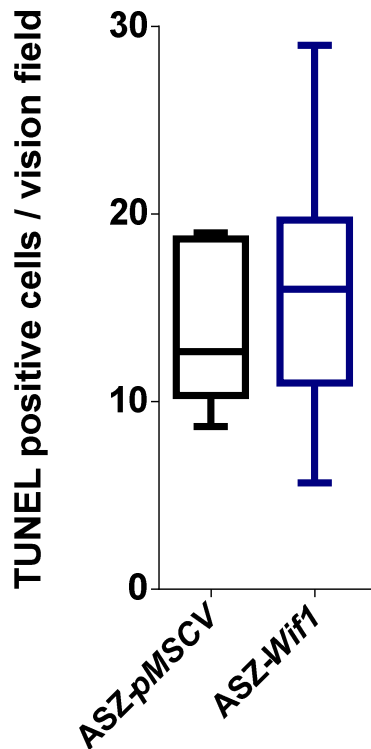


**Fig. 43: TUNEL staining of ASZ-pMSCV and ASZ-Wif1 allografts**

Number of positive cells staining was calculated using the Alpha View software. Analyzed were 3 images of 7 allograft samples each. All data are represented as a box-whisker plot: median (horizontal line), 25-75 percentile (box), 5-95 percentile (whiskers). Statistical significance was tested using Wilcoxon test.

Together, these data show that induction of apoptosis is not the mechanism underlying reduced tumor growth of ASZ-*Wif1* allografts.

#### **IV.5.2.5 Effect of Wif1 on deposition of extracellular matrix *in vivo***

Remodelling of extracellular matrix (ECM) is necessary for tumor cell migration and metastasis. However, whether ECM is protective or not is highly context specific and depends on the composition of ECM components (Honma *et al.* 2007; Fullar *et al.* 2015). To investigate whether Wif1 changes the global deposition of collagen which is a main component of the ECM, Ladewig staining of paraffin sections was performed in the Department of Neuropathology, University Medical Center Göttingen. This method results in blue coloring of collagens. Shown in Fig. 44 are examples of paraffin sections

from ASZ-*pMSCV* and ASZ-*Wif1* derived allografts (top row). The collagen was stained in blue and after image software based extraction of the blue channel a black and white image was generated (bottom row) allowing for automated quantification of the collagen proportion using FIJI software (see Fig. 44).

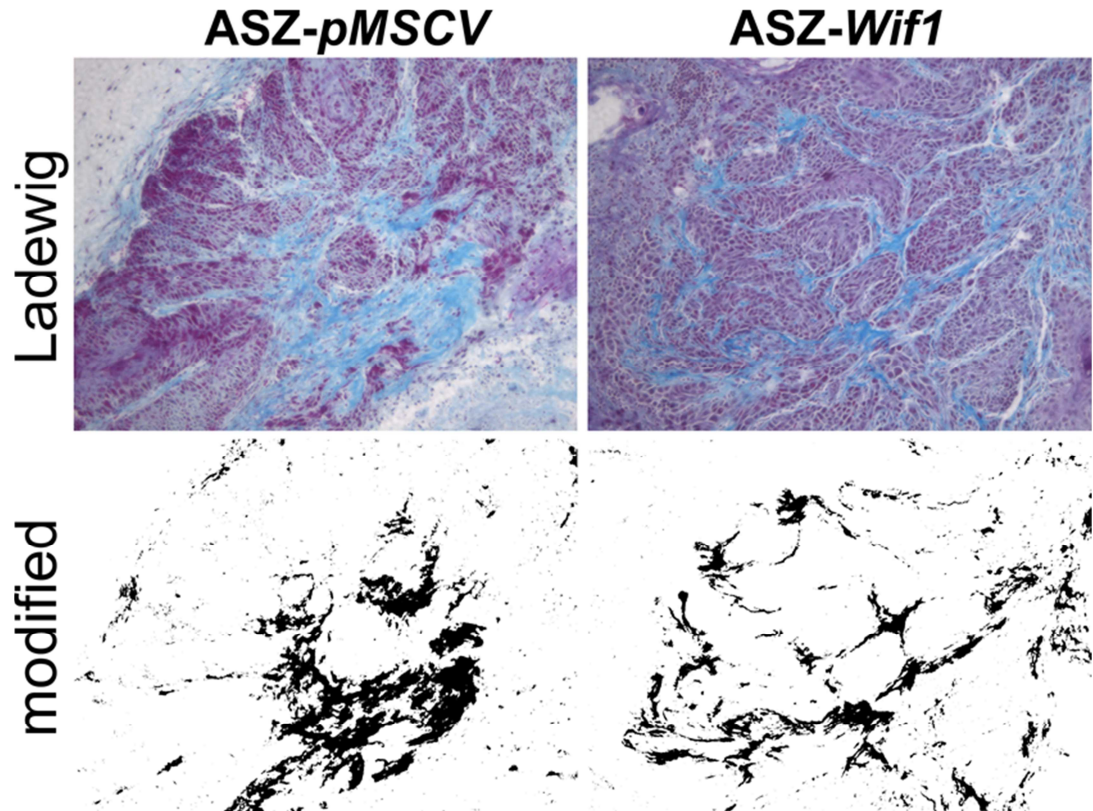


**Fig. 44: Ladewig staining of ASZ-*pMSCV* and ASZ-*Wif1* allografts**

Ladewig staining of paraffin sections of ASZ-*pMSCV* and ASZ-*Wif1* allografts was performed according to standard protocols. Collagens are stained in blue (top row). Using image software FIJI the blue channel was extracted and a black and white image was generated (bottom row).

Since the tumors also contained necrotic areas (see Fig. 28), the proportion of collagen within the vital as well as in the necrotic tumor tissue was calculated. Shown in Fig. 45 is the mean proportion of collagen per vision field and the 95% confidence interval (CI). In both, the viable tumor areas and necrotic areas, ASZ-*Wif1* derived allografts exhibited an increased proportion of collagen. However, this was only significant for the necrotic areas.

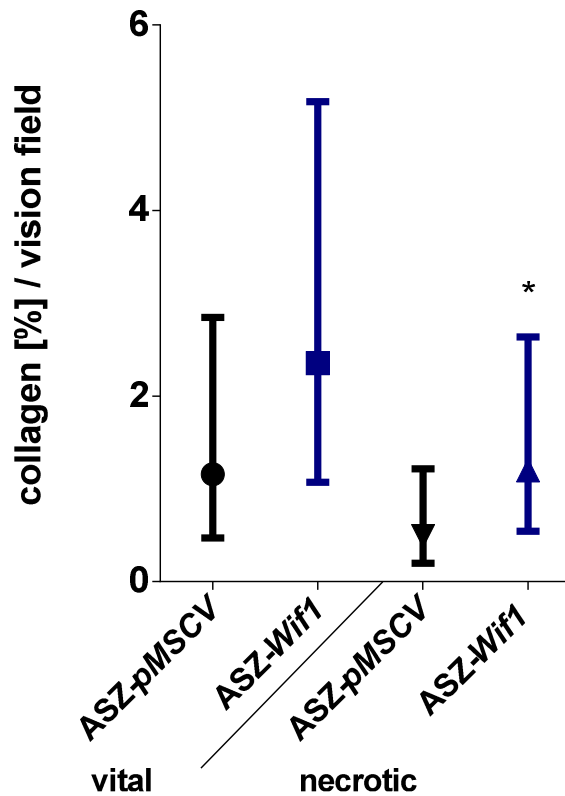


**Fig. 45: Collagen proportion in ASZ-pMSCV and ASZ-Wif1 allografts**

Using image software FIJI the proportion of blue stained collagen was calculated for each image. Each value represents the mean and the 95% CI of 11 tumors for which 3 images each were analyzed. Statistical significance was tested using mixed linear model. \*  $p < 0.05$ .

As Wif1 can bind to HSGPs in the extracellular space we speculated whether Sdc-2, a main component of HSPGs, is also affected by Wif1 overexpression. For this purpose, a Western blot was performed (see Fig. 46). In both *in vitro* samples no Sdc-2 expression was detectable.

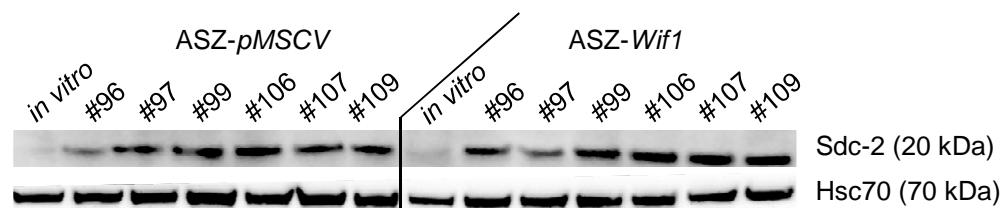


**Fig. 46: Western blot of Sdc-2 in ASZ-pMSCV and ASZ-Wif1 allografts**

Protein samples from *in vitro* cultures and from allografts (#96-109) were analyzed. Sdc-2 antibody detects total Sdc-2 protein with a size of 20 kDa. Hsc70 served as loading control. Please note that Hsc70 loading control in this Figure is identical with that in Fig. 34 and 36 as all proteins were detected using the same membrane.

### IV.5.2.6 Effect of Wif1 on proliferation *in vivo*

In order to evaluate the impact of Wif1 overexpression on proliferative capacity of ASZ-*pMSCV* and ASZ-*Wif1* derived tumors, immunohistochemical stainings of the S-phase associated marker Ki67 was performed.

ASZ-*Wif1* derived allografts revealed a significantly reduced number of Ki67 positive nuclei per 1000 cells compared to ASZ-*pMSCV* derived allografts. This indicates that ASZ-*Wif1* allografts show a lower proliferative capacity (see Fig. 47).

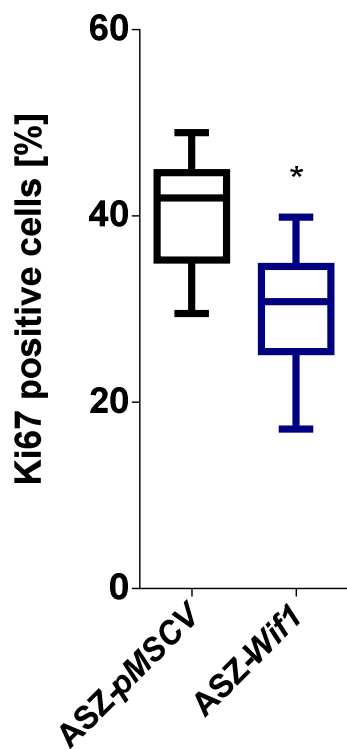


**Fig. 47: Evaluation of Ki67 staining of ASZ-*pMSCV* and ASZ-*Wif1* allografts**

Total number of nuclei and Ki67 positive nuclei per paraffin section of ASZ-*pMSCV* and ASZ-*Wif1* allografts were counted using image processing software FIJI. 3 images per section derived from 9 different tumor samples were analyzed for ASZ-*pMSCV* and ASZ-*Wif1* derived allografts. Statistical significance was analyzed using Wilcoxon test. \*  $p < 0.05$ .

Since Wnt signaling is known to induce cyclin D1 expression (Shtutman *et al.* 1999; Zhang *et al.* 2012), which is a key regulator of cell cycle progression, we also analyzed cyclin D1 protein expression levels by means of Western blot. However, no obvious differences in the expression levels between ASZ-*pMSCV* and ASZ-*Wif1* derived tumors were observed (see Fig. 48).

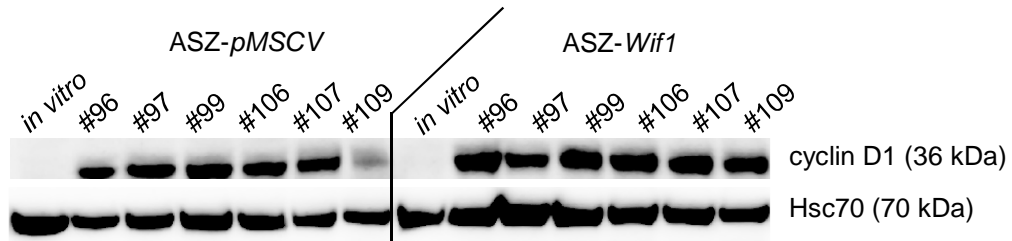


**Fig. 48: Western blot of cyclin D1 in ASZ-pMSCV and ASZ-Wif1 allografts.**

Protein samples from in vitro cultures and from allografts (#96-109) were analyzed. Cyclin D1 antibody detects total cyclin D1 protein with a size of 36 kDa. Hsc70 served as loading control.

Tumor-associated macrophages (TAMs) and cancer-associated fibroblasts (CAFs) are known to affect cancer cell proliferation (Bingle *et al.* 2002; Augsten 2014). For example, the reduced proliferation of ASZ-Wif1 derived tumors could have been a result of decreased infiltration with TAMs or CAFs. To investigate whether the latter cellular components show a different distribution in ASZ-pMSCV and ASZ-Wif1 derived tumors, antibody staining of F4/80 and alpha smooth muscle actin ( $\alpha$ Sma) as markers for TAMs and CAFs, respectively, was performed.

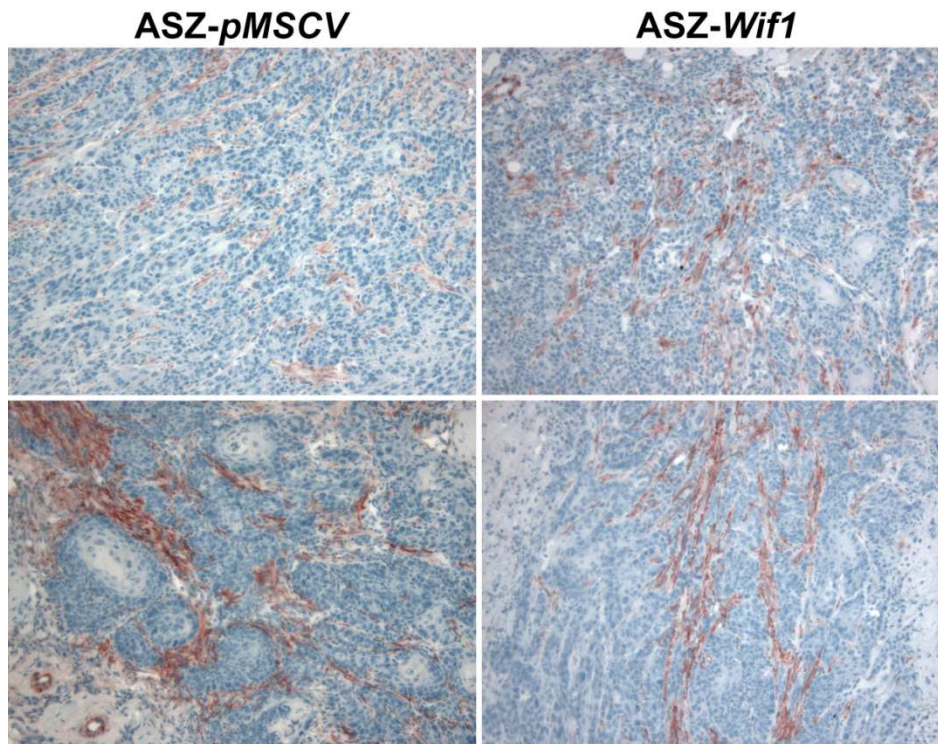


**Fig. 49: antibody staining of F4/80 in ASZ-pMSCV and ASZ-Wif1 allografts**

Antibody stainings of F4/80 (red) on paraffin sections derived from ASZ-pMSCV and ASZ-Wif1 allografts. Two examples each are shown. Staining reaction was performed using AEC.

Neither the quantity of F4/80 positive cells nor the staining pattern was obviously different between *ASZ-pMSCV* and *ASZ-Wif1* derived allografts (see Fig. 49). Similar results were obtained with the  $\alpha$ Sma antibody that also did not show any differences concerning quantity of stained cells or staining pattern (see Fig. 50).

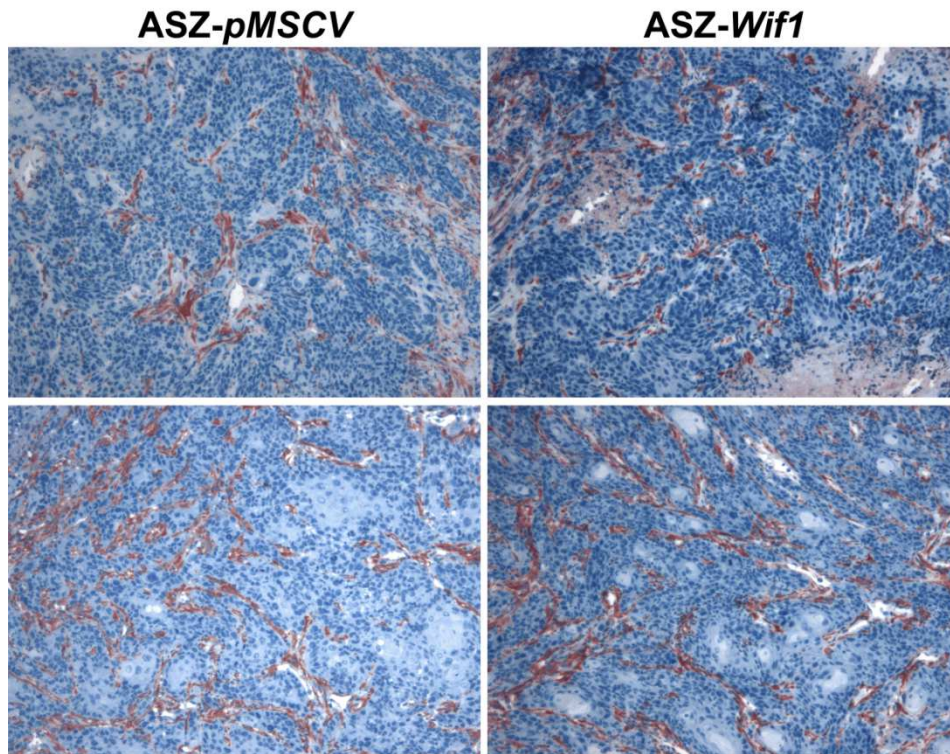


**Fig. 50: Antibody staining of  $\alpha$ Sma in *ASZ-pMSCV* and *ASZ-Wif1* allografts**

Antibody stainings of  $\alpha$ Sma on paraffin sections derived from *ASZ-pMSCV* and *ASZ-Wif1* allografts. Two examples each are shown. Staining reaction was performed using AEC.

Together these results suggest that the infiltration of the tumors with TAM and CAF is not responsible for the different growth behaviour of *ASZ-pMSCV* and *ASZ-Wif1* derived tumors.

### **IV.5.3 Summary of the effects of Wif1 overexpression**

Overexpression of Wif1 in the BCC cell line ASZ001 resulted in reduced tumor growth when the cells were transplanted into nude mice. This did not involve Hh, Wnt or PI3K/Akt signaling, apoptosis, stromal composition or differentiation. Furthermore, it does not require an interaction with tumor-associated fibroblasts or macrophages. Instead, the deposition of collagen

was increased and the proliferative capacity of the transplanted cells was reduced. This correlated with increased PKC and Erk1 phosphorylation which might indicate a putative role in EGF signaling.

## IV.6 Targeted disruption of *Wif1* in murine BCC

For further analysis of the function of *Wif1* *in vivo* we employed the *Ptch<sup>flox/flox</sup>CreERT2<sup>T/-</sup>* BCC mouse model in which mice develop BCC upon tamoxifen induction. BCC of these mice express *Wif1*. The expression is already detectable 45d after tamoxifen induced BCC development (see Fig. 52). The expression persists at least 90 days after tamoxifen injection (see Fig. 52). As in humans (see Fig. 8) the expression is detected tumor intrinsically as well as in the tumor stroma with a highly heterogeneous distribution in the latter (see Fig. 51).

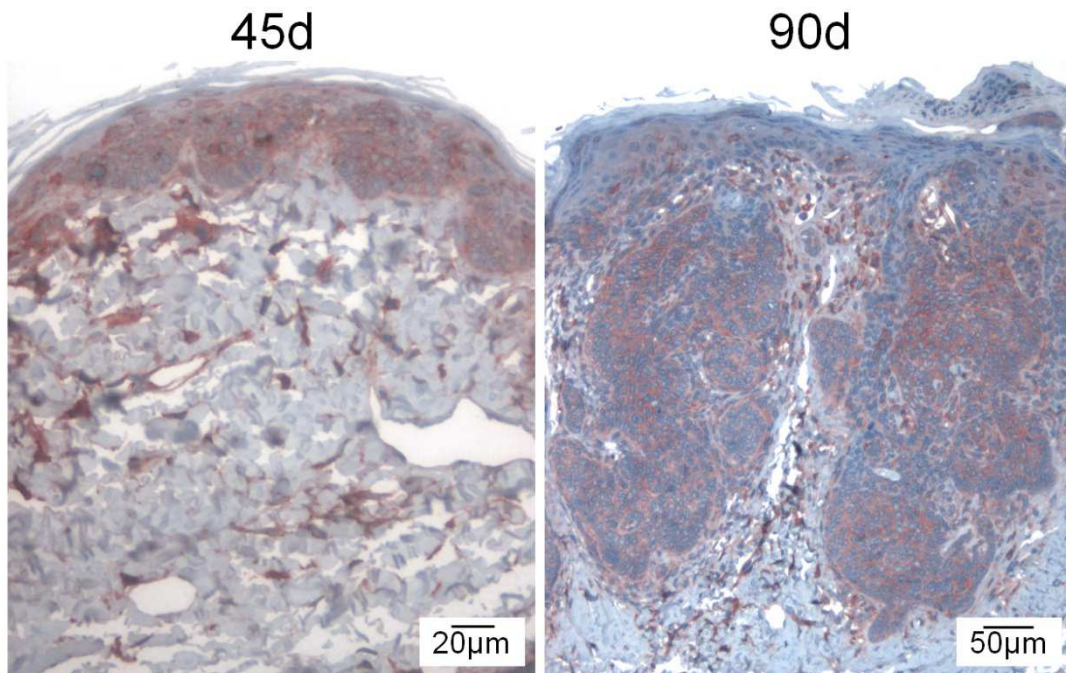


**Fig. 51: Antibody staining of *Wif1* in murine BCC**

Anti-*Wif1* antibody staining of paraffin sections derived from 45d (left) and 90d (right) BCC of *Ptch<sup>flox/flox</sup>CreERT2<sup>T/-</sup>* mice. Staining reaction was performed using AEC.

In order to investigate whether BCC growth is dependent on *Wif1*, *Wif1* function was disrupted in BCC by breeding *Ptch<sup>flox/flox</sup>CreERT2<sup>T/-</sup>* mice with

*Wif1*<sup>-/-</sup> mice. In the *Wif1*<sup>-/-</sup> mouse model a *LacZ*-ORF is inserted into exon 1 of the *Wif1* gene which results in several in frame stop codons and thus in loss of function of *Wif1*. In the resulting offspring i.e. *Ptch*<sup>flox/flox</sup>*CreERT2*<sup>T/-</sup>*Wif1*<sup>-/-</sup> and *Ptch*<sup>flox/flox</sup>*CreERT2*<sup>T/-</sup> BCC were induced by tamoxifen injection at an age of 8 weeks. Both *Ptch*<sup>flox/flox</sup>*CreERT2*<sup>T/-</sup>*Wif1*<sup>-/-</sup> and *Ptch*<sup>flox/flox</sup>*CreERT2*<sup>T/-</sup> mice were randomized in 2 cohorts. In the first cohort BCC were analyzed 45 days after tamoxifen injection (45d) (Nitzki *et al.* 2010). The second cohort was analyzed 90 days after BCC induction. *Wif1* wild-type littermates i.e. *Ptch*<sup>flox/flox</sup>*CreERT2*<sup>T/-</sup> and littermates lacking Cre-recombinase i.e. *Ptch*<sup>flox/flox</sup>*Wif1*<sup>-/-</sup> served as controls. None of the littermates lacking Cre-recombinase that were treated with tamoxifen developed BCC. In contrast, all *Ptch*<sup>flox/flox</sup>*CreERT2*<sup>T/-</sup> and *Ptch*<sup>flox/flox</sup>*CreERT2*<sup>T/-</sup>*Wif1*<sup>-/-</sup> animals developed tumors. Macroscopically no difference between both BCC backgrounds was detectable. As expected *Wif1* protein was not detected in skin samples from *Ptch*<sup>flox/flox</sup>*CreERT2*<sup>T/-</sup>*Wif1*<sup>-/-</sup> animals (see Fig. 52).

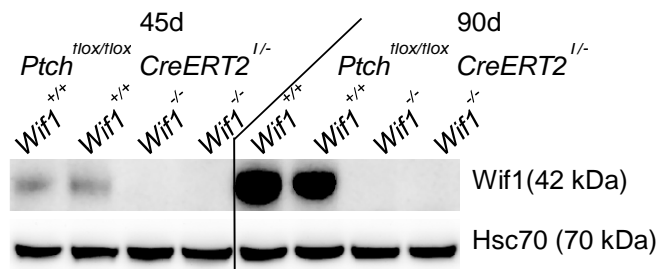


**Fig. 52: Western blot of *Wif1* in murine BCC**

Skin samples from 45d and 90d cohorts of *Ptch*<sup>flox/flox</sup>*CreERT2*<sup>T/-</sup> and *Ptch*<sup>flox/flox</sup>*CreERT2*<sup>T/-</sup>*Wif1*<sup>-/-</sup> animals were analyzed regarding *Wif1* protein expression.

To assess the tumor load of *Ptch*<sup>flox/flox</sup>*CreERT2*<sup>T/-</sup> and *Ptch*<sup>flox/flox</sup>*CreERT2*<sup>T/-</sup>*Wif1*<sup>-/-</sup> animals the tumor size was measured on H&E stained paraffin sections (3 images from sections of 5 different animals each) using cellSens software. As demonstrated in Fig. 53 BCC of mice lacking *Wif1* expression had the same size compared with *Wif1* wild-type littermate 45d after induction. However, in 90 day cohorts the size of BCC in mice lacking *Wif1* expression was unambiguously larger compared with *Wif1* wild-type littermates (see Fig. 54).

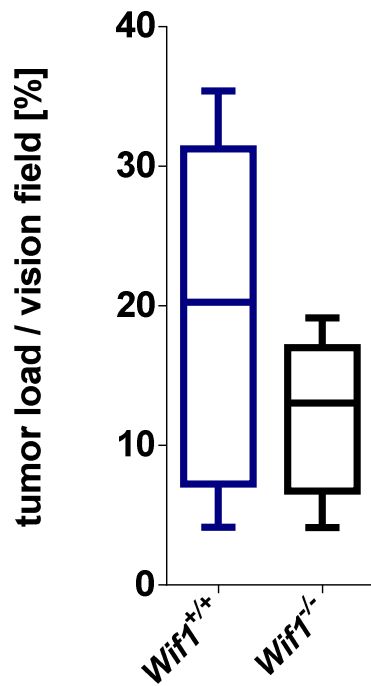


Fig. 53: Planimetric measurement of tumor size in *Ptch<sup>flox/flox</sup>CreERT2<sup>T/-</sup>* and *Ptch<sup>flox/flox</sup>CreERT2<sup>T/-</sup>Wif1<sup>-/-</sup>* skin samples 45d after induction

3 images of each 5 Skin samples from *Ptch<sup>flox/flox</sup>CreERT2<sup>T/-</sup>* and *Ptch<sup>flox/flox</sup>CreERT2<sup>T/-</sup>Wif1<sup>-/-</sup>* animals were analyzed using software cellSens.

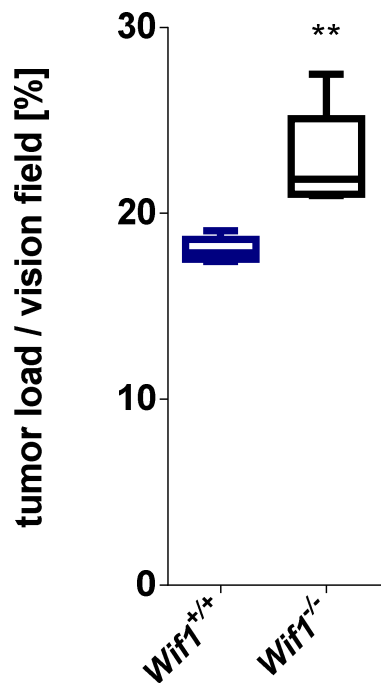
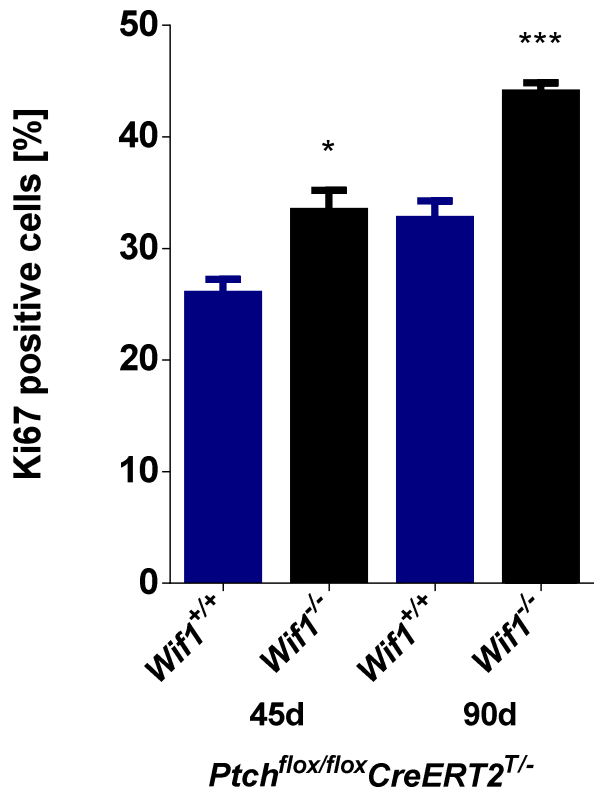


Fig. 54: Planimetric measurement of tumor size in *Ptch<sup>flox/flox</sup>CreERT2<sup>T/-</sup>* and *Ptch<sup>flox/flox</sup>CreERT2<sup>T/-</sup>Wif1<sup>-/-</sup>* skin samples 90d after induction

3 images of each 5 Skin samples from *Ptch<sup>flox/flox</sup>CreERT2<sup>T/-</sup>* and *Ptch<sup>flox/flox</sup>CreERT2<sup>T/-</sup>Wif1<sup>-/-</sup>* animals were analyzed using software cellSens.

Next, in order to investigate the proliferative capacity of the tumors, an anti-Ki67 antibody staining was performed on paraffin embedded sections. As shown in Fig. 55 the percentage of Ki67 positive cells was significantly higher on a *Wif1* deficient background in both, the 45d and 90d, cohorts.

Together, these data indicate that in accordance with the allograft experiments (see Fig. 26) *Wif1* is a factor that is necessary to restrict BCC growth.



**Fig. 55: Evaluation of anti-Ki67 antibody staining in *Ptch*<sup>flox/flox</sup>*CreERT2*<sup>T/-</sup> and *Ptch*<sup>flox/flox</sup>*CreERT2*<sup>T/-</sup>*Wif1*<sup>-/-</sup> skin samples 45d and 90d after induction**

Ki67 positive cells were counted using AlphaView software. 3 images of 3 skin samples each were analyzed. Exclusively BCC cells were counted. All data are represented as a mean + SEM. Statistical significance was evaluated using Mann-Whitney *U* test. \* *p* < 0.05, \*\*\* *p* < 0.001.

## V Discussion

### V.1 WIF1 in human tumors of the skin

As shown by antibody staining, WIF1 is highly expressed in human and also murine BCC. Indeed, all analyzed human BCC samples exhibited tumor-intrinsic WIF1 expression. This is in line with data from the human protein atlas webpage where 5 out of 6 samples from BCC patients were described to express at least weak WIF1 protein levels in antibody stainings.

Using immortalized rat kidney cells it was found that GLI1 transduction induced the expression of *Wif1* (Louro *et al.* 2002). Because at that time WIF1 was already known as a potential tumor suppressor gene, the authors already speculated that WIF1 expression may be responsible for the infrequent occurrence of metastases in BCC patients (Louro *et al.* 2002). Even though this speculation was not formally proven, the authors proposed that a *Wif1* knockout could demonstrate its tumor suppressive function in skin cancer. In line with this assumption, *WIF1* was found to be downregulated in melanomas compared with nevi (Haqq *et al.* 2005). Taken together, this drove us to hypothesize that *Wif1* might keep BCC semi-malignant and prevents it from malignant transformation. We also speculated that *WIF1* is absent or present at significantly lower levels in invasive BCC, SCC and malignant melanomas compared to indolent-growth subtypes of BCC. However, as shown by our data this was not the case.

In our experiments we used qRT-PCR to quantify *WIF1* expression in indolent-growth and invasive variants of BCC, SCC and malignant melanomas. Whereas antibody staining does not allow comparative quantification of gene expression in different tumor samples and entities, qRT-PCR does. Thus, laser microdissection of paraffin-embedded tumor tissue was performed and *WIF1* mRNA levels were analyzed. *WIF1* expression in invasive BCC, SCC and melanomas was at comparable levels and expression in SCC and melanomas was significantly higher compared to the indolent-growth variants of BCC, i.e. superficial and nodular BCC. Although this contradicted our working hypothesis that WIF1 is a tumor suppressor in BCC and as such should be expressed at higher levels in

indolent-growth subtypes of BCC when compared to more malignant skin tumors, our consecutive data showed that *Wif1* inhibited BCC growth in mouse models. This leaves several possibilities for interpretation: First, *Wif1* exerts its tumor suppressive functions only in the mouse. However, this is unlikely since there is only one report suggesting an oncogenic function of *WIF1*, whereas all other studies unambiguously showed that *WIF1* acts as a tumor suppressor in diverse human tumor entities. Furthermore, in melanoma *WIF1* gene transfer was shown to inhibit tumor growth in a xenograft model by suppressing proliferation (Lin *et al.* 2007). This supports the hypothesis of *WIF1* being a tumor suppressor also in malignant skin tumors. Second, *WIF1* could also have distinct functions in BCC, SCC and melanoma. For example, *WIF1* promotes melanogenesis in melanocytes (Park *et al.* 2014) suggesting a distinct function in melanomas compared with BCC and SCC. Third, I only have determined *WIF1* expression on mRNA level ignoring possible post-transcriptional, translational and post-translational regulatory mechanisms.

Another aspect about *WIF1* expression in BCC is the following: Although invasive BCC express higher *WIF1* levels than indolent-growth subtypes the differences of *WIF1* expression were statistically not significant. This might be different if a larger sample set would have been analyzed. In case this would be true, there would be an explanation to it: *GLI1* was shown to induce *Wif1* expression in rat kidney cells (Louro *et al.* 2002). Furthermore, *Gli1* is the effector driving tumor formation in BCC (Nilsson *et al.* 2000). Thus elevated *GLI1* activity in invasive BCC could be the cause for elevated *WIF1* expression levels. However, so far this is pure speculation because *GLI1* mRNA levels in invasive versus indolent-growth variants of BCC have not been quantified. Prospectively, this experiment will be conducted in our lab using the samples from the microdissections.

Noteworthy, beside tumor-intrinsic expression *WIF1* was obviously also highly expressed in cells of inflammatory infiltrates and in fibroblasts of the tumor stroma (see Fig. 8). *WIF1* expression in fibroblasts of the skin has been previously reported to be involved in melasma development (Kim *et al.* 2013). In contrast, the role of *WIF1* in inflammation of the skin is currently absolutely unknown. However, it was shown that abrogation of Wnt secretion

in keratinocytes resulted in infiltration of immune cells and inflammation of the skin (Augustin *et al.* 2013). This might also suggest an implication of WIF1 in the promotion of inflammation by inhibiting Wnt signaling.

Thus, WIF1 seems to exert a variety of functions in the skin and it cannot be ruled out that tumor-extrinsic WIF1 also affects BCC development. However, in this thesis I will focus on the putative tumor suppressive function of tumor-intrinsic WIF1 as this appears to be a general phenomenon that applies for a variety of different cancer entities.

## **V.2 Wif1 overexpression in the BCC cell line ASZ001**

ASZ001 is the only available BCC cell line derived from *Ptch*<sup>+/-</sup> mice. Even though derived from a tumor that exhibited *Wif1* expression, this cell line expresses *Wif1* at low to undetectable levels (data not shown). This is in line with lost WIF1 expression in human cultured proliferating keratinocytes (Schluter *et al.* 2013). Thus, a *Wif1* overexpression plasmid was generated. Using the stably transduced cell line ASZ-*Wif1* the effect of *Wif1* on BCC growth was examined.

### **V.2.1 Validation of *Wif1* overexpression, secretion and functionality**

Effective *Wif1* overexpression in ASZ-*Wif1* cells was shown on RNA as well as protein level (see Fig. 12 and Fig. 13). Since *Wif1* is a secreted protein exhibiting its function in the extracellular space by sequestration of Wnt ligands, its secretion was analyzed by concentrating the medium of ASZ-*Wif1* and subsequent Western blot analysis. In fact, *Wif1* is secreted by ASZ-*Wif1* into the medium (see Fig. 14). Unfortunately, I was not able to analyze the functionality of the secreted *Wif1* by *TOP/FOP* reporter assay when the parental cell line ASZ001 was used. This was due to the fact that neither Wnt3a nor an active form of  $\beta$ -catenin induced *TOP* activity in this cell line.

*TOP* activity is dependent on functional Lef1 which binds to Tcf/Lef binding sites of the *TOP* vector when activated by  $\beta$ -catenin. Thus, it is possible that ASZ001 simply does not express a functional form of Lef1. Alternatively, the transduction efficiency was insufficient to facilitate luciferase expression. Therefore, HEK-293 cells were employed as an alternative. In this experimental setup concentrated supernatant from ASZ-*Wif1* significantly inhibited the action of Wnt3a conditioned medium as measured by the *TOP/FOP* reporter assay. This demonstrated that functionally active Wif1 was successfully overexpressed and secreted by ASZ-*Wif1* cells. Therefore, ASZ-*Wif1* cells served as basis for subsequent investigations on the role of Wif1 in BCC.

## **V.2.2 Effects of Wif1 overexpression on the BCC cell line ASZ001**

The effect of Wif1 overexpression on BCC cell growth was analyzed *in vitro* and *in vivo*. For *in vivo* analyses the cell lines ASZ-*Wif1* and ASZ-*pMSCV* were subcutaneously transplanted in the flanks of nude mice.

Similarly to xenografts of melanoma, kidney cancer and cervical cancer cells (Lin *et al.* 2007; Kawakami *et al.* 2009; Ramachandran *et al.* 2012) the overexpression of Wif1 resulted in reduced BCC growth (see Fig. 26) which was also reflected by reduced tumor weight (see Fig. 27). Reduced tumor growth can be a result of alterations in diverse cellular processes. Therefore, I examined the effect of Wif1 on signaling pathway activity, cell viability, apoptosis, differentiation, EMT, migration, cell cycle regulation, proliferation, and on the tumor microenvironment.

### **V.2.2.1 Effect of Wif1 on Wnt, Hh and EGFR signaling pathways**

It has been shown that shifted, the *Drosophila* orthologue of Wif1, increased stabilization and diffusion of Hh (Glise *et al.* 2005) and promoted Hh signaling

mediated by Hh co-receptors interference hedgehog (Ihog) and brother of Ihog Boi (Avanesov and Blair 2013). Furthermore, overexpression of Wif1 in hematopoietic stem cells induced Shh expression resulting in Hh pathway activation (Schaniel *et al.* 2011). As these results suggested that Wif1 may also induce Hh signaling in BCC, Hh signaling activity was determined by *Gli1* qRT-PCR in ASZ-*Wif1* and ASZ-*pMSCV* cells. However, overexpression of Wif1 did not alter *Gli1* gene expression neither *in vitro* nor *in vivo* (see Fig. 17 and 31). Although ASZ001 were derived from BCC that had activated Hh signaling, they express relatively low *Gli1* mRNA levels (So *et al.* 2006). Thus, we would have expected an upregulation of *Gli1* expression if Wif1 would have been able to activate Hh signaling. Taken together, it can be hypothesized that ASZ001 either i) lacks required coreceptors, ii) is not able to upregulate Shh or iii) is insensitive towards Shh due to its Ptch mutation. On the contrary, it has been shown that Wif1 is downstream of Gli1 as *GLI1* transduction induced Wif1 expression in rat kidney cells (Louro *et al.* 2002). Moreover, the *Wif1* promoter region contains a GLI-kruppel binding site as a regulatory element (Reguart *et al.* 2004), suggesting that Wif1 is downstream and not upstream of activated Hh signaling in BCC. If this is also true for Wif1 expression in ASZ001 it consequently did not alter Hh signaling in ASZ-*Wif1* cells and allografts.

As a Wnt inhibitor Wif1 can bind to several Wnts and prevent them from binding to their receptors. Activated canonical Wnt signaling leads to a translocation of  $\beta$ -catenin into the nucleus and ultimately to the induction of target gene expression including *Axin2* and *c-Myc*. In order to analyze whether the overexpression of Wif1 is sufficient to inhibit canonical target gene expression, the expression of *Axin2* and *c-Myc* was analyzed by qRT-PCR. In addition, the subcellular localization of  $\beta$ -catenin was estimated by antibody staining. No changes in the target gene expression and no nuclear  $\beta$ -catenin were detectable (see Fig. 17, 31 and 32). Although nuclear  $\beta$ -catenin is currently debated as a reliable read-out for active canonical Wnt signaling, absence of nuclear  $\beta$ -catenin in combination with the unaffected target gene expression strongly suggests that canonical Wnt signaling is inactive in the ASZ001-derived cell lines and respective allografts. Thus, it is

possible that *Wif1* overexpression was not able to further decrease the already very low levels of *Axin2* and *c-Myc*.

Next, the activation status of  $\text{Wnt}/\text{Ca}^{2+}$  and  $\text{Wnt}/\text{PCP}$  pathways were determined as *Wif1* is able to bind and inhibit several Wnts that are implicated in activation of non-canonical Wnt signaling (e.g. *Wnt4*, *5a*, *7a* and *11*) (Surmann-Schmitt *et al.* 2009; Vassallo *et al.* 2015). However, JNK as mediator of active  $\text{Wnt}/\text{PCP}$  pathway was unphosphorylated. This rather suggests inactive  $\text{Wnt}/\text{PCP}$  signaling. Furthermore, the cytoplasmic  $\text{Ca}^{2+}$  levels of *ASZ-pMSCV* and *ASZ-Wif1* as an indicator for activated  $\text{Wnt}/\text{Ca}^{2+}$  signaling were examined. Neither the basal  $\text{Ca}^{2+}$  concentrations nor the maximum  $\text{Ca}^{2+}$  flux ratio was altered in *ASZ-Wif1* (see Fig. 18). This indicates that  $\text{Wnt}/\text{Ca}^{2+}$  signaling is either not affected by *Wif1* or that the sensitivity of this assay does not allow for discrimination between small differences in  $\text{Ca}^{2+}$  concentrations. Moreover, CaMKII was unphosphorylated in allografts and in *in vitro* samples supporting that  $\text{Wnt}/\text{Ca}^{2+}$  signaling is not affected.

However, I found PKC phosphorylation to be upregulated *in vitro* and to be maintained in *ASZ-Wif1* allografts. The antibody detects PKC isoforms  $\alpha$ ,  $\beta$ I,  $\beta$ II,  $\delta$ ,  $\epsilon$ ,  $\eta$  and  $\theta$  (78-85 kDa) when phosphorylated at serine 660. Due to the minor differences in the size of the isoforms they cannot be discriminated by Western blot analysis. However, PKC  $\alpha$ ,  $\beta$  and  $\delta$  isoforms are expressed in keratinocytes and BCC (Neill *et al.* 2003; Breitkreutz *et al.* 2007). Interestingly, loss of PKC  $\alpha$  is associated with enhanced tumor growth in BCC (Neill *et al.* 2003). Previous results of our group showed that an antibody detecting  $\alpha$  and  $\beta$ II isoforms recapitulated pan-PKC expression in BCC samples (Carstens 2010). Thus, it is highly probable that the detected PKC was constituted of  $\alpha$  and  $\beta$ II isoforms.

The aspect about PKC phosphorylation is of particular interest as PKC is not only involved in  $\text{Wnt}/\text{Ca}^{2+}$  signaling but also mediates EGFR (Fan *et al.* 2009). As *Wif1* contains 5 EGF-like domains, all high-affinity ErbB ligands contain an EGF-like domain (Yarden and Sliwkowski 2001) and since  $\text{Ca}^{2+}$  was not affected in *ASZ-Wif1* cell lines, it is tempting to speculate that *Wif1*

might also have affected EGFR signaling. Indeed, one investigation identified Wif1 as a binding partner for ErbB2, 3 and 4 that are isoforms of the EGFR (Curak 2010). Since BCC usually express EGFR (Eberl *et al.* 2012) and because EGFR activity can result in activation of Akt and Ras signaling the phosphorylation status of Akt, S6 and Erk1/2 was analyzed. Akt and S6 display an inconsistent phosphorylation pattern, which however did not significantly vary between ASZ-*Wif1* and ASZ-*pMSCV* allografts. Erk1 and 2 were both phosphorylated and thus activated when the cell lines were cultured *in vitro* with slightly increased phosphorylation of Erk1 in ASZ-*Wif1*. Interestingly, when the cell lines were transplanted in nude mice, the phosphorylation status of Erk2 remained at equal levels in both cell lines. In contrast, Erk1 phosphorylation was only maintained in the ASZ-*Wif1* allografts whereas it vanished in ASZ-*pMSCV* allografts.

Firstly, these data may indicate that Erk1 phosphorylation in the *in vitro* situation is fostered by specific growth factors provided by FCS that is a supplement of the culture medium. The fact that Erk1 phosphorylation was maintained exclusively in ASZ-*Wif1* allografts could be a result of the concomitantly observed maintenance of PKC phosphorylation. Moreover, it could be part of activated Wnt/Ca<sup>2+</sup> signaling or active EGFR signaling (see above) (Kolch 2005; Mendoza *et al.* 2011). Whether the maintenance of PKC and Erk1 phosphorylation is indeed part of one or both signaling pathways and how and whether Wif1 participates in this process remains to be elucidated in the future.

Secondly, the maintenance of Erk1 phosphorylation in ASZ-*Wif1* cells may be related to inhibition of tumor growth. Although, at the first glance this seems to come into conflict with the traditionally regarded role of pERK1/2 as tumor promoters, overexpression of ERK1 in NIH/3T3 cells inhibits Ras-mediated proliferation and tumorigenicity while ERK2 does not (Vantaggiato *et al.* 2006). Furthermore, it has been reported that the cell cycle is promoted when Erk1/2 is persistently and moderately activated, while transient Erk1/2 activation fails to do so (Yamamoto *et al.* 2006). In addition, sustained Raf/Mek/Erk pathway over-activation can trigger cell cycle arrest (Samuels *et al.* 1993; Guegan *et al.* 2014), which can be mediated by elevated expression levels of the cell cycle inhibitor p21cip1 that blocks cyclin E/CDK2 complexes

inhibiting S-phase entry (LaBaer *et al.* 1997; Sewing *et al.* 1997). Finally, temporally elevated Erk1/2 activation at the G2/M transition can block entry into mitosis (Rahmouni *et al.* 2006). Thus, the consequence of Erk1/2 signaling is considered to depend on the duration, intensity and time point of activation. Accordingly, it is possible that persistent high Erk1 activation in combination with sustained Erk2 activity in ASZ-*Wif1* cells may have resulted in cell cycle arrest and thus could ultimately explain the reduced tumor growth of ASZ-*Wif1* allografts. This highly interesting topic will be investigated in the future.

In this context it is also interesting to know, that Erk1 and 2 share about 84% amino acid sequence identity, that they are coexpressed in most tissues, have similar subcellular localization, substrate specificity and stimuli leading to their activation (Samuels *et al.* 2008; Guihard *et al.* 2010; Woodson and Kedes 2012). Thus, most investigations did not discriminate between both isoforms. However, and as already mentioned above, increasing evidence supports distinct functions and different outcomes of Erk1 and Erk2 phosphorylation (Pages and Pouyssegur 2004). First hints that they execute different functions came from observations that the levels of Erk1 and Erk2 vary depending on the tissue context (Pages and Pouyssegur 2004). Subsequently, it was shown that loss of ERK1 significantly facilitated proliferation in contrast to knockdown of ERK2 which resulted in reduced proliferation. *Vice versa* and as already mentioned above, overexpression of ERK1 in NIH/3T3 cells inhibited Ras-mediated proliferation and tumorigenicity while ERK2 does not. Notably, ERK1 function was kinase-independent in this case, as expression of a catalytically inactive form of ERK1 was equally effective (Vantaggiato *et al.* 2006). The authors proposed a model in which ERK1 and ERK2 compete in binding to the upstream kinase MEK. By means of this molecular process ERK1 negatively interferes with the growth promoting ERK2 signaling. However, coming back to ASZ-*Wif1* cells the total amounts of Erk1 and 2 were not significantly altered but Erk1 phosphorylation was maintained *in vivo*. Thus, a distinct mechanism may be involved for the tumor-suppressive role of Erk1 in ASZ-*Wif1* cells. Indeed, it was hypothesized that Erk1 is a partial agonist of Erk signaling. Thus, Erk1 may bind to the same signaling effectors but is not able to elicit the maximum

possible response that is produced by the full agonist Erk2. With increasing ratios of Erk1 to Erk2 activity this would result in the inhibition of Erk signaling (Brambilla and Ratto 2009). Thus, increased phosphorylation of Erk1 could possibly inhibit growth promoting effect of Erk2 by competing with its signaling effectors, thereby suppressing ASZ-*Wif1* tumor growth *in vivo*. However, this is pure speculation and remains to be established in the future.

### **V.2.2.2 Effect of Wif1 on proliferation**

In line with inhibition of proliferation in keratinocytes (Schluter *et al.* 2013) and with the above-mentioned speculations about the relation of Erk1 and Erk2 activation levels, proliferation and growth of ASZ-*Wif1* allografts was suppressed. This was shown by decreased tumor size and weight, which went along with a significantly reduced number of Ki67 positive tumor cells (see Fig. 47). This showed that *Wif1* can suppress tumor growth of BCC cells *in vivo*.

*Wif1* has been shown to induce a G1 cell cycle arrest in invasive bladder cancer cell lines (Tang *et al.* 2009) and to suppress proliferation in keratinocytes of the interfollicular epidermis (Schluter *et al.* 2013). Indeed, an *in vitro* cell cycle analysis showed that ASZ-*Wif1* cells had the tendency to accumulate in G1 phase, however this was statistically not significant (see Fig. 21). In addition, the *in vitro* analysis revealed no significant differences between ASZ-*Wif1* and ASZ-*pMSCV* cells by BrdU assay (see Fig. 22). As *Wif1* overexpression did not suppress proliferation *in vitro* but *in vivo* we initially hypothesized that the *Wif1*-mediated inhibition of proliferation *in vivo* might require a crosstalk with the tumor microenvironment. Within the microenvironment TAMs and CAFs play essential roles in the regulation of tumor cell proliferation (Bingle *et al.* 2002; Augsten 2014). Therefore, ASZ-*Wif1* and ASZ-*pMSCV* cells were cocultured with several fibroblast cell lines and BMDMs and the proliferative capacity of the BCC cell lines were analyzed. However, no significant difference of the proliferation between both cell lines was observed (see Fig. 23). Thus, the *in vivo* inhibition of proliferation caused by *Wif1* cannot only be explained by an interaction with

fibroblasts (simulating CAFs) or BMDMs (simulating TAMs) and must rely on additional or different cellular and/or molecular components. Alternatively, and as outlined in the previous section, the Wif1-mediated inhibitory effect on BCC cell proliferation might depend on maintenance of Erk1 phosphorylation in ASZ-*Wif1* cells, which may have required cultivation in the absence of FCS. In conclusion, Wif1 inhibits the proliferation of ASZ001 *in vivo* but not *in vitro*, at least not in the presence of FCS.

### **V.2.2.3 Effect of Wif1 on apoptosis**

Since the proliferative capacity of tumor cells is frequently negatively correlated with their metabolic activity and apoptotic processes, WST-1 assay and Annexin V staining were performed. Indeed, WIF1 induces caspase mediated apoptosis in cervical cancer and hepatocellular carcinoma cells (Hu *et al.* 2009; Ramachandran *et al.* 2012). Moreover, active Erk1/2 signaling can be associated with both, suppression and induction of apoptosis (Cagnol and Chambard 2010). However, overexpression of Wif1 neither reduced *in vitro* cell viability as shown by WST-1 assay nor induced cell death as revealed by analysis of Caspase 3 cleavage and Annexin V assay. In accordance, ASZ-*Wif1* allografts did not show hints for cell death as determined by TUNEL and p53 antibody staining. Thus, the reduced growth of ASZ-*Wif1* allografts did not seem to involve the induction of apoptosis.

### **V.2.2.4 Effect of Wif1 on differentiation**

As Wif1 expression has been shown to induce differentiation of several cancer entities and also regulates differentiation processes during development (Ramachandran *et al.* 2014; Baker *et al.* 2015), I determined whether reduced BCC proliferation was accompanied by an induction of keratinocyte differentiation marker expression. For this reason, the expressions of early markers (loricrin and involucrin) as well as markers for late differentiation (keratin 1 and 10) were analyzed in the ASZ-derived

allografts. However, no significant differences were detectable. The lack of difference in gene expression together with similar proportions of keratinization in allograft sections (see Fig. 25, 37 and 38) indicates that the anti-proliferative effect mediated by Wif1 is unrelated to induction of differentiation processes.

#### **V.2.2.5 Effect of Wif1 on EMT**

EMT is a prerequisite for the induction of migration that could lead to extravasation and ultimately to metastasis. Thus, migration can serve as a read out for *in vitro* induction of EMT in epithelial cells (Kalluri and Weinberg 2009). Since Wif1 can induce EMT reversal and can inhibit migration and invasion in prostate cancer cells (Yee *et al.* 2010), the impact of Wif1 on expression of EMT marker genes and migration was determined.

*In vitro*, Wif1 did not change the migratory capacity of ASZ001 (see Fig. 24). In accordance with this, the expression of EMT markers *Cdh1*, *Cdh2* and *Fn1* did not differ between ASZ-*Wif1* and ASZ-*pMSCV* allografts. This is in line with the microscopically unaffected cell morphology *in vitro*. Admittedly, we did not expect a significant difference in EMT marker expression or migration as ASZ001 already show a strict epithelial phenotype. In addition, these cells are derived from a well differentiated semi-malignant tumor entity, which is maintained when the cells were transplanted in mice and formed tumors (see Fig. 28). Taken together, we conclude that Wif1 probably does not affect EMT in BCC. Furthermore, Wif1 seems to be unable to induce a more epithelial phenotype of an already well differentiated epithelial tumor.

#### **V.2.2.6 Effect of Wif1 on the tumor microenvironment**

As discussed in section IV.5.2.6 antibody staining of the S-phase marker Ki67 showed reduced proliferation of ASZ-*Wif1* derived tumors. Since invasion of TAMs and CAFs can affect tumor growth, antibody stainings

using an anti-F4/80 antibody and an anti- $\alpha$ Sma antibody, respectively, were conducted.

TAMs and CAFs can either promote or inhibit tumor growth and the respective outcome is apparently context-specific (Bingle *et al.* 2002; Augsten 2014). TAMs and CAFs secrete a variety of growth factor, including EGF, hepatocyte growth factor (HGF), basic fibroblastic growth factor (bFGF), vascular endothelial growth factor (VEGF) and platelet derived growth factor (PDGF) (Koontongkaew 2013) that can modulate tumor growth. Thus, the recruitment or absence of TAMs and/or CAFs could have been a cause of the growth inhibitory effect of *Wif1*.

However, no obvious differences in the number of F4/80 and  $\alpha$ Sma positive cells were detected in *ASZ-Wif1* and *ASZ-pMSCV* derived tumors when stained with the respective antibodies (see Fig. 49 and 50). Admittedly, this does not categorically exclude differences in e.g. activity or secretion of growth factors of TAMs or CAFs. However, the similar infiltration pattern of the tumor samples together with the fact that the corresponding coculture experiments also did not result in proliferation changes of the BCC cells (see section IV.4.3 and Fig. 23) kept us from further extensions of the experiments.

Furthermore, extracellular matrix (ECM) proteins including collagens can significantly influence tumor growth and invasiveness. This is due to the fact that tumor progression directly depends on the ECM composition, structure and organization (Yu *et al.* 2011). Traditionally, ECM deposition is considered as an antagonistic response of the host stroma to the development of the tumor.

Undoubtedly, tumor cells change their microenvironment to ensure their survival (Bissell and Radisky 2001). Furthermore, previous data showed that inhibition of integrins that mediate cell-ECM interactions results in restoration of a “close-to-benign” phenotype of tumor cells (Weaver *et al.* 1997). Moreover, it is well known that tumor-derived ECM is biochemically distinct in its composition compared to normal ECM. This is responsible for a stiffening of the tumor stroma compared to normal stroma (Kass *et al.* 2007; Levental *et al.* 2009). Thus, ECM deposition has been linked to tumor growth.

However, in contrast it also has been reported that overexpression of type I collagen, which is a main component of the ECM, can reduce tumor growth *in vivo* (Honma *et al.* 2007).

Due to the importance of ECM in tumor growth processes, the collagen deposition was analyzed in ASZ-derived allograft sections by means of Ladewig staining. Collagen deposition was significantly increased in deeper necrotic areas of ASZ-*Wif1* allografts when compared to ASZ-*pMSCV* allografts. Outer regions of the allografts with mainly vital tumor tissue showed a tendency of elevated collagen levels that, however, was not significant. Nevertheless, it would be certainly of interest to study the effects of *Wif1* on production of collagen and thus on ECM in more detail. In addition, it would be also interesting to analyze whether *Wif1* changes the composition of the ECM or modulates the expression of e.g. metalloproteases that are well known ECM degrading enzymes.

Admittedly, it remains to be said that the increased amount of collagen found in the necrotic tumor regions may have originated from the Matrigel that served as substrate for the cells transplanted cells into nude mice.

Nevertheless, the collagen accumulation in ASZ-*Wif1* allografts is an interesting feature that certainly deserves further investigations.

### V.3 Wif1 depletion in murine BCC

The tumor suppressive role of *Wif1* in BCC was verified in a genetic approach. *Wif1* disruption led to tumor promotion, which supported the anti-tumorigenic role of *Wif1* in BCC. In this genetic approach the *Ptch<sup>flox/flox</sup>CreERT2<sup>T/-</sup>* BCC mouse model was bred onto a *Wif1* deficient background. The resulting *Ptch<sup>flox/flox</sup>CreERT2<sup>T/-</sup>Wif1<sup>-/-</sup>* offspring lacked *Wif1* expression in BCC as estimated by Western blot. *Ptch<sup>flox/flox</sup>CreERT2<sup>T/-</sup>* and *Ptch<sup>flox/flox</sup>Wif1<sup>-/-</sup>* littermates served as controls. For each genotype 2 cohorts were sacrificed 45d and 90d after tamoxifen injection. Macroscopically, first tumors were visible about 4 weeks after tamoxifen injection in *Ptch<sup>flox/flox</sup>CreERT2<sup>T/-</sup>Wif1<sup>-/-</sup>* and *Ptch<sup>flox/flox</sup>CreERT2<sup>T/-</sup>* mice without significant differences between the genotypes. As expected Cre lacking *Ptch<sup>flox/flox</sup>Wif1<sup>-/-</sup>*

mice remained tumor free. In the cohorts that were sacrificed 45d after tamoxifen injection both  $Ptch^{flox/flox}CreERT2^{T/-}Wif1^{-/-}$  and  $Ptch^{flox/flox}CreERT2^{T/-}$  mice developed histologically confirmed BCC. At that time the tumor load of the animals was undistinguishable. Taken together with lacking differences in tumor onset, this suggests that *Wif1* does not affect tumor initiation. However, when the animals were sacrificed 90d after tumor induction the tumor load of  $Ptch^{flox/flox}CreERT2^{T/-}Wif1^{-/-}$  was significantly increased when compared to  $Ptch^{flox/flox}CreERT2^{T/-}$  mice. In addition, we confirmed the enhanced proliferative capacity of the tumors as the number of Ki67 positive cells was significantly higher in tumors lacking *Wif1*. Together, this experiment confirmed that *Wif1* plays a tumor suppressive role in BCC progression.

## V.4 Outlook

Planimetric measurement and Ki67 staining show that BCC growth is enhanced in *Ptch* knockout mice on a *Wif1*-deficient background. *Vice versa*, tumor-intrinsic *Wif1* overexpression in the BCC cell line ASZ001 inhibits tumor growth in mice. This does not involve apoptosis, Akt, Wnt or Hh signaling or activation of apoptosis. It also does not involve changes in tumor differentiation or alterations in stromal composition of transplanted cells in host mice. Furthermore it does not seem to require an interaction with tumor associated fibroblasts or macrophages. Because tumor-intrinsic *Wif1* expression only inhibits cellular proliferation *in vivo* but not *in vitro* the data suggest that *Wif1* probably prevents tumor-promoting effects of soluble Wnt or other factors secreted by the tumor environment.

The tumor suppressive effect of *Wif1* was exclusively observed *in vivo*. Thus, *Wif1* could elicit its effects via two potential mechanisms. First, secreted *Wif1* may result in the activation of Wnt/ $Ca^{2+}$  or affect EGFR signaling and ultimately lead to PKC and Erk1 phosphorylation of the secreting cells in an autocrine fashion. Second, secreted *Wif1* may also affect cells of the tumor stroma in a paracrine fashion. Mediated by the inhibition of Wnt signaling or by affecting EGFR signaling in adjacent stromal cells, *Wif1* might change the

secretome of these cells, which in turn could result in the outcome described above (see Fig. 56). In order to elucidate whether paracrine signaling mechanisms are participating in the observed molecular events one could perform expression analyses using antibody staining or Western blot detecting putatively involved signaling molecules comparing ASZ-*Wif1* and ASZ-*pMSCV* allografts.

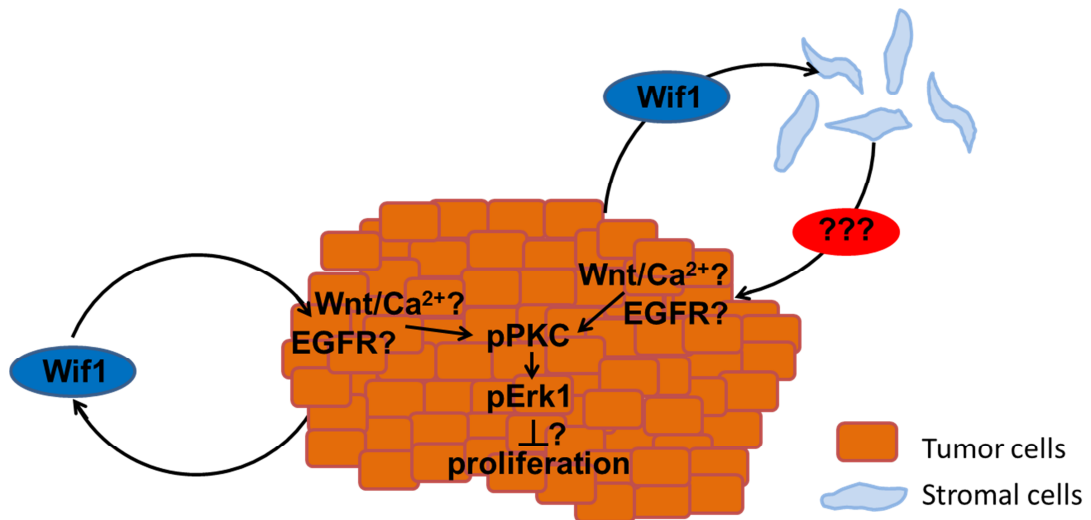


Fig. 56: Putative autocrine and paracrine signaling mechanism in ASZ-*Wif1* allografts

To examine the causative mechanism underlying these observations one should firstly analyse the proliferative capacity of ASZ-*Wif1* in the absence of FCS, because the surplus of growth factors in FCS may have impeded the *Wif1*-dependent inhibition of proliferation *in vitro*. Furthermore, in the same experimental setting an incubation of ASZ-*pMSCV* with concentrated ASZ-*Wif1* supernatant would confirm whether *Wif1* inhibits proliferation.

Most interestingly, the *Wif1*-mediated prevention of *in vivo* tumor growth was accompanied by maintenance of phosphorylation of PKC and Erk1 that was already seen in cell cultures, whereas phosphorylation of both proteins vanished in the faster growing control cells. This indicates that *Wif1* may permit  $Wnt/Ca^{2+}$  signaling mediated by PKC phosphorylation resulting in Erk1 activation. Alternatively, *Wif1* might also affect EGFR signaling. Nevertheless, specific inhibition of Erk1 would demonstrate whether Erk1 phosphorylation could result in the suppression of proliferation. Unfortunately, specific Erk1 inhibitors are not available. However, inhibition of Mek1/2 by U0126 resulting in inhibition of Erk1/2 was shown to inhibit proliferation of

ASZ001 (Xie *et al.* 2001). Therefore, one should also anticipate an Erk1 knockdown/-out experiments in ASZ-*Wif1* cells. This experiment would help to elucidate the function of Erk1 in proliferation *in vitro* and tumor growth suppression in an allograft experiment.

To investigate whether EGFR signaling participates in Erk1 activation, protein samples from the respective *in vitro* cultures as well as allograft samples should be analyzed regarding EGFR signaling activity. First, the phosphorylation status of EGF receptors ErbB2, ErbB3, and ErbB4 that are able to bind *Wif1* should be determined. Downstream of ErbB, receptor components of the signaling pathway that are known to be regulators of Erk1 activity (e.g. Ras, Raf, Mek1) and effector proteins that are known to be regulated by Erk1 and control proliferation should be analyzed regarding their activity in subsequent experiments.

In summary, our data indicate that *Wif1* exerts a tumor suppressive function in BCC. Therefore, it might be worth testing purified and concentrated, topically applied *Wif1* in a therapeutic treatment approach in the *Ptch* mouse model for BCC.

## VI References

- Abdulla, FR, Feldman, SR, Williford, PM, Krowchuk, D and Kaur, M (2005). "Tanning and skin cancer." *Pediatr Dermatol* 22(6): 501-512.
- Arteaga, CL and Engelman, JA (2014). "ERBB receptors: from oncogene discovery to basic science to mechanism-based cancer therapeutics." *Cancer Cell* 25(3): 282-303.
- Athar, M, Tang, X, Lee, JL, Kopelovich, L and Kim, AL (2006). "Hedgehog signalling in skin development and cancer." *Exp Dermatol* 15(9): 667-677.
- Augsten, M (2014). "Cancer-associated fibroblasts as another polarized cell type of the tumor microenvironment." *Front Oncol* 4: 62.
- Augustin, I, Gross, J, Baumann, D, Korn, C, Kerr, G, Grigoryan, T, Mauch, C, Birchmeier, W and Boutros, M (2013). "Loss of epidermal Evi/Wls results in a phenotype resembling psoriasiform dermatitis." *J Exp Med* 210(9): 1761-1777.
- Avanesov, A and Blair, SS (2013). "The Drosophila WIF1 homolog Shifted maintains glypican-independent Hedgehog signaling and interacts with the Hedgehog co-receptors Ihog and Boi." *Development* 140(1): 107-116.
- Avanesov, A, Honeyager, SM, Malicki, J and Blair, SS (2012). "The role of glypicans in Wnt inhibitory factor-1 activity and the structural basis of Wif1's effects on Wnt and Hedgehog signaling." *PLoS Genet* 8(2): e1002503.
- Baker, EK, Taylor, S, Gupte, A, Chalk, AM, Bhattacharya, S, Green, AC, Martin, TJ, Strbenac, D, Robinson, MD, Purton, LE and Walkley, CR (2015). "Wnt inhibitory factor 1 (WIF1) is a marker of osteoblastic differentiation stage and is not silenced by DNA methylation in osteosarcoma." *Bone* 73: 223-232.
- Banziger, C, Soldini, D, Schutt, C, Zipperlen, P, Hausmann, G and Basler, K (2006). "Wntless, a conserved membrane protein dedicated to the secretion of Wnt proteins from signaling cells." *Cell* 125(3): 509-522.
- Basset-Seguin, N, Sharpe, HJ and de Sauvage, FJ (2015). "Efficacy of Hedgehog Pathway Inhibitors in Basal Cell Carcinoma." *Mol Cancer Ther*.
- Beachy, PA, Hymowitz, SG, Lazarus, RA, Leahy, DJ and Siebold, C (2010). "Interactions between Hedgehog proteins and their binding partners come into view." *Genes Dev* 24(18): 2001-2012.
- Beachy, PA, Karhadkar, SS and Berman, DM (2004). "Tissue repair and stem cell renewal in carcinogenesis." *Nature* 432(7015): 324-331.
- Becker, M (2011). "The Role of Wif1 in Basal Cell Carcinoma" Master Thesis
- Behrens, J, von Kries, JP, Kuhl, M, Bruhn, L, Wedlich, D, Grosschedl, R and Birchmeier, W (1996). "Functional interaction of beta-catenin with the transcription factor LEF-1." *Nature* 382(6592): 638-642.

- Bingle, L, Brown, NJ and Lewis, CE (2002). "The role of tumour-associated macrophages in tumour progression: implications for new anticancer therapies." *J Pathol* 196(3): 254-265.
- Bissell, MJ and Radisky, D (2001). "Putting tumours in context." *Nat Rev Cancer* 1(1): 46-54.
- Boonchai, W, Green, A, Ng, J, Dicker, A and Chenevix-Trench, G (2000). "Basal cell carcinoma in chronic arsenicism occurring in Queensland, Australia, after ingestion of an asthma medication." *J Am Acad Dermatol* 43(4): 664-669.
- Bowman, T, Garcia, R, Turkson, J and Jove, R (2000). "STATs in oncogenesis." *Oncogene* 19(21): 2474-2488.
- Brambilla, R and Ratto, GM (2009). "The controversy on the differential role of ERK1 and ERK2 MAP kinases in cell signaling" Letter to the editor of *Cell Cycle*
- Breitkreutz, D, Braiman-Wiksman, L, Daum, N, Denning, MF and Tennenbaum, T (2007). "Protein kinase C family: on the crossroads of cell signaling in skin and tumor epithelium." *J Cancer Res Clin Oncol* 133(11): 793-808.
- Briscoe, J, Chen, Y, Jessell, TM and Struhl, G (2001). "A hedgehog-insensitive form of patched provides evidence for direct long-range morphogen activity of sonic hedgehog in the neural tube." *Mol Cell* 7(6): 1279-1291.
- Burke, R, Nellen, D, Bellotto, M, Hafen, E, Senti, KA, Dickson, BJ and Basler, K (1999). "Dispatched, a novel sterol-sensing domain protein dedicated to the release of cholesterol-modified hedgehog from signaling cells." *Cell* 99(7): 803-815.
- Cadigan, KM and Waterman, ML (2012). "TCF/LEFs and Wnt signaling in the nucleus." *Cold Spring Harb Perspect Biol* 4(11).
- Cagnol, S and Chambard, JC (2010). "ERK and cell death: mechanisms of ERK-induced cell death--apoptosis, autophagy and senescence." *FEBS J* 277(1): 2-21.
- Cancer Facts & Figures (2015). Atlanta: American Cancer Society
- Carstens, PO (2010). "Untersuchungen zur Rolle von Wnt5a Beim Basalzellkarzinom" Dissertation
- Cebrot, M, Strzadala, L and Kisielow, P (2004). "Wnt inhibitory factor-1: a candidate for a new player in tumorigenesis of intestinal epithelial cells." *Cancer Lett* 206(1): 107-113.
- Chang, SC, Mulloy, B, Magee, AI and Couchman, JR (2011). "Two distinct sites in sonic Hedgehog combine for heparan sulfate interactions and cell signaling functions." *J Biol Chem* 286(52): 44391-44402.
- Chong, CR and Janne, PA (2013). "The quest to overcome resistance to EGFR-targeted therapies in cancer." *Nat Med* 19(11): 1389-1400.
- Clevers, H and Nusse, R (2012). "Wnt/beta-catenin signaling and disease." *Cell* 149(6): 1192-1205.
- Crowson, AN (2006). "Basal cell carcinoma: biology, morphology and clinical implications." *Mod Pathol* 19 Suppl 2: S127-147.

- Curson, C and Weedon, D (1979). "Spontaneous regression in basal cell carcinomas." *J Cutan Pathol* 6(5): 432-437.
- Dessinioti, C, Antoniou, C, Katsambas, A and Stratigos, AJ (2010). "Basal cell carcinoma: what's new under the sun." *Photochem Photobiol* 86(3): 481-491.
- Devenport, D (2014). "The cell biology of planar cell polarity." *J Cell Biol* 207(2): 171-179.
- Dogliani, C, Piccinin, S, Demontis, S, Cangi, MG, Pecciarini, L, Chiarelli, C, Armellin, M, Vukosavljevic, T, Boiocchi, M and Maestro, R (2003). "Alterations of beta-catenin pathway in non-melanoma skin tumors: loss of alpha-ABC nuclear reactivity correlates with the presence of beta-catenin gene mutation." *Am J Pathol* 163(6): 2277-2287.
- Eberl, M, Klingler, S, Mangelberger, D, Loipetzberger, A, Damhofer, H, Zoidl, K, Schnidar, H, Hache, H, Bauer, HC, Solca, F, Hauser-Kronberger, C, Ermilov, AN, Verhaegen, ME, Bichakjian, CK, Dlugosz, AA, Nietfeld, W, Sibilica, M, Lehrach, H, Wierling, C and Aberger, F (2012). "Hedgehog-EGFR cooperation response genes determine the oncogenic phenotype of basal cell carcinoma and tumour-initiating pancreatic cancer cells." *EMBO Mol Med* 4(3): 218-233.
- Ecke, I (2008). "Überprüfung neuer Therapieansätze für Patched-assoziierte Tumoren im Mausmodell" Dissertation
- El-Bahrawy, M, El-Masry, N, Alison, M, Poulson, R and Fallowfield, M (2003). "Expression of beta-catenin in basal cell carcinoma." *Br J Dermatol* 148(5): 964-970.
- Epstein, EH (2008). "Basal cell carcinomas: attack of the hedgehog." *Nat Rev Cancer* 8(10): 743-754.
- Euhus, DM, Hudd, C, LaRegina, MC and Johnson, FE (1986). "Tumor measurement in the nude mouse." *J Surg Oncol* 31(4): 229-234.
- Fan, QW, Cheng, C, Knight, ZA, Haas-Kogan, D, Stokoe, D, James, CD, McCormick, F, Shokat, KM and Weiss, WA (2009). "EGFR signals to mTOR through PKC and independently of Akt in glioma." *Sci Signal* 2(55): ra4.
- Fullar, A, Dudas, J, Olah, L, Hollosi, P, Papp, Z, Sobel, G, Karaszi, K, Paku, S, Baghy, K and Kovalszky, I (2015). "Remodeling of extracellular matrix by normal and tumor-associated fibroblasts promotes cervical cancer progression." *BMC Cancer* 15: 256.
- Glise, B, Miller, CA, Crozatier, M, Halbisen, MA, Wise, S, Olson, DJ, Vincent, A and Blair, SS (2005). "Shifted, the Drosophila ortholog of Wnt inhibitory factor-1, controls the distribution and movement of Hedgehog." *Dev Cell* 8(2): 255-266.
- Goppner, D and Leverkus, M (2011). "Basal cell carcinoma: from the molecular understanding of the pathogenesis to targeted therapy of progressive disease." *J Skin Cancer* 2011: 650258.
- Gorfinkiel, N, Sierra, J, Callejo, A, Ibanez, C and Guerrero, I (2005). "The Drosophila ortholog of the human Wnt inhibitor factor Shifted controls the diffusion of lipid-modified Hedgehog." *Dev Cell* 8(2): 241-253.

- Green, J, Nusse, R and van Amerongen, R (2014). "The role of Ryk and Ror receptor tyrosine kinases in Wnt signal transduction." *Cold Spring Harb Perspect Biol* 6(2).
- Guegan, JP, Ezan, F, Gailhouste, L, Langouet, S and Baffet, G (2014). "MEK1/2 overactivation can promote growth arrest by mediating ERK1/2-dependent phosphorylation of p70S6K." *J Cell Physiol* 229(7): 903-915.
- Guihard, S, Clay, D, Cocault, L, Saulnier, N, Opolon, P, Souyri, M, Pages, G, Pouyssegur, J, Porteu, F and Gaudry, M (2010). "The MAPK ERK1 is a negative regulator of the adult steady-state splenic erythropoiesis." *Blood* 115(18): 3686-3694.
- Habas, R, Dawid, IB and He, X (2003). "Coactivation of Rac and Rho by Wnt/Frizzled signaling is required for vertebrate gastrulation." *Genes Dev* 17(2): 295-309.
- Hafner, C, Landthaler, M and Vogt, T (2010). "Activation of the PI3K/AKT signalling pathway in non-melanoma skin cancer is not mediated by oncogenic PIK3CA and AKT1 hotspot mutations." *Exp Dermatol* 19(8): e222-227.
- Hahn, H, Wicking, C, Zaphiropoulos, PG, Gailani, MR, Shanley, S, Chidambaram, A, Vorechovsky, I, Holmberg, E, Uden, AB, Gillies, S, Negus, K, Smyth, I, Pressman, C, Leffell, DJ, Gerrard, B, Goldstein, AM, Dean, M, Toftgard, R, Chenevix-Trench, G, Wainwright, B and Bale, AE (1996). "Mutations of the human homolog of Drosophila patched in the nevoid basal cell carcinoma syndrome." *Cell* 85(6): 841-851.
- Hallikas, O, Palin, K, Sinjushina, N, Rautiainen, R, Partanen, J, Ukkonen, E and Taipale, J (2006). "Genome-wide prediction of mammalian enhancers based on analysis of transcription-factor binding affinity." *Cell* 124(1): 47-59.
- Haqq, C, Nosrati, M, Sudilovsky, D, Crothers, J, Khodabakhsh, D, Pulliam, BL, Federman, S, Miller, JR, 3rd, Allen, RE, Singer, MI, Leong, SP, Ljung, BM, Sagebiel, RW and Kashani-Sabet, M (2005). "The gene expression signatures of melanoma progression." *Proc Natl Acad Sci U S A* 102(17): 6092-6097.
- Hemmings, BA and Restuccia, DF (2015). "The PI3K-PKB/Akt pathway." *Cold Spring Harb Perspect Biol* 7(4).
- Hogan, PG, Chen, L, Nardone, J and Rao, A (2003). "Transcriptional regulation by calcium, calcineurin, and NFAT." *Genes Dev* 17(18): 2205-2232.
- Honma, K, Miyata, T and Ochiya, T (2007). "Type I collagen gene suppresses tumor growth and invasion of malignant human glioma cells." *Cancer Cell Int* 7: 12.
- Hsieh, JC, Kodjabachian, L, Rebbert, ML, Rattner, A, Smallwood, PM, Samos, CH, Nusse, R, Dawid, IB and Nathans, J (1999). "A new secreted protein that binds to Wnt proteins and inhibits their activities." *Nature* 398(6726): 431-436.

- Hu, J, Dong, A, Fernandez-Ruiz, V, Shan, J, Kawa, M, Martinez-Anso, E, Prieto, J and Qian, C (2009). "Blockade of Wnt signaling inhibits angiogenesis and tumor growth in hepatocellular carcinoma." *Cancer Res* 69(17): 6951-6959.
- Huang, S, Zhong, X, Gao, J, Song, R, Wu, H, Zi, S, Yang, S, Du, P, Cui, L, Yang, C and Li, Z (2014). "Coexpression of SFRP1 and WIF1 as a prognostic predictor of favorable outcomes in patients with colorectal carcinoma." *Biomed Res Int* 2014: 256723.
- Hui, CC and Angers, S (2011). "Gli proteins in development and disease." *Annu Rev Cell Dev Biol* 27: 513-537.
- Johnson, RL, Rothman, AL, Xie, J, Goodrich, LV, Bare, JW, Bonifas, JM, Quinn, AG, Myers, RM, Cox, DR, Epstein, EH, Jr. and Scott, MP (1996). "Human homolog of patched, a candidate gene for the basal cell nevus syndrome." *Science* 272(5268): 1668-1671.
- Kalluri, R and Weinberg, RA (2009). "The basics of epithelial-mesenchymal transition." *J Clin Invest* 119(6): 1420-1428.
- Kansara, M, Tsang, M, Kodjabachian, L, Sims, NA, Trivett, MK, Ehrich, M, Dobrovic, A, Slavin, J, Choong, PF, Simmons, PJ, Dawid, IB and Thomas, DM (2009). "Wnt inhibitory factor 1 is epigenetically silenced in human osteosarcoma, and targeted disruption accelerates osteosarcomagenesis in mice." *J Clin Invest* 119(4): 837-851.
- Kass, L, Erler, JT, Dembo, M and Weaver, VM (2007). "Mammary epithelial cell: influence of extracellular matrix composition and organization during development and tumorigenesis." *Int J Biochem Cell Biol* 39(11): 1987-1994.
- Kaucka, M, Petersen, J, Janovska, P, Radaszkiewicz, T, Smyckova, L, Daulat, AM, Borg, JP, Schulte, G and Bryja, V (2015). "Asymmetry of VANGL2 in migrating lymphocytes as a tool to monitor activity of the mammalian WNT/planar cell polarity pathway." *Cell Commun Signal* 13: 2.
- Kawakami, K, Hirata, H, Yamamura, S, Kikuno, N, Saini, S, Majid, S, Tanaka, Y, Kawamoto, K, Enokida, H, Nakagawa, M and Dahiya, R (2009). "Functional significance of Wnt inhibitory factor-1 gene in kidney cancer." *Cancer Res* 69(22): 8603-8610.
- Kim, GH and Han, JK (2005). "JNK and ROKalpha function in the noncanonical Wnt/RhoA signaling pathway to regulate *Xenopus* convergent extension movements." *Dev Dyn* 232(4): 958-968.
- Kim, J, You, L, Xu, Z, Kuchenbecker, K, Raz, D, He, B and Jablons, D (2007). "Wnt inhibitory factor inhibits lung cancer cell growth." *J Thorac Cardiovasc Surg* 133(3): 733-737.
- Kim, JY, Lee, TR and Lee, AY (2013). "Reduced WIF-1 expression stimulates skin hyperpigmentation in patients with melasma." *J Invest Dermatol* 133(1): 191-200.
- Kispert, A, Vainio, S and McMahon, AP (1998). "Wnt-4 is a mesenchymal signal for epithelial transformation of metanephric mesenchyme in the developing kidney." *Development* 125(21): 4225-4234.

- Kolch, W (2005). "Coordinating ERK/MAPK signalling through scaffolds and inhibitors." *Nat Rev Mol Cell Biol* 6(11): 827-837.
- König, S (2012). "Die Rolle von Wnt5a bei der Regression des Basalzellkarzinoms" Dissertation
- Koontongkaew, S (2013). "The tumor microenvironment contribution to development, growth, invasion and metastasis of head and neck squamous cell carcinomas." *J Cancer* 4(1): 66-83.
- Korinek, V, Barker, N, Morin, PJ, van Wichen, D, de Weger, R, Kinzler, KW, Vogelstein, B and Clevers, H (1997). "Constitutive transcriptional activation by a beta-catenin-Tcf complex in APC<sup>-/-</sup> colon carcinoma." *Science* 275(5307): 1784-1787.
- Krahn, G, Leiter, U, Kaskel, P, Udart, M, Utikal, J, Bezold, G and Peter, RU (2001). "Coexpression patterns of EGFR, HER2, HER3 and HER4 in non-melanoma skin cancer." *Eur J Cancer* 37(2): 251-259.
- Kuhl, M, Sheldahl, LC, Malbon, CC and Moon, RT (2000). "Ca<sup>2+</sup>/calmodulin-dependent protein kinase II is stimulated by Wnt and Frizzled homologs and promotes ventral cell fates in *Xenopus*." *J Biol Chem* 275(17): 12701-12711.
- Kulesz-Martin, M, Kilkenny, AE, Holbrook, KA, Digernes, V and Yuspa, SH (1983). "Properties of carcinogen altered mouse epidermal cells resistant to calcium-induced terminal differentiation." *Carcinogenesis* 4(11): 1367-1377.
- LaBaer, J, Garrett, MD, Stevenson, LF, Slingerland, JM, Sandhu, C, Chou, HS, Fattaey, A and Harlow, E (1997). "New functional activities for the p21 family of CDK inhibitors." *Genes Dev* 11(7): 847-862.
- Lam, CW, Xie, J, To, KF, Ng, HK, Lee, KC, Yuen, NW, Lim, PL, Chan, LY, Tong, SF and McCormick, F (1999). "A frequent activated smoothed mutation in sporadic basal cell carcinomas." *Oncogene* 18(3): 833-836.
- Levental, KR, Yu, H, Kass, L, Lakins, JN, Egeblad, M, Ertler, JT, Fong, SF, Csiszar, K, Giaccia, A, Wenginger, W, Yamauchi, M, Gasser, DL and Weaver, VM (2009). "Matrix crosslinking forces tumor progression by enhancing integrin signaling." *Cell* 139(5): 891-906.
- Li, VS, Ng, SS, Boersema, PJ, Low, TY, Karthaus, WR, Gerlach, JP, Mohammed, S, Heck, AJ, Maurice, MM, Mahmoudi, T and Clevers, H (2012). "Wnt signaling through inhibition of beta-catenin degradation in an intact Axin1 complex." *Cell* 149(6): 1245-1256.
- Li, XJ, Zhang, X, Johnson, MA, Wang, ZB, Lavaute, T and Zhang, SC (2009). "Coordination of sonic hedgehog and Wnt signaling determines ventral and dorsal telencephalic neuron types from human embryonic stem cells." *Development* 136(23): 4055-4063.
- Lim, X and Nusse, R (2013). "Wnt signaling in skin development, homeostasis, and disease." *Cold Spring Harb Perspect Biol* 5(2).
- Lin, YC, You, L, Xu, Z, He, B, Yang, CT, Chen, JK, Mikami, I, Clement, G, Shi, Y, Kuchenbecker, K, Okamoto, J, Kashani-Sabet, M and Jablons, DM (2007). "Wnt inhibitory factor-1 gene transfer inhibits melanoma cell growth." *Hum Gene Ther* 18(4): 379-386.

- Liu, F, van den Broek, O, Destree, O and Hoppler, S (2005). "Distinct roles for *Xenopus* Tcf/Lef genes in mediating specific responses to Wnt/beta-catenin signalling in mesoderm development." *Development* 132(24): 5375-5385.
- Lories, RJ, Corr, M and Lane, NE (2013). "To Wnt or not to Wnt: the bone and joint health dilemma." *Nat Rev Rheumatol* 9(6): 328-339.
- Louro, ID, Bailey, EC, Li, X, South, LS, McKie-Bell, PR, Yoder, BK, Huang, CC, Johnson, MR, Hill, AE, Johnson, RL and Ruppert, JM (2002). "Comparative gene expression profile analysis of GLI and c-MYC in an epithelial model of malignant transformation." *Cancer Res* 62(20): 5867-5873.
- Lustig, B, Jerchow, B, Sachs, M, Weiler, S, Pietsch, T, Karsten, U, van de Wetering, M, Clevers, H, Schlag, PM, Birchmeier, W and Behrens, J (2002). "Negative feedback loop of Wnt signaling through upregulation of conductin/axin2 in colorectal and liver tumors." *Mol Cell Biol* 22(4): 1184-1193.
- Ma, Y, Erkner, A, Gong, R, Yao, S, Taipale, J, Basler, K and Beachy, PA (2002). "Hedgehog-mediated patterning of the mammalian embryo requires transporter-like function of dispatched." *Cell* 111(1): 63-75.
- Malinauskas, T, Aricescu, AR, Lu, W, Siebold, C and Jones, EY (2011). "Modular mechanism of Wnt signaling inhibition by Wnt inhibitory factor 1." *Nat Struct Mol Biol* 18(8): 886-893.
- Malinauskas, T and Jones, EY (2014). "Extracellular modulators of Wnt signalling." *Curr Opin Struct Biol* 29: 77-84.
- Mancuso, M, Pazzaglia, S, Tanori, M, Hahn, H, Merola, P, Rebessi, S, Atkinson, MJ, Di Majo, V, Covelli, V and Saran, A (2004). "Basal cell carcinoma and its development: insights from radiation-induced tumors in *Ptch1*-deficient mice." *Cancer Res* 64(3): 934-941.
- Mazieres, J, He, B, You, L, Xu, Z, Lee, AY, Mikami, I, Reguart, N, Rosell, R, McCormick, F and Jablons, DM (2004). "Wnt inhibitory factor-1 is silenced by promoter hypermethylation in human lung cancer." *Cancer Res* 64(14): 4717-4720.
- McCubrey, JA, Steelman, LS, Chappell, WH, Abrams, SL, Franklin, RA, Montalto, G, Cervello, M, Libra, M, Candido, S, Malaponte, G, Mazzarino, MC, Fagone, P, Nicoletti, F, Basecke, J, Mijatovic, S, Maksimovic-Ivanic, D, Milella, M, Tafuri, A, Chiarini, F, Evangelisti, C, Cocco, L and Martelli, AM (2012). "Ras/Raf/MEK/ERK and PI3K/PTEN/Akt/mTOR cascade inhibitors: how mutations can result in therapy resistance and how to overcome resistance." *Oncotarget* 3(10): 1068-1111.
- Mendoza, MC, Er, EE and Blenis, J (2011). "The Ras-ERK and PI3K-mTOR pathways: cross-talk and compensation." *Trends Biochem Sci* 36(6): 320-328.
- Molenaar, M, van de Wetering, M, Oosterwegel, M, Peterson-Maduro, J, Godsave, S, Korinek, V, Roose, J, Destree, O and Clevers, H (1996). "XTcf-3 transcription factor mediates beta-catenin-induced axis formation in *Xenopus* embryos." *Cell* 86(3): 391-399.

- Morin, PJ, Sparks, AB, Korinek, V, Barker, N, Clevers, H, Vogelstein, B and Kinzler, KW (1997). "Activation of beta-catenin-Tcf signaling in colon cancer by mutations in beta-catenin or APC." *Science* 275(5307): 1787-1790.
- Nakayama, M, Tabuchi, K, Nakamura, Y and Hara, A (2011). "Basal cell carcinoma of the head and neck." *J Skin Cancer* 2011: 496910.
- Neill, GW, Ghali, LR, Green, JL, Ikram, MS, Philpott, MP and Quinn, AG (2003). "Loss of protein kinase Calpha expression may enhance the tumorigenic potential of Gli1 in basal cell carcinoma." *Cancer Res* 63(15): 4692-4697.
- Nilsson, M, Unden, AB, Krause, D, Malmqwist, U, Raza, K, Zaphiropoulos, PG and Toftgard, R (2000). "Induction of basal cell carcinomas and trichoepitheliomas in mice overexpressing GLI-1." *Proc Natl Acad Sci U S A* 97(7): 3438-3443.
- Nitzki, F (2008). "Patched-assoziierte Tumoren: Modifikatorgene und Pathogenese" Dissertation
- Nitzki, F, Zibat, A, König, S, Wijgerde, M, Rosenberger, A, Brembeck, FH, Carstens, P-O, Frommhold, A, Uhmann, A, Klingler, S, Reifenberger, J, Pukrop, T, Aberger, F, Schulz-Schaeffer, W and Hahn, H (2010). "Tumor stroma-derived Wnt5a induces differentiation of basal cell carcinoma of Ptch mutant mice via CaMKII." *Cancer Res* in press.
- Noubissi, FK, Kim, T, Kawahara, TN, Aughenbaugh, WD, Berg, E, Longley, BJ, Athar, M and Spiegelman, VS (2014). "Role of CRD-BP in the growth of human basal cell carcinoma cells." *J Invest Dermatol* 134(6): 1718-1724.
- Nyati, MK, Morgan, MA, Feng, FY and Lawrence, TS (2006). "Integration of EGFR inhibitors with radiochemotherapy." *Nat Rev Cancer* 6(11): 876-885.
- Oliva, JL, Griner, EM and Kazanietz, MG (2005). "PKC isozymes and diacylglycerol-regulated proteins as effectors of growth factor receptors." *Growth Factors* 23(4): 245-252.
- Oro, AE, Higgins, KM, Hu, Z, Bonifas, JM, Epstein, EH, Jr. and Scott, MP (1997). "Basal cell carcinomas in mice overexpressing sonic hedgehog." *Science* 276(5313): 817-821.
- Pages, G and Pouyssegur, J (2004). "Study of MAPK signaling using knockout mice." *Methods Mol Biol* 250: 155-166.
- Palmer, HG, Anjos-Afonso, F, Carmeliet, G, Takeda, H and Watt, FM (2008). "The vitamin D receptor is a Wnt effector that controls hair follicle differentiation and specifies tumor type in adult epidermis." *PLoS One* 3(1): e1483.
- Park, TJ, Kim, M, Kim, H, Park, SY, Park, KC, Ortonne, JP and Kang, HY (2014). "Wnt inhibitory factor (WIF)-1 promotes melanogenesis in normal human melanocytes." *Pigment Cell Melanoma Res* 27(1): 72-81.
- Pasca di Magliano, M and Hebrok, M (2003). "Hedgehog signalling in cancer formation and maintenance." *Nat Rev Cancer* 3(12): 903-911.
- Patthy, L (2000). "The WIF module." *Trends Biochem Sci* 25(1): 12-13.

- Peterson, SC, Eberl, M, Vagnozzi, AN, Belkadi, A, Veniaminova, NA, Verhaegen, ME, Bichakjian, CK, Ward, NL, Dlugosz, AA and Wong, SY (2015). "Basal Cell Carcinoma Preferentially Arises from Stem Cells within Hair Follicle and Mechanosensory Niches." *Cell Stem Cell* 16(4): 400-412.
- Petrova, R and Joyner, AL (2014). "Roles for Hedgehog signaling in adult organ homeostasis and repair." *Development* 141(18): 3445-3457.
- Rahmouni, S, Cerignoli, F, Alonso, A, Tsutji, T, Henkens, R, Zhu, C, Louisdit-Sully, C, Moutschen, M, Jiang, W and Mustelin, T (2006). "Loss of the VHR dual-specific phosphatase causes cell-cycle arrest and senescence." *Nat Cell Biol* 8(5): 524-531.
- Ramachandran, I, Ganapathy, V, Gillies, E, Fonseca, I, Sureban, SM, Houchen, CW, Reis, A and Queimado, L (2014). "Wnt inhibitory factor 1 suppresses cancer stemness and induces cellular senescence." *Cell Death Dis* 5: e1246.
- Ramachandran, I, Thavathiru, E, Ramalingam, S, Natarajan, G, Mills, WK, Benbrook, DM, Zuna, R, Lightfoot, S, Reis, A, Anant, S and Queimado, L (2012). "Wnt inhibitory factor 1 induces apoptosis and inhibits cervical cancer growth, invasion and angiogenesis in vivo." *Oncogene* 31(22): 2725-2737.
- Reguart, N, He, B, Xu, Z, You, L, Lee, AY, Mazieres, J, Mikami, I, Batra, S, Rosell, R, McCormick, F and Jablons, DM (2004). "Cloning and characterization of the promoter of human Wnt inhibitory factor-1." *Biochem Biophys Res Commun* 323(1): 229-234.
- Reifenberger, J, Wolter, M, Knobbe, CB, Kohler, B, Schonicke, A, Scharwachter, C, Kumar, K, Blaschke, B, Ruzicka, T and Reifenberger, G (2005). "Somatic mutations in the PTCH, SMOH, SUFUH and TP53 genes in sporadic basal cell carcinomas." *Br J Dermatol* 152(1): 43-51.
- Roberg-Larsen, H, Strand, MF, Krauss, S and Wilson, SR (2014). "Metabolites in vertebrate Hedgehog signaling." *Biochem Biophys Res Commun* 446(3): 669-674.
- Robinson, JK and Dahiya, M (2003). "Basal cell carcinoma with pulmonary and lymph node metastasis causing death." *Arch Dermatol* 139(5): 643-648.
- Rubin, AI, Chen, EH and Ratner, D (2005). "Basal-cell carcinoma." *N Engl J Med* 353(21): 2262-2269.
- Ruvinsky, I and Meyuhas, O (2006). "Ribosomal protein S6 phosphorylation: from protein synthesis to cell size." *Trends Biochem Sci* 31(6): 342-348.
- Salto-Tellez, M, Peh, BK, Ito, K, Tan, SH, Chong, PY, Han, HC, Tada, K, Ong, WY, Soong, R, Voon, DC and Ito, Y (2006). "RUNX3 protein is overexpressed in human basal cell carcinomas." *Oncogene* 25(58): 7646-7649.
- Samuels, IS, Karlo, JC, Faruzzi, AN, Pickering, K, Herrup, K, Sweatt, JD, Saitta, SC and Landreth, GE (2008). "Deletion of ERK2 mitogen-

- activated protein kinase identifies its key roles in cortical neurogenesis and cognitive function." *J Neurosci* 28(27): 6983-6995.
- Samuels, ML, Weber, MJ, Bishop, JM and McMahon, M (1993). "Conditional transformation of cells and rapid activation of the mitogen-activated protein kinase cascade by an estradiol-dependent human raf-1 protein kinase." *Mol Cell Biol* 13(10): 6241-6252.
- Schaniel, C, Sirabella, D, Qiu, J, Niu, X, Lemischka, IR and Moore, KA (2011). "Wnt-inhibitory factor 1 dysregulation of the bone marrow niche exhausts hematopoietic stem cells." *Blood* 118(9): 2420-2429.
- Schindelin, J, Arganda-Carreras, I, Frise, E, Kaynig, V, Longair, M, Pietzsch, T, Preibisch, S, Rueden, C, Saalfeld, S, Schmid, B, Tinevez, JY, White, DJ, Hartenstein, V, Eliceiri, K, Tomancak, P and Cardona, A (2012). "Fiji: an open-source platform for biological-image analysis." *Nat Methods* 9(7): 676-682.
- Schluter, H, Stark, HJ, Sinha, D, Boukamp, P and Kaur, P (2013). "WIF1 is expressed by stem cells of the human interfollicular epidermis and acts to suppress keratinocyte proliferation." *J Invest Dermatol* 133(6): 1669-1673.
- Schnidar, H, Eberl, M, Klingler, S, Mangelberger, D, Kasper, M, Hauser-Kronberger, C, Regl, G, Kroismayr, R, Moriggl, R, Sibilia, M and Aberger, F (2009). "Epidermal growth factor receptor signaling synergizes with Hedgehog/GLI in oncogenic transformation via activation of the MEK/ERK/JUN pathway." *Cancer Res* 69(4): 1284-1292.
- Sewing, A, Wiseman, B, Lloyd, AC and Land, H (1997). "High-intensity Raf signal causes cell cycle arrest mediated by p21Cip1." *Mol Cell Biol* 17(9): 5588-5597.
- Sheldahl, LC, Park, M, Malbon, CC and Moon, RT (1999). "Protein kinase C is differentially stimulated by Wnt and Frizzled homologs in a G-protein-dependent manner." *Curr Biol* 9(13): 695-698.
- Shtutman, M, Zhurinsky, J, Simcha, I, Albanese, C, D'Amico, M, Pestell, R and Ben-Ze'ev, A (1999). "The cyclin D1 gene is a target of the beta-catenin/LEF-1 pathway." *Proc Natl Acad Sci U S A* 96(10): 5522-5527.
- So, PL, Langston, AW, Daniellinia, N, Hebert, JL, Fujimoto, MA, Khaimskiy, Y, Aszterbaum, M and Epstein, EH, Jr. (2006). "Long-term establishment, characterization and manipulation of cell lines from mouse basal cell carcinoma tumors." *Exp Dermatol* 15(9): 742-750.
- Soleymani, AD, Scheinfeld, N, Vasil, K and Bechtel, MA (2008). "Metastatic basal cell carcinoma presenting with unilateral upper extremity edema and lymphatic spread." *J Am Acad Dermatol* 59(2 Suppl 1): S1-3.
- Staal, FJ, Noort Mv, M, Strous, GJ and Clevers, HC (2002). "Wnt signals are transmitted through N-terminally dephosphorylated beta-catenin." *EMBO Rep* 3(1): 63-68.
- Staples, MP, Elwood, M, Burton, RC, Williams, JL, Marks, R and Giles, GG (2006). "Non-melanoma skin cancer in Australia: the 2002 national survey and trends since 1985." *Med J Aust* 184(1): 6-10.

- Surmann-Schmitt, C, Widmann, N, Dietz, U, Saeger, B, Eitzinger, N, Nakamura, Y, Rattel, M, Latham, R, Hartmann, C, von der Mark, H, Schett, G, von der Mark, K and Stock, M (2009). "Wif-1 is expressed at cartilage-mesenchyme interfaces and impedes Wnt3a-mediated inhibition of chondrogenesis." *J Cell Sci* 122(Pt 20): 3627-3637.
- Tang, Y, Simoneau, AR, Liao, WX, Yi, G, Hope, C, Liu, F, Li, S, Xie, J, Holcombe, RF, Journak, FA, Mercola, D, Hoang, BH and Zi, X (2009). "WIF1, a Wnt pathway inhibitor, regulates SKP2 and c-myc expression leading to G1 arrest and growth inhibition of human invasive urinary bladder cancer cells." *Mol Cancer Ther* 8(2): 458-468.
- Taniguchi, H, Yamamoto, H, Hirata, T, Miyamoto, N, Oki, M, Nosho, K, Adachi, Y, Endo, T, Imai, K and Shinomura, Y (2005). "Frequent epigenetic inactivation of Wnt inhibitory factor-1 in human gastrointestinal cancers." *Oncogene* 24(53): 7946-7952.
- Taylor, MD, Zhang, X, Liu, L, Hui, CC, Mainprize, TG, Scherer, SW, Wainwright, B, Hogg, D and Rutka, JT (2004). "Failure of a medulloblastoma-derived mutant of SUFU to suppress WNT signaling." *Oncogene* 23(26): 4577-4583.
- Tomayko, MM and Reynolds, CP (1989). "Determination of subcutaneous tumor size in athymic (nude) mice." *Cancer Chemother Pharmacol* 24(3): 148-154.
- Trakatelli, M, Ulrich, C, del Marmol, V, Euvrard, S, Stockfleth, E and Abeni, D (2007). "Epidemiology of nonmelanoma skin cancer (NMSC) in Europe: accurate and comparable data are needed for effective public health monitoring and interventions." *Br J Dermatol* 156 Suppl 3: 1-7.
- Uhmann, A, Dittmann, K, Nitzki, F, Dressel, R, Koleva, M, Frommhold, A, Zibat, A, Binder, C, Adham, I, Nitsche, M, Heller, T, Armstrong, V, Schulz-Schaeffer, W, Wienands, J and Hahn, H (2007). "The Hedgehog receptor Patched controls lymphoid lineage commitment." *Blood* 110(6): 1814-1823.
- Ulloa, F, Itasaki, N and Briscoe, J (2007). "Inhibitory Gli3 activity negatively regulates Wnt/beta-catenin signaling." *Curr Biol* 17(6): 545-550.
- van Amerongen, R and Nusse, R (2009). "Towards an integrated view of Wnt signaling in development." *Development* 136(19): 3205-3214.
- van de Wetering, M, Cavallo, R, Dooijes, D, van Beest, M, van Es, J, Loureiro, J, Ypma, A, Hursh, D, Jones, T, Bejsovec, A, Peifer, M, Mortin, M and Clevers, H (1997). "Armadillo coactivates transcription driven by the product of the *Drosophila* segment polarity gene dTCF." *Cell* 88(6): 789-799.
- Vantaggiato, C, Formentini, I, Bondanza, A, Bonini, C, Naldini, L and Brambilla, R (2006). "ERK1 and ERK2 mitogen-activated protein kinases affect Ras-dependent cell signaling differentially." *J Biol* 5(5): 14.
- Vassallo, I, Zinn, P, Lai, M, Rajakannu, P, Hamou, MF and Hegi, ME (2015). "WIF1 re-expression in glioblastoma inhibits migration through attenuation of non-canonical WNT signaling by downregulating the lncRNA MALAT1." *Oncogene*.

- Vidal, D, Matias-Guiu, X and Alomar, A (2004). "Efficacy of imiquimod for the expression of Bcl-2, Ki67, p53 and basal cell carcinoma apoptosis." *Br J Dermatol* 151(3): 656-662.
- Wang, Y (2009). "Wnt/Planar cell polarity signaling: a new paradigm for cancer therapy." *Mol Cancer Ther* 8(8): 2103-2109.
- Watanabe, N and Higashida, C (2004). "Formins: processive cappers of growing actin filaments." *Exp Cell Res* 301(1): 16-22.
- Weaver, VM, Petersen, OW, Wang, F, Larabell, CA, Briand, P, Damsky, C and Bissell, MJ (1997). "Reversion of the malignant phenotype of human breast cells in three-dimensional culture and in vivo by integrin blocking antibodies." *J Cell Biol* 137(1): 231-245.
- Wei, C, Peng, B, Han, Y, Chen, WV, Rother, J, Tomlinson, GE, Boland, CR, Chaussabel, M, Frazier, ML and Amos, CI (2015). "Mutations of HNRNPA0 and WIF1 predispose members of a large family to multiple cancers." *Fam Cancer* 14(2): 297-306.
- Weidinger, G and Moon, RT (2003). "When Wnts antagonize Wnts." *J Cell Biol* 162(5): 753-755.
- Wendel, HG, De Stanchina, E, Fridman, JS, Malina, A, Ray, S, Kogan, S, Cordon-Cardo, C, Pelletier, J and Lowe, SW (2004). "Survival signalling by Akt and eIF4E in oncogenesis and cancer therapy." *Nature* 428(6980): 332-337.
- Woodson, EN and Kedes, DH (2012). "Distinct roles for extracellular signal-regulated kinase 1 (ERK1) and ERK2 in the structure and production of a primate gammaherpesvirus." *J Virol* 86(18): 9721-9736.
- Xie, J, Aszterbaum, M, Zhang, X, Bonifas, JM, Zachary, C, Epstein, E and McCormick, F (2001). "A role of PDGFRalpha in basal cell carcinoma proliferation." *Proc Natl Acad Sci U S A* 98(16): 9255-9259.
- Xie, J, Murone, M, Luoh, SM, Ryan, A, Gu, Q, Zhang, C, Bonifas, JM, Lam, CW, Hynes, M, Goddard, A, Rosenthal, A, Epstein, EH, Jr. and de Sauvage, FJ (1998). "Activating Smoothed mutations in sporadic basal-cell carcinoma." *Nature* 391(6662): 90-92.
- Yamamoto, T, Ebisuya, M, Ashida, F, Okamoto, K, Yonehara, S and Nishida, E (2006). "Continuous ERK activation downregulates antiproliferative genes throughout G1 phase to allow cell-cycle progression." *Curr Biol* 16(12): 1171-1182.
- Yang, SH, Andl, T, Grachtchouk, V, Wang, A, Liu, J, Syu, LJ, Ferris, J, Wang, TS, Glick, AB, Millar, SE and Dlugosz, AA (2008). "Pathological responses to oncogenic Hedgehog signaling in skin are dependent on canonical Wnt/beta3-catenin signaling." *Nat Genet* 40(9): 1130-1135.
- Yao, S, Lum, L and Beachy, P (2006). "The ihog cell-surface proteins bind Hedgehog and mediate pathway activation." *Cell* 125(2): 343-357.
- Yarden, Y and Pines, G (2012). "The ERBB network: at last, cancer therapy meets systems biology." *Nat Rev Cancer* 12(8): 553-563.
- Yarden, Y and Sliwkowski, MX (2001). "Untangling the ErbB signalling network." *Nat Rev Mol Cell Biol* 2(2): 127-137.
- Yee, DS, Tang, Y, Li, X, Liu, Z, Guo, Y, Ghaffar, S, McQueen, P, Atreya, D, Xie, J, Simoneau, AR, Hoang, BH and Zi, X (2010). "The Wnt

- inhibitory factor 1 restoration in prostate cancer cells was associated with reduced tumor growth, decreased capacity of cell migration and invasion and a reversal of epithelial to mesenchymal transition." *Mol Cancer* 9: 162.
- Yoshikawa, S, McKinnon, RD, Kokel, M and Thomas, JB (2003). "Wnt-mediated axon guidance via the Drosophila Derailed receptor." *Nature* 422(6932): 583-588.
- Youssef, KK, Lapouge, G, Bouvree, K, Rorive, S, Brohee, S, Appelstein, O, Larsimont, JC, Sukumaran, V, Van de Sande, B, Pucci, D, Dekoninck, S, Berthe, JV, Aerts, S, Salmon, I, del Marmol, V and Blanpain, C (2012). "Adult interfollicular tumour-initiating cells are reprogrammed into an embryonic hair follicle progenitor-like fate during basal cell carcinoma initiation." *Nat Cell Biol* 14(12): 1282-1294.
- Youssef, KK, Van Keymeulen, A, Lapouge, G, Beck, B, Michaux, C, Achouri, Y, Sotiropoulou, PA and Blanpain, C (2010). "Identification of the cell lineage at the origin of basal cell carcinoma." *Nat Cell Biol* 12(3): 299-305.
- Yu, H, Mouw, JK and Weaver, VM (2011). "Forcing form and function: biomechanical regulation of tumor evolution." *Trends Cell Biol* 21(1): 47-56.
- Zhang, J, Gill, AJ, Issacs, JD, Atmore, B, Johns, A, Delbridge, LW, Lai, R and McMullen, TP (2012). "The Wnt/beta-catenin pathway drives increased cyclin D1 levels in lymph node metastasis in papillary thyroid cancer." *Hum Pathol* 43(7): 1044-1050.
- Zibat, A, Uhmman, A, Nitzki, F, Wijgerde, M, Frommhold, A, Heller, T, Armstrong, V, Wojnowski, L, Quintanilla-Martinez, L, Reifenberger, J, Schulz-Schaeffer, W and Hahn, H (2009). "Time-point and dosage of gene inactivation determine the tumor spectrum in conditional Ptch knockouts." *Carcinogenesis* 30(6): 918-926.

## VII Abbreviations

#	number
%	percent
&	and
‘	minute
”	second
°	degree
μ	micro
∞	unlimited
+	positive
+	wild-type
-	minus
-	knockout
A	Ampere
Ab	antibody
<i>ad libitum</i>	lat. at liberty
AEC	3-amino-9 ethylcarbazole
AG	stock company (german: Aktiengesellschaft)
Akt	v-akt murine thymoma viral oncogene homolog
Ankrd	ankyrin repeat domain
Apc	adenomatosis polyposis coli
a.u.	arbitrary unit
A <sub>xxx</sub>	absorbance at xxx nm
b	y-intercept
BAD	BCL2 antagonist of cell death
BCC	basal cell carcinoma
Bcl2	B cell leukemia/lymphoma 2
Bcl9	B cell CLL/lymphoma 9
BCNS	basal cell nevus syndrome
bFGF	basic fibroblastic growth factor

Boc	biregional cell adhesion molecule-related/down-regulated by oncogenes (Cdon) binding protein
Boi	brother of lhog
bp	base pair
BrdU	5-bromo-2'-deoxyuridine
BSA	bovine serum albumin
C	Celsius
c	centi
c	concentration
Ca <sup>2+</sup>	calcium
CaCl <sub>2</sub>	calcium chloride
CAFs	cancer-associated fibroblasts
CaMKII	calcium/calmodulin-dependent protein kinase II
Cbp	CREB-binding protein
CD	cluster of differentiation
Cdh	cadherin
CDK	cyclin-dependent kinase
cDNA	complementary DNA
Cdo1	cysteine dioxygenase 1, cytosolic
Ci	cubitus interruptus
CM	conditioned medium
CMV	cytomegalovirus
Cn	calcinurin
Co.	company
CO <sub>2</sub>	carbon dioxide
Cre	causes recombination
Creb	cAMP responsive element binding protein
Csnk1a1	casein kinase 1, alpha 1
Ct	threshold cycle
C-terminal	carboxyterminal
Daam1	Dvl associated activator of morphogenesis 1
dATP	2'-deoxyadenosine 5'-triphosphate

## VII

## Abbreviations

DAG	1,2 diacylglycerol
DB	database
dCTP	2'-deoxycytidine 5'-triphosphate
ddH <sub>2</sub> O	double-distilled water
del	deleted, deletion
dGTP	2'-deoxyguanosine 5'-triphosphate
Dhh	Dessert hedgehog
Disp	Dispatched
Dkk	dickkopf
DMEM	Dulbecco's modified eagle medium
DMSO	dimethyl sulfoxide
DNA	deoxyribonucleic acid
DNase	deoxyribonuclease
dNTP	deoxynucleotide
dpc	days post coitum
Drl	derailed
DTT	dithiothreitol
dTTP	2'-deoxythymidine 5'-triphosphate
Dvl	dishevelled
E. coli	Escherichia coli
ECM	extracellular matrix
<i>e.g.</i>	<i>exempli gratia</i> (lat. for example)
EDTA	ethylenediaminetetraacetic acid
EGF	epidermal growth factor
EGFR	epidermal growth factor receptor
EGTA	ethylene glycol tetraacetic acid
eGFP	enhanced GFP
EMT	epithelial-to-mesenchymal transition
ER	endoplasmic reticulum
ErbB	v-erb-b2 erythroblastic leukemia viral oncogene homolog
Erk	extracellular-signal regulated kinase

ERT	tamoxifen-inducible estrogen receptor
<i>et al.</i>	<i>et alii</i> (lat. and others)
EtOH	ethanol
FCS	fetal calf serum
FDA	Federal Drug Agency
Fig.	figure
FITC	fluorescein isothiocyanate
flox	floxed
Fn1	fibronectin 1
FOP	SuperFOP <i>Flash</i> expression plasmid
FOXO	Forkhead (FKHR) family of transcription factors
Fu	Fused
Fzd	frizzled
g	gramm
g	g-force
GAPDH	glyceraldehyde 3-phosphate dehydrogenase
gDNA	genomic DNA
GFP	green fluorescent protein
Gli	Glioma-associated oncogene family member
GliR	Gli repressor form
GmbH & Co KG	limited partnership with a limited liability company as general partner (german: Gesellschaft mit beschränkter Haftung Compagnie und Kommanditgesellschaft)
GmbH	limited liability company (german: Gesellschaft mit beschränkter Haftung)
GPCR	G-protein coupled receptor
G-Phase	gap phase
Gsk3	glycogen synthase kinase 3
h	hour
H <sub>2</sub> O <sub>2</sub>	hydrogen peroxyde
HCl	hydrochloric acid

## VII

## Abbreviations

H&E	haematoxylen and eosin
HEPES	4-(2-hydroxyethyl)-1-piperazineethanesulfonic acid
HEK-293	human embryonic kidney cells 293
HGF	hepatocyte growth factor
Hh	Hedgehog
HNRNPA0	heterogeneous nuclear ribonucleoprotein A0
Hprt	hypoxanthine phosphoribosyltransferase 1
HRP	horse-raddish peroxidase
HRPO	horse-raddish peroxidase
Hsc70	heat-shock protein 70
HSPGs	heparan sulfate proteoglycans
<i>i.e.</i>	<i>id est</i> (lat. that is)
Ig	immunoglobulin
Igf2bp1	insulin-like growth factor 2 mRNA binding protein 1
IHC	immunohistochemistry
Ihh	Indian hedgehog
Ihog	interference hedgehog
i.m.	intramuscular
Inc.	incorporated
i.p.	intraperitoneal
IP <sub>3</sub>	inositol 1,4,5-triphosphate
IvI	involucrin
JNK	c-Jun N-terminal kinase
k	kilo
K1	keratin 1
K10	keratin 10
kb	kilobase
KCl	potassium chloride
KH <sub>2</sub> PO <sub>4</sub>	monopotassium phosphate
KG	limited Partnership (german: Kommanditgesellschaft)

## VII

## Abbreviations

I	liter
LacZ	$\beta$ -Galactosidase
LAR II	Luciferase Assay Reagent II
LB	lysogeny broth
Lef	lymphoid enhancer factor
LiCl	lithium chloride
log	logarithm
LOH	loss-of -heterozygosity
Lor	loricrin
Lrp	LDL receptor-related protein
Ltd.	limited
m	meter
m	milli
m	murine
m	slope
M	molar
Map	Mitogen-activated protein
Mapk	Mitogen-activated protein kinase
Map3k	Mitogen-activated protein kinase kinase kinase
MB	medulloblastoma
MEF	mouse embryonic fibroblast
Mek	MAPK/ERK kinase
MgCl <sub>2</sub>	magnesium dichloride
MetOH	methanol
min	minute
mRNA	messenger ribonucleic acid
MSCV	murine stem cell virus
mTOR	mammalian target of rapamycin
Myc	myelocytomatosis oncogene
n	nano
Na	sodium
Na <sub>2</sub> HPO <sub>4</sub>	disodium hydrogen phosphate

NaCl	sodium chloride
Nfat	nuclear factor associated with T cells
Nf- $\kappa$ B	kappa light polypeptide gene enhancer in B cells
NIH	National Institutes of Health
NMSC	non-melanoma skin cancer
n.s.	not significant
N-terminal	aminoterminal
OD	optical density
O/N	overnight
p	pico
p	plasmid
p	phospho
PBS	Phosphate-buffered sodium chloride-solution
PBST	Phosphate-buffered sodium chloride-solution with Tween-20
PCR	polymerase chain reaction
PCP	planar cell polarity
PDGF	platelet derived growth factor
PDGFR	platelet derived growth factor receptor
pH	lat. potentia hydrogenii
PI	propidium iodide
PI3K	phosphatidylinositol-4,5-bisphosphate 3-kinase
PIP <sub>3</sub>	phosphatidylinositol-3,4,5-triphosphate
Pk	prickle
PKC	protein kinase C
PLB	passive lysis buffer
PLC	protein lipase C
POD	peroxidase
Porcn	palmitoyltransferase porcupine
PS	penicillin/streptomycin
PSMF	phenylmethanesulfonylfluoride
Ptch	patched1

Ptch2	patched2
Ptk7	protein tyrosine kinase 7
Puro	puromycin
Pygo	pygopus
qRT-PCR	quantitative real-time PCR
Raf	
Ras	rat sarcoma virus oncogene homolog
RIPA buffer	radioimmunoprecipitation assay buffer
Rlu	relative light units
RMS	rhabdomyosarcoma
RNA	ribonucleic acid
RNase	ribonuclease
Rock	Rho-associated coiled-coil containing protein kinase
Ror	receptor tyrosine kinase-like orphan receptor
rRNA	ribosomal RNA
RT	room temperature
RYK	receptor tyrosine kinase
S6	ribosomal protein S6
SAPK	stress-activated phospho-kinases
SCC	squamous cell carcinoma
SDS	sodium dodecyl sulfate
Sdc-2	syndecan-2
sec	second
SEM	standard error of the mean
Sfrp	secreted frizzled-related protein
Shh	sonic hedgehog
Sma	smooth muscle actin
Smo	smoothened
SmoM2	constitutively active W539L point mutation of the mouse smoothened homolog gene
SN	supernatant
SOC	super optimal broth with catabolite repression

SOS	son of sevenless
SPF	specified pathogen-free
S-Phase	synthesis phase
St.	saint (german: Sankt)
STAT	signal transducer and activator of transcription
stauro	staurosporine
Sufu	suppressor of fused homolog
SYBR	Synergy Brands Inc.
TAMs	tumor-associated macrophages
Taq	thermos aquaticus
TBE	Tris-boric acid-EDTA-solution
Tbp	TATA box binding protein
TBS	Tris-buffered sodium chloride-solution
TBST	Tris-buffered sodium chloride-solution containing Tween-20
Tcf	T-cell factor
TE	Tris/EDTA buffer
TF	transcription factor
TGF- $\beta$	Transforming growth factor beta
Tgm1	transglutaminase 1
TK	thymidine kinase
Tle	transducin-like enhancer of split
TOP	SuperTOP <i>Flash</i> expression plasmid
TP53	tumor protein p53
$\beta$ -TrCP	beta-transducin repeat containing protein
Tris	tris(hydroxymethyl)aminomethane
TUNEL	TdT-mediated dUTP-biotin nick end labeling
U	unit
USA	United States of America
UV	ultraviolet
V	Volt
v	volume

Vangl	vang-like
VEGF	vascular endothelial growth factor
vs	versus
W	Watt
w	weight
WD	WIF domain
WHO	World Health Organization
Wif1	Wnt inhibitory factor 1
wk	week
Wls	wntless
Wnt	wingless-type MMTV integration site family
WST-1	water soluble tetrazolium salt 1
wt	wild-type
x	fold

## VIII Acknowledgements

This thesis would not have been possible without the support and aid of all the people which accompanied me on my way to complete this study. First of all I would like express my endless gratitude to my supervisor Prof. Dr. Heidi Hahn. Thank you for your support, continuous mentoring, numerous discussions and proofreading of this thesis. Thank you for giving me the opportunity to work on this exciting project.

Many thanks also to the members of my thesis committee Prof. Dr. Matthias Dobbelstein and Prof. Dr. Tobias Pukrop for your helpful input and numerous ideas.

Special thanks go to Dr. Kai Dittmann for all your support and advice in all the experiment requiring flow cytometry and for the joyful small talks that made my visits in the department of immunology a pleasant stay.

A big thank to Prof Dr. Walter Schulz-Schaeffer for the interpretation of all my antibody stainings.

I also would like to thank Prof. Dr. Michael Schön for his support and for providing human tissue samples.

Special thanks also go to the animal care takers, especially Susann Peter and Jennifer Flemming for the excellent animal care and being a memory aid when my animals desperately needed to “retire”.

Countless thanks go to the people of the lab I loved to work with, many of them became more than colleagues. In particular, I would like to thank Dr. Frauke Nitzki for your patients and guidance in the very beginning of this project and Benedikt Linder for always having an open ear, for all the discussions, BBQs and hours in the gym to forget the lab for a while. Moreover, I would like to thank Anke Frommhold, Ina Heß and Eva Stetter for your great support and backup during all the time. You rock! Many Thanks also to all the other current and former lab members, Dr. Anja Uhmann, Dr. Simone König, Dr. Diana Rettberg, Dr. Penelope Pelczar, Rosalie Ridzewski, Julia Dräger, Joana Pyczek, Nicole Cuvelier and Tobias Goldak

for your support and making this a wonderful experience. It was great to work with all of you.

I would also like to thank Prof. Peter Burfeindt and Dr. Silke Kaulfuß for adopting me for lunch and all the funny moments and discussion during all the years.

Especially, I would like to thank my friends and my parents Ingrid and Herbert, to whom I would like to dedicate this thesis, for their endless support and encouragement during my studies and my thesis. I would not have made it without you. Thank you with all my heart!

Finally, I would like to express special thanks to Pia who supported me throughout the critical phase. Thank you for your patience and your warmness.

## IX Curriculum vitae

### Personal information

Name: Marco Becker

Date of Birth: 23.07.1985

Place of Birth: Gelsenkirchen, Germany

Citizenship: German

- 01/2012-09/2015    **Research assistant (Ph. D. candidate),  
Georg-August-University Göttingen**  
University Medical Center Göttingen; Institute of Human Genetics, Tumor Genetics group  
Within the Göttingen Graduate School for Neurosciences, Biophysics and Molecular Biosciences (GGNB) and the doctoral program Molecular biology of cells that is part of GAUSS (Georg-August University School of Science)  
Thesis title: "Wif1 Inhibits the Growth of Basal Cell Carcinoma"
- 10/2009-01/2012    **M.Sc., Georg-August-University Göttingen**  
Within the master program "Developmental, Neural and Behavioral Biology" with focus on "Cell and Developmental Biology".  
Thesis title: "The Role of Wif1 in Basal Cell Carcinoma"
- 10/2006-07/2009    **B.Sc., Georg-August-University Göttingen**  
Within the bachelor program "Biology" with focus on "Molecular Biosciences".  
Thesis title: "Aspects of the Putative Pluripotency Gene Stra8"
- 07/2005            **Abitur, Gymnasium-Petrum Dorsten.**

### Publications

Frauke Nitzki, **Marco Becker**, Anke Frommhold, Walter Schulz-Schaeffer and Heidi Hahn (2012) "*Patched Knockout Mouse Models of Basal Cell Carcinoma*"; Journal of Skin Cancer, Volume 2012 (2012), Article ID 907543